University of Aveiro
2014
Department of Materials Engineering and Ceramics

Priscila Cristina Soares Melo

Electromechanical Poly(L-lactic acid) (PLLA) platforms for regenerative medicine

Plataformas electromecânicas de Poli(L- ácido láctico) (PLLA) para medicina regenerativa

University of Aveiro
2014
Department of Materials Engineering and Ceramics

Priscila Cristina Soares Melo

Electromechanical Poly(L-lactic acid) PLLA platforms for regenerative medicine

Plataformas electromecânicas de Poli(L-ácido láctico) (PLLA) para medicina regenerativa

Master thesis presented to the University of Aveiro in order to accomplish all the necessary requirements to obtain a Master Degree in Biomedical Materials and Devices, elaborated under the scientific orientation of Dra. Maria Helena Fernandes and Dra. Paula Vilarinho, both associated professors of the Department of Materials and Ceramics Engineering from the University of Aveiro.

I dedicate this work to my parents, Ana and Manuel.

Examiners

President

Prof. Dr. José Maria da Fonte Ferreira
Associate Professor with aggregation of the University of Aveiro

Prof. Dr. Carlos Jorge Mariano Miranda Dias
Assistant professor of the New University of Lisbon

Prof. Dr. Maria Helena Figueira Vaz Fernandes
Associate Professor of the University of Aveiro

Acknowledgments

I will never be able to thank enough, but I'll start by doing it here, to my friend Natalie Barroca for all the support, patience, ideas and wise advice along the whole way, because without her everything would have been much hard to execute and accomplish. Another special thank goes to my friend Cátia whose affection and sense of humour kept me going during the most difficult times. To my friends and colleagues João, Alicia, Rui, Pedro D., Pedro L, I appreciate all the help, laughs and motivation that kept me focused. I'm also thankful to my mentors Dra. Maria Helena Fernandes and Dra. Paula Vilarinho for making my ideas possible, providing me with guidance and means to execute them. I acknowledge to the technicians from and out of the ceramics department that participated in my analysis. I'm very grateful to Doc. Abílio Almeida and his Post Doc Yonny Romaguera for receiving me and orienting me like a member of their own and providing me with their knowledge. A special acknowledgment to my parents Ana and Manuel for making this dream possible with their sacrifices and trust in my abilities to do it. I want to thank my life friends, Maria João and Maria Inês for believing in me and being there when I needed, especially in the final step when family is essential. Finally, to the ones who were far, I am grateful for the trust and strength even if separated by half Atlantic Ocean.

palavras-chave PLLA, piezoelectricidade, biomteriais, osso, regeneração.

resumo A descoberta da piezoeletricidade no osso por Fukada levou à ideia de usar materiais piezoeléctricos para melhorar o crescimento ósseo. Polímeros piezoeléctricos como o poli (L-ácido láctico) (PLLA), um poliéster semi-cristalino sintético que combina biodegradabilidade e propriedades físicas ajustáveis, destacam-se pois podem ser utilizados como estruturas temporárias para a regeneração óssea. Para além disso, alguns produtos feitos à base de PLLA estão já aprovados para implantação no corpo humano pela Food and Drug Administration (FDA).Neste trabalho foram produzidos filmes de PLLA com diferentes cristalinidades e espessuras com o intuito de melhorar as propriedades dielétricas do material e a adesão celular. O grau de cristalinidade máximo obtido foi de aproximadamente 35%. Efectuou-se uma caracterização completa dos filmes com diferentes cristalinidades e espessuras. As medidas dielétricas realizadas abrangeram permitividade relativa, perda dielétrica e polarização. O valor mais alto de permitividade relativa medido foi de 52,58 para o filme amorfo, a 120 ºC e 153 kHz. A perda dielétrica atingiu o seu máximo nos filmes cristalinos aos 27 ºC para uma frequência de 1 MHz, com o valor de 1,64. A polarização foi estudada segundo a técnica TSDC (Thermal Stimulation Depolarization Current), um método que mede a polarização do material através do estímulo térmico. Em termos de polarização os valores aumentaram proporcionalmente com a cristalinidade, sendo o mais elevado 180 $\mu C/cm^2$ para as amostras cristalinas polarizadas durante meia hora.

Para além dos ensaios celulares, existe a metabolómica, hoje em dia uma ferramenta poderosa pois pode fornecer informações detalhadas sobre as vias metabólicas específicas que respondem e permitem a adaptação celular a cada uma das formulações de materiais selecionados. O trabalho realizado neste projecto constitui a primeira etapa de um programa mais amplo de caracterização biológica *in vitro*. É apresentado o primeiro estudo de metabolómica, utilizando osteoblastos humanos, em contato com o piezoelétrico PLLA, utilizando filmes de PLLA standard, 3% de cristalinidade, polarizados negativamente.

keywords PLLA, piezoelectricity, biomaterials, bone, regeneration.

abstarct The discovery of piezoelectricity in bone by Fukada brought to light the idea of using piezoelectrics to enhance bone growth. Piezoelectric polymers like poly (L-lactic) acid (PLLA), a synthetic semi-crystalline polyester combining adjustable biodegradability and physical properties, stands out and therefore can be used as scaffolds for bone regeneration. In addition, some PLLA products have been approved for implantation in human body by the Food and Drug Administration (FDA). In the present work PLLA films with different crystallinities and thicknesses were produced in order to improve the dielectric properties and cellular adhesion. The maximum crystalline degree obtained was 35%. A complete characterization of PLLA films with different thicknesses and crystallinities was performed. The dielectric analysis included permittivity, dielectric loss and polarization. The highest relative permittivity value was 52.58 for amorphous samples at 120 ºC and 153 kHz. Dielectric loss reached its maximum at 27 ºC for a frequency of 1 MHz, being the value 1.64 on crystalline films. Polarization was studied by the technique Thermal Stimulated Depolarization Currents (TSDC), a method that measures polarization through thermal stimulus. In terms of polarization, the values increase proportionally with crystallinity, being the highest values 180 μC/cm^2 on crystalline samples polarized during half an hour.
In addition to cell-based assays, exists the metabolomics studies, a powerful tool since it can provide detailed information on the specific metabolic pathways responding and adapting to each of the selected material formulations. The work carried out in this project is the first stage of a wider program including *in vitro* biological characterization. It is presented the first metabolomics study using human osteoblasts in contact with piezoelectric PLLA, on PLLA standard films with 3% crystallinity, negatively poled.

Index

Figures Index

Table Index

Abbreviations

AC – Alternated Current

BG - Bioglass

BTE – Bone Tissue Engineering

DC – Direct Current

DP – Direct Polycondensation

DSC – Differential Scanning Calorimetry

E – Electrical Field

ECM – Extracellular Matrix

EF – Endogenous Fields

FDA – Food and Drug Administration

GF – Growth factors

HR-MAS – High Resolution Magic Angle Spinning

NMR – Nuclear Magnetic Resonance

PLLA – Poly(L-lactic acid)

POM – Polarized light Optical Microscopy

PVDF – Polyvinylidene Fluoride

ROP – Ring Opening Polymerization

SBF – Simulated Body Fluid

SEM – Scanning Electron Microscopy

TDR – Time Domain Reflectometry

TE – Tissue Engineering

TSDC – Thermal Stimulation Depolarization Current

XRD - X-Ray Diffraction

WAXD – Wide Angle X-Ray Diffraction

Chapter 1

Motivation and Objectives

1. Chapter I – Motivation and Objectives

1.1 The necessity

Nowadays, bone defects represent a major challenge for orthopaedic and reconstructive surgeons because no adequate bone substitute has been developed yet. Materials science brought improvements to the field of bone substitution and has been providing the means to create devices that can regenerate or substitute bone itself. However these solutions are not good enough, per year 1000 000 000 cases of bone defects emerge and the number are increasing due to the high life expectancy. This has socioeconomic consequences once the demand is higher than the offer. According to a report made on the U.S. market for orthopaedic biomaterials for bone repair and regeneration, by 2017, this market will reach an estimated value of 3.5 billion dollars. [1, 2]

Until the present time the most efficient devices available to regenerate or substitute bone are autologous and autogenous bone grafts and prosthesis. In the case of bone grafts, compatibility factors are in favour. Autologous grafts are biocompatible once they belong to the individual but the amount possible to obtain is limited and cannot be used on big fractures/sites of resorption. Autogeneous grafts have the risk of an immune response that will lead to infection of the affected site, or worse, to another part of the body. [2]

Prosthetics have advantages and disadvantages, both depending on the material used. Metals are applied with frequency because they provide immediate mechanical support, however they are poor in biocompatibility and can induce bone fatigue. Ceramics are the most popular because they promote osteointegration due to calcium phosphate content and their bioactivity. Having low density, ceramics are brittle materials being inefficient on torsion or bending sites. Facing the actual facts, the new solution passes through the regeneration of bone appealing to Tissue Engineering (TE) techniques. Cell growth is a complicated process involving many factors such as: growth factors (GF), extracellular matrix components (ECM) and intercellular communications. Cells can be cultured *in vitro,* growing in a 2D mode, once transplanted to bone they must form a 3D structure and consequently their behaviour changes drastically. To surpass this problem biomaterial made platforms have been investigated all over the world, being scaffolds the most popular for bone because of the 3D architecture. [2, 3]

In terms of biomaterials, a market study showed that polymers are the most used now and the tendency will not change until 2017. That is completely logic once polymers are easier and cheaper to produce and manipulate, also having a wider range of applications. In 2010, polymeric materials had an estimated sale of 21.7 billion dollars, having an estimated profit of approximately 53 billion dollars by 2017 and a market share of 63%. [4]

In Tissue Engineering, polymers have been one of the most studied biomaterials, with special attention of biodegradable non toxic materials like lactides, glycolides and their copolymers. PLA in its D and L form has been one of the most used and studied polymers for biomedical devices, more

recently for Bone Tissue Engineering (BTE) where properties like piezoelectricity gave rise to a whole new series of studies.

1.2 Motivation

For this work, since its main objective is related with biopolymers, it is pertinent to talk about polymers for medical applications. In terms of medical care, polymers have been used in preventive medicine, clinical inspections and surgical treatments of diseases. Our body composing materials are all biodegradable, like the skeleton frame and tissue matrix because they gradually lose mass unless additional treatments are given when our heart stops beating. This fact attracted much attention to biodegradable medical polymers. Producing these biodegradable materials, in this case polymers, involves the consideration of many factors: structure, physical and chemical properties. The combination of properties should aim the material biocompatibility. The polymer degradation process is also important and should be studied before implantation because if the products of degradation are toxic for cells, an immune response will be triggered and consequently the organism will reject the material. The residues of degradation may include anti-oxidants, pigments, and fragments of polymerization initiator catalysts. Among the mostly used biodegradable polymers in medicine is Poly (L-lactic acid) (PLLA) for fracture fixation, ligament augmentation and sutures. [5, 6]

Although artificial organs have been an effective solution in short terms their biocompatibility is not satisfactory enough to prevent foreign-body reactions and to fully perform the objective aimed for patients. In these conditions, a new technology emerged, Tissue Engineering, based on self-healing of the human body, only by using cells, biomacromolecules (differentiation and growth factors) and biomaterials designed to direct the organization, growth and differentiation of the cells during tissue formation. [2, 3, 5]

In TE, biodegradable polymers are required for: substrate fabrication aiming cell proliferation and differentiation which results on tissue regeneration, and for sustained release of growth factors at the injury location. Currently, some of the polymers used as platforms are collagen, glycolide-lactide copolymers, lactides and crosslinked polysaccharides. [6]

In the ambit of TE, this work aims to exploit the electromechanical (namely piezoelectricity) of Poly (L-lactic acid) (PLLA) for bone tissue regeneration. PLLA is a U.S. FDA (Food and Drug Administration) approved important biocompatible, biodegradable, piezoelectric polymer. Its biodegradation rate and mechanical properties can be altered by changing the quantity and characteristics of crystalline phases through the processing conditions. [3, 7-9]

Bone is a connective tissue composed by a mineralized organic matrix with living cells incorporated in it. This tissue function is to protect organs, allow movement and grant mechanical support. Besides this, it acts as storage for essential minerals like calcium and phosphate, contributing for the regulation of their concentration in the extracellular fluid. Bone grows in size and shape through the collective activities of cells which produce, mineralize, and resorb bone

matrix. Osteoblasts produce bone matrix and facilitate mineralization while osteoclasts, specialized multinucleated cells, are responsible for the resorption process. These processes control is based on intricate interactions among individual's genetic potential, environment, and nutritional factors. The mechanisms behind bone mineralization are not yet entirely known. [2, 10, 11]

During the study of bone properties, early in the 40's, Yasuda, a Japanese orthopedic surgeon started to investigate the bone because by that time scientist thought that bone callus formation was not inextricably linked to bone fracture. Between 1939 and 1953, Yasuda made new experiments and demonstrated that the application of a direct electrical current (DC) with 1-100 μA produced callus in the medullary canal of rabbits, and the application of external mechanical forces also resulted in the production of electricity and consequently callus. This resulted in the discovery of piezoelectricity in bone later in 1962-1968. The study of both piezoelectric and dielectric properties of bone showed that these two characteristics depend on the frequency, direction of the applied load and relative humidity, among other parameters. [12]

According to previous studies, this phenomenon in bone is associated to the piezoelectric character of collagen fibers and their alignment in response to an applied electric field. The discovery of piezoelectricity in bone brought to light the idea of using materials with these characteristic as platforms for tissue growth, in this case bone growth. Although a large number of materials exhibit piezoelectric properties, only after 1970 the idea gained interest for the biomedical field. Some biomaterials have been tested for this purpose: ceramics, like barium titanate ($BaTi_2O_5$); polymers such as polyvinylidene fluoride (PVDF) and PLLA, and some composites. [13]

As it was referred before, PLLA is a U. S. FDA approved polymer with approved implantable and extracorporal applications in the market, for example sutures. [6].

In 2012 the polymer stability was experimented and the results showed that by stretching this polymer uniaxially it was possible to enhance bone growth and the proportion of grown bone tissue. These results were related to the influence of stretched ratio on the piezoelectric constant of PLLA. Some of the most recent studies on PLLA as a piezoelectric material in TE have been conducted by Barroca *et al*. [14, 15] at the University of Aveiro. Firstly, Barroca and coworkers tested the adsorption of adhesion-promotion proteins, namely Fibronectin, and the results clearly showed that the protein adhesion was considerably enhanced by electrically induced poling. Barroca also studied polarization on PLLA thin films, polarized by PFM. It was observed that the various crystalline forms of PLLA, α and α' have different mechanical properties. Mechanical properties influence cells behavior since the molecular pathways are triggered by the adhesion forces between the cells and the substrate, through transcellular structures. Topography and roughness, originated by the different crystalline forms also influence cells adhesion, for example, the cytoskeleton organization of primary human condrocytes that adopt a much more elongated shape when the PLLA spherulites were bigger. [15, 16]

The relationship between the electrical response and crystalline form of the polymer is not studied yet but it is assumed that different crystalline forms may have different polarization behaviors, namely, regarding the polarization stability. In her study Barroca demonstrated that,

when poled at room temperature, both PLLA crystalline structures presented a rapid loss of the polarization but it was α-PLLA that showed better results. It has a more ordered structure and consequently more stability, and, when polarized above T_g, the PLLA films showed a durable polarization of approximately 10 days. These results proved that PLLA is appropriate as a platform for the study of the interaction between poled substrates-proteins-cells and ultimately as a stimulated platform for tissue growth. [15]

1.3 Objectives

Within this context and in the continuation of the work already developed the main objective of this work is to study the electrical and physical-chemical characteristics of PLLA films with different degrees of crystallization. It is intended to use these films in new and different biological assays and metabolomics studies. The specific objectives of the work are:

- Fabrication of PLLA films by solvent casting (Standard films);
- Inducing different crystallization degrees by thermal treatment of standard films (Amorphous and Crystalline);
- Complete physical-chemical characterization of the different films;
- Electrical characterization of the prepared films:
  - Polarization of the films by Corona
  - Quantification of the polarization by Thermal Stimulated Depolarization Current (TSDC);
  - Dielectric characterization (relative permittivity and dielectric loss);
- Establishment of the relations between electric response of PLLA films and cell adhesion parameters.

Chapter 2

State of the Art

2. Chapter 2 - State of the Art

2.1 Bioelectricity

Everything started many centuries ago with the searching of water and ores by dowsing. Dowsing consists on the use of a Y-shaped wooden twig or L-shaped metal wire where the dowser walks with the rod in his hands over the investigated area. When they are near or in the exact site where water is, the Y-shaped twig (Figure 1, left) bends vertically and the L-shaped wires (Figure 1, right) moves horizontally. [17]

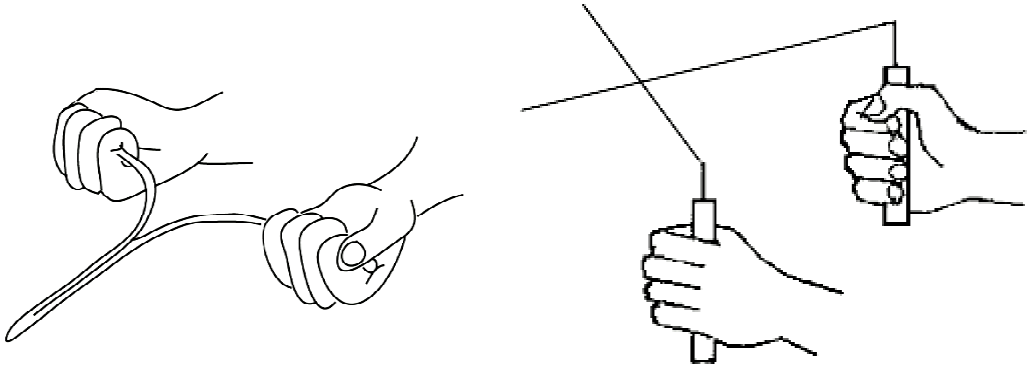

Figure 1 - Dowsing rods. Left: Y-shaped; Right: L-Shaped. [18, 19]

This knowledge on dowsing is very old, so old that the bible mentions that Moses used to search for water with a stick, and writings from the 16th century tell about dowsing on ore prospecting. In the 20th century, Yasuda discovered bone bioelectricity and later Fukada found that bone was piezoelectric. Piezoelectricity in bone explained why dowsing was an effective method. Since the bone is piezoelectric, it is sensitive to soil magnetic fields alterations which results in bone deformation and consequently involuntary muscular movements that lead to the inclination of the rod. [17]

During the study of bone properties, early in the 40's, Yasuda, a japanese orthopedic surgeon started to investigate the bone because by that time scientists thought that bone callus formation was not inextricably linked to bone fracture. To prove this, he applied thermal, chemical and mechanical stimulus to bone which resulted in the formation of callus, even without fracture. The mechanical forces were applied to long bones showing callus formation in nontraumatized areas under compression. By doing the experiment in viable and boiled bones he observed the presence of an electrical signal when subjected to the mechanical deformation and that compression areas showed a negative sign while tension areas showed a positive one. With this, Yasuda assumed that callus formation was related to the electrical activity. To prove these observations, between 1939 and 1953, he made new experiments and demonstrated that the application of a DC with 1-

100 µA produced callus in the medullary canal of rabbits, and the application of external mechanical forces also resulted in the production of electricity and consequently callus. This data led to the discovery of piezoelectricity in bone later between1962-1968. [20]

In 1957, Yasuda joined Fukada (also a japanese orthopedist) and measured the numerical value of the piezoelectric constant of a dry bone by applying a shearing force along the bone axis, causing voltage to appear on the bone surface parallel to the axis. The reverse phenomenon was also experimented and confirmed. In the end, they concluded that the piezoelectric effect in bone was about one tenth of that exhibited by quartz crystals and quantified as 0.2 pC/N. [20]

Other scientists worked on these experiments trying to find out what was behind the bone remodeling and repairing mechanisms. Basset and Becker [21-26] reasoned that if stress-generated electricity could directly affect bone cells promoting bone growth, then externally applied current ought to affect bone growth in a polarity-dependent fashion. The assumptions were that the negative electrode would promote bone growth and the positive one bone resorption. This knowledge was tested in dogs in 1964, where a DC current of 3 µA originated more bone growth in the cathode area than in the anode area. The authors interpreted that the failure in observing bone formation in the anode was probably due to the non-physiological nature of the electric signal (continuous application during 21 days instead of intermittent electrical signal that would be associated to an adaptive osteogenic response). [20]

Other scientists tried experiments with DC current but all of them were ambiguous because the dose applied was difficult to control in this method. Later, Friedenberg *et al.* [27-29] overcame this difficulty by employing a current-controlled implantable circuitry, establishing electrical osteogenesis as a real phenomenon. Friedenberg tested 6 current intensities, 1, 5, 10, 20, 50 and 100 µA, for 10 days. He concluded that 5-20 µA was the optimum intensity for bone formation at the cathode and that bone destruction occurred at the anode with 1 µA or less. In the 70´s, the experiments done proved that DC current enhanced callus formation, causing the acceleration of the healing phenomenon. Richez *et al.*, [30] in 1972 did not observe a polarity-dependent effect by using platinum electrodes, and later other reports came up concluding the same. In 1981, Brighton *et al*. [31], presented evidence that pulsed DC current was less effective than DC current in an experiment with rabbits. [20]

One of the most important, but unanswered questions in bone bioelectricity is: which kind of potential should be identified as a feedback signal for adaptive remodeling, admitting that the body works as a circuitry in loop? The possibilities assumed were piezoelectricity, originated by the application of shearing forces along the bone axis, and streaming potentials, also derived from mechanical forces that cause electrical signals due to the motion of ions carrying extracellular fluid in the bone matrix. [20, 32, 33]

The human body is seen as a set of electric batteries expending a significant proportion of its energy generating electricity. Every cell in the organism maintains a voltage across its external organelles membrane due to the active ion transport (Sodium, Na, and Potassium, K) against their concentration gradients. This transport process establishes a charge separation that constitutes a

potential difference or voltage of the order of the millivolts (mV) in magnitude. If there is a conducting pathway, the movement of ions within the tissues produces an electric current in the microampere range (mA). [34]

Bioelectricity influences cell behavior, even in non-excitable cells (cells unable to generate an action potential) there are voltage-gate channels controlling the passage of Na and K ions. At a tissue level, endogenous fields (EF), the electrical fields generated by the organism, are intrinsic to a number of metabolic processes, including development, adaptation and tissue repairing. When connective tissues, such as bone and tendon, are stressed, adaptive modifications occur in the extracellular matrix, which in case of damage, will set up currents that appear to drive elements of the healing response. The current diminishes with healing progress, until normal values are established and healing is complete. [34]

Since bioelectricity is intrinsic to the human body and is involved in healing processes it is pertinent to study this phenomenon, especially regarding bone repair. In bone repair, as it was demonstrated above, electricity is directly associated to the healing process, being responsible for important phenomena like cell migration. It is also scientifically important to establish the relations between bioelectricity in the bone and the piezoelectric nature of the bone.[34]

2.1.1 Bioelectricity in the human bone

In order to understand the influence of electricity in bone formation and how tissue engineering acts in this field, it is necessary to review some concepts about the bone and its remodeling processes.

There are 206 bones in the human skeleton presented in varied sizes and shapes. Bones five main functions are:

- Support – To provide a hard framework that supports the body;
- Protection – To cradle the soft organs;
- Movement – Skeletal muscles are attached to the bones by tendons using them as levers to move the body and its parts. The arrangement of bones and joint design dictates the type of movement possible to execute;
- Mineral storage – Serves as a reservoir for minerals like Calcium (Ca) and Phosphorus (P). These minerals are released in the bloodstream as ions for distribution to all parts of the body;
- Blood cells formation – The bone marrow of certain bones houses the process of haematopoiesis. [35]

At the naked eye, bones are divided in 2 parts: compact bone (calcified outer layer) and cancellous bone (vascularized inner layer). [35]

At microscopic level, bone is composed by the bone matrix and cells. The bone matrix is produced by the bone cells and it is 35% organic and 65% inorganic, being responsible for the

maintenance of all functional characteristics. The organic part is composed by bone cells and the osteoid (proteoglycans, glycoproteins and collagen), and the mineral part by hydroxyapatite (HAp), composed by calcium phosphate crystals (CaP). Collagen confers mechanical resistance and flexibility to the matrix while the mineral components act as cement, giving the matrix the resistance to compression tensions. [36]

In cellular terms, there are 3 types of bone cells: osteoblasts, osteocytes and osteoclasts (Figure 2). Osteoblasts are responsible for the formation of bone (osteogenesis) by producing collagen and proteoglycans which are then stored in their Golgi vesicles. They also form vesicles that accumulate calcium and phosphate ions and some enzymes. These ions are released to form HAp crystals, originating the mineralized bone matrix. [35, 36]

Osteocytes are mature osteoblasts, almost inactive, that are already surrounded by bone matrix. Their function is to keep the production of matrix components in order to maintain it. These spider-shaped cells occupy cavities (lacunae), at the junctions of lamellae. The lacunae are connected to each other and to the central canal by canaliculi (hair-like canals). Once the matrix hardens it becomes impermeable for nutrients, so this connection form allows a faster and more efficient exchange of nutrients and release of wastes. [35]

Osteoclasts, also known as “bone breakers”, are multinucleated cells that arise from the same hematopoietic stem cells that differentiate into macrophages and are in charge of the resorption process (destruction of old bone). When osteoclasts contact with the matrix they attach to it via numerous membrane projections, creating a border. Once attached to the respective receptors, they release hydrogen ions to create an acid medium that will cause bone resorption. [35, 36]

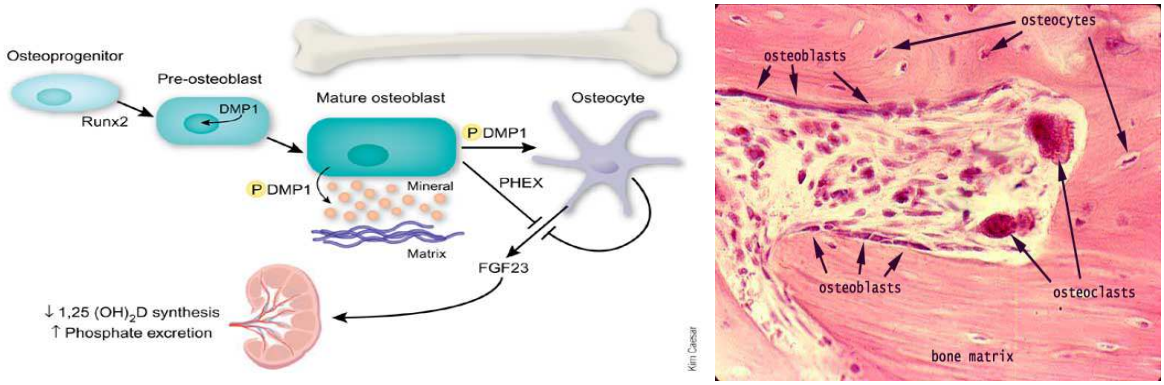

Figure 2 – Bone cells formation and differentiation. [37, 38]

As mentioned before, bone is divided in two types: cancellous and compact (Figure 3). Compact bone, despite its dense appearance, is riddled with passageways that serve as conduits for nerves, blood and lymphatic vessels. Its structural unit is the osteon also called Haversian system. Osteons are seen as pillars, not only because of their elongated cylindrical shape (parallel to the long axis of the bone) but also for their weight-bearing function. It is composed by matrix tubes, named lamellae, made of collagen fibers aligned in the same direction. The fibers in the

adjacent lamellae run in the opposite direction, forming a pattern that allows the resistance to torsion stresses. The same happens with the HAp crystals. [35, 36]

Cancellous bone, in contrast to compact bone, consists of trabeculae, a honeycomb of small needle-like or flat pieces 50-400 µm thick. Despite the poor organization, the tiny bone struts are carefully positioned and align precisely along lines of stress, helping the bone to resist that stress. It is a porous structure where the empty spaces are filled with bone marrow and blood vessels and the trabeculae, a few cell layers thick, contains arranged lamellae and osteocytes interconnected by canaliculi. The canaliculi permit the passage of nutrients that diffuse from the capillaries in the endosteum surrounding the trabeculae. [35, 36]

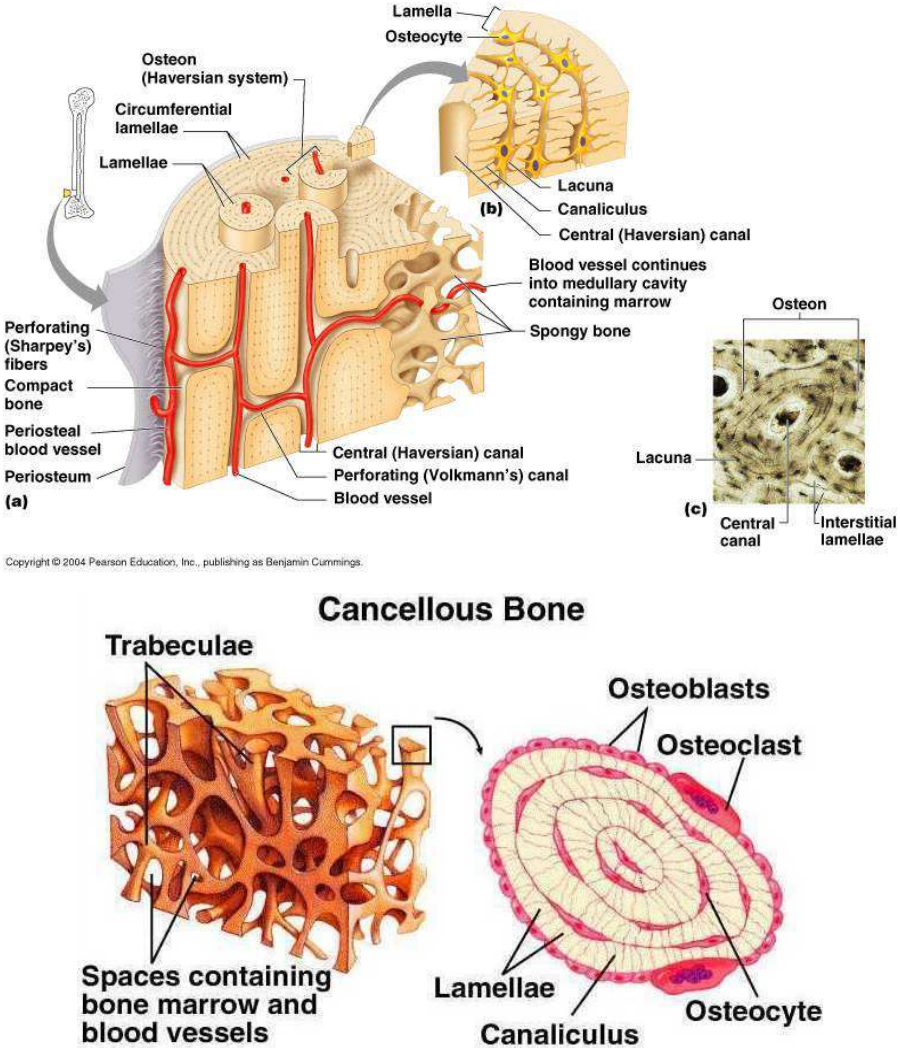

Figure 3 – Bone structure. Up: Compact bone; Down: Trabecular bone. [39]

The process of bone tissue formation is called osteogenesis or ossification (Figure 4) and is affected by nutrition and hormones. [35, 36]

In embryos osteogenesis starts after the 8th week with bony skeleton formation where fibrous and cartilage structures are replaced by bone tissue. For the skull and clavicles, which are flat bones, the process is called Intramembranous Ossification, which uses the fibrous connective tissue membranes derived from mesenchymal cells. The rest of bones are formed by Endochondral Ossification, which starts at the 2nd month and uses hyaline cartilage bones as a model for bone construction. [35]

During infancy and youth, all bones grow in thickness by appositional growth and long bones lengthen by interstitial growth of the cartilage followed by appositional growth. [35]

Interstitial growth is similar to the Endochondral Ossification process. It starts with a fast division of the cartilage cells at the top of the bone (epiphyseal side) that will bring distance between the epiphysis and the diaphysis (middle section of the long bone) causing the entire long bone to lengthen. Meanwhile, the older condrocytes positioned close to the transformation zone, hypertrophy causing the calcification of the surrounding cartilage matrix. This calcified zone is invaded by marrow elements, namely osteoclasts that erode it then, osteoblasts cover the area with bone matrix forming the spongy bone. [35]

In Appositional growth, osteoblasts beneath the periosteum secrete bone matrix on the external bone surface as osteoclasts on the endosteal surface of the diaphysis remove bone. The breaking down is less than the forming, allowing equilibrium in bone thickness and weight. [35]

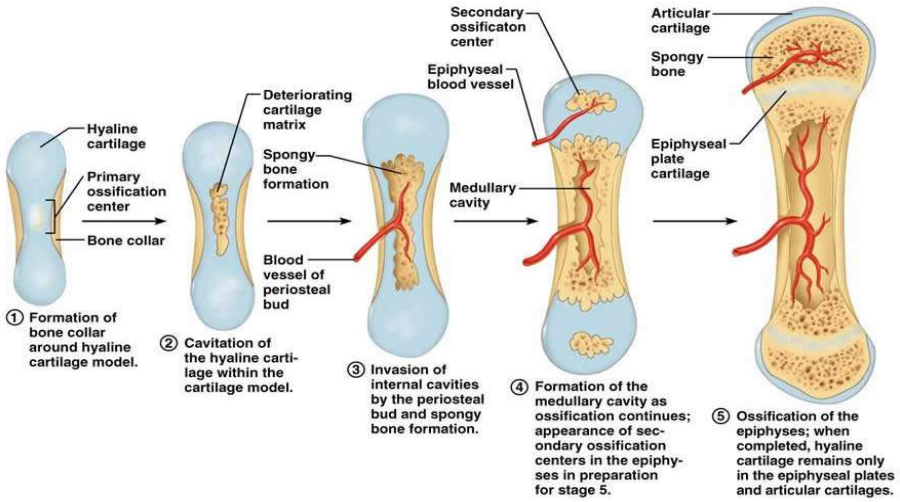

Figure 4 – Bone growth process. [40]

Bone remodelling

Bones appear to be “death” organs, but in fact, changes in their architecture happen every week and 5 to 7% of the bone mass is recycled. Spongy bone is replaced every 3 to 4 years and compact bone, approximately, every 10 years. [35]

Bone remodeling in the adult, skeleton bone consists of 2 processes: removal of mature bone tissue by osteoclasts and deposition of new bone by osteoblasts. Bone deposition is done at the

periosteal and endosteal surfaces (Figure 5). The rates of these processes are equal, once the bone mass remains constant, but are not uniform because some bones are more remodeled than others. The thickness is maintained because, while osteoclasts remove inner tissue, osteoblasts add new tissue on the exterior. [35, 36]

The process of remodeling is involved in:

- bone growth;
- bone modification and configuration;
- bone adaptation to mechanical stresses;
- bone repairing;
- Calcium ions regulation in the organism. [36]

The formation of new osteons in compact bone is also part of the remodeling process and can happen in two ways where both leave behind portions of old bone, also called interstitial lamellae. [36]

In the first phase, osteoclasts penetrate in the central canal of pre-existing osteons through blood vessels and start removing the old bone, producing a tunnel along the bone. New concentric lamellae are formed around the blood vessel until the new osteons fill the area occupied by the old ones.[36]

In the second phase, some osteoclasts from the periosteum remove bone causing the formation of a drip along the bone surface. Periosteum capillaries settle in those drips and are involved in a tunnel form while osteoblasts fabricate new bone. New lamellae are added to the interior of the central canal originating a new osteon. [36]

The control of bone remodeling is done by two control loops: a negative feedback hormonal mechanism that maintains Ca^{2+} homeostasis in blood, and the response mechanism to mechanical and gravitational forces acting on the skeleton. [35]

The hormonal mechanism consists on release of the parathyroid hormone (PTH) in the bloodstream when the levels of calcium are low. These hormones stimulate the osteoclasts that start to resorb the bone, releasing calcium to the blood. When the levels rise, the hormone calcitonin is released inhibiting bone resorption and encouraging salt deposit in the bone matrix, reducing calcium levels.[35]

The response to mechanical stress mechanism works by Wolff's law which is based on three concepts from the 19th century: *"Bone is deposited and resorbed to achieve an optimum balance between strength and weight, trabeculae in cancellous bone tend to line up with the directions of principal stresses that they experience, and both phenomena occur through self-regulating mechanisms that respond to mechanical forces acting upon bone tissues."* [41]. Studies were done showing that under deformation bone produces an electrical current. Compressed and stretched regions are oppositely charged, suggesting that the electrical signs direct the remodeling process. [35]

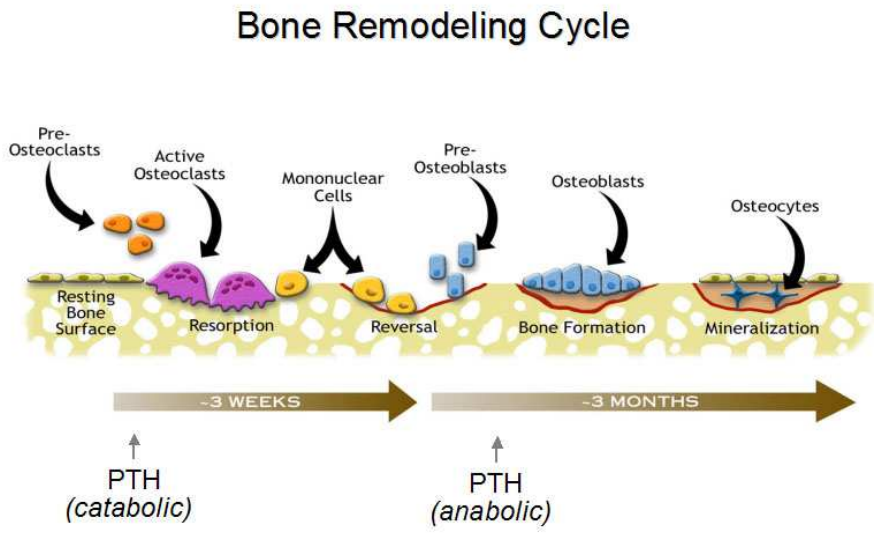

Figure 5 – Bone remodelling process. [42]

Bone repairing

The mechanism of bone repairing is applied when bone fractures. It involves 4 main phases:

I. Hematoma formation – a result of an hemorrhage caused by the breaking of blood vessels. This leads to the lack of nutrients to the bone cells causing their death and, consequently, an inflammation;

II. Fibrocartilaginous callus formation – capillaries grow into the hematoma and phagocyte cells invade the area beginning to clean the debris. Meanwhile, fibroblasts and osteoblasts migrate to the site, starting the process of bone reconstruction;

III. Bony callus formation – due to osteoblasts action, the new trabeculae appear in the fibrocartilaginous callus and gradually convert it into bony callus of spongy bone. This process takes place 3 or 4 weeks after the fracture and lasts until 2 or 3 months after it, when a firm union is formed;

IV. Bone remodeling – it starts along with the bony callus formation and continues several months after it ends. During this process, the excess of material in the bone shaft is removed and compact bone is laid down to reconstruct the shaft walls. [35, 36]

A number of experimental approaches through new materials, therapies or combinations have been explored to induce bone remodeling and repairing pursuing the ultimate goal of bone regeneration. As it was suggested by Fukada, bone remodeling and repairing are directly related to the bioelectricity present in the human body, in particular to the piezoelectric phenomenon. Knowing this, new studies exploring this property started and results are already published. [12, 14, 15, 43]

2.1.2 Piezoelectricity in bone

Piezoelectric Phenomenon

The piezoelectric effect was first discovered in 1880 by the Curie brothers, Jacques and Pierre. The scientists decided to combine their knowledge on pyroelectricity and crystal structures to test various crystals like tourmaline and quartz (SiO_2) and evaluate the effect of mechanical stress on electricity production. One year later, Gabriel Lippman studied the theory and found out that an inverse effect was also possible. [44]

Piezoelectricity is a reversible phenomenon that is defined by the amount of electricity created when certain materials are subjected to compression or tension. On crystals it relies on the absence of a symmetry center in the crystal unit cell (Figure 6). For polymers, it consists on dipole alignment according to the direction of the electric field or tension applied. [44, 45]

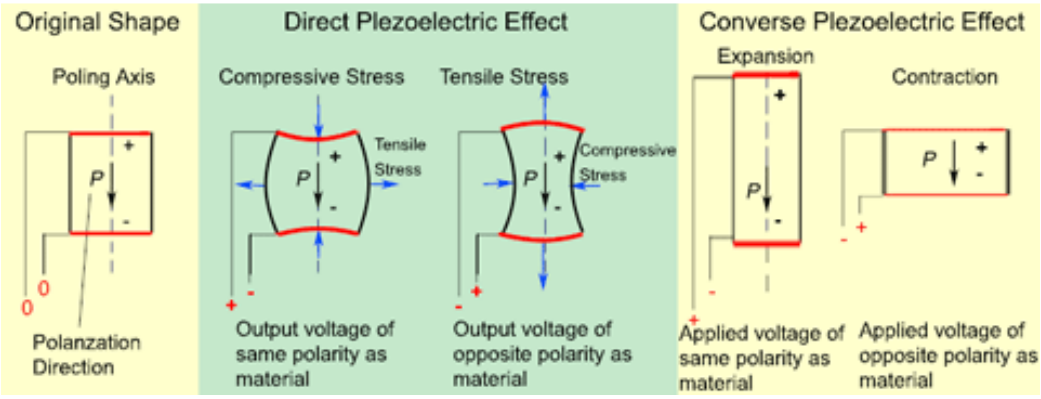

Figure 6 – Direct and Converse Piezoelectric effect. [46]

Some piezoelectric materials are also ferroelectric. Ferroelectric materials have a spontaneous polarization which is reversible upon the application of an electric field. This spontaneous polarization is similar to the one that happens in ferromagnetic materials. A material can also be paraelectric which means it does not need a permanent dipole to become polarized under an electric field, and once the field is removed, polarization returns to 0. Finally, dielectric materials can be classified as electrets if they have a net charge or quasi-permanent time polarization. [45, 47, 48]

When the material is poled, negative and positive charges are separated. At a temperature slightly below the Curie temperature (T_C, temperature at which a materials permanent magnetism changes to induced magnetism), the dipoles align with that same field and the polarization also increases until the full alignment is completed. Once aligned, even if the field keeps rising, the polarization will remain the same, which means, the material reached the saturation polarization (P_s). When the field is reduced to zero, the dipoles become less strongly aligned but do not lose the orientation because they are bound to certain preferred directions with the individual region,

remaining in the direction most close to the initial electric field. Since there is still a high degree of alignment, the polarization remains although in a lower value, also known as remnant polarization (P_r). [44, 49]

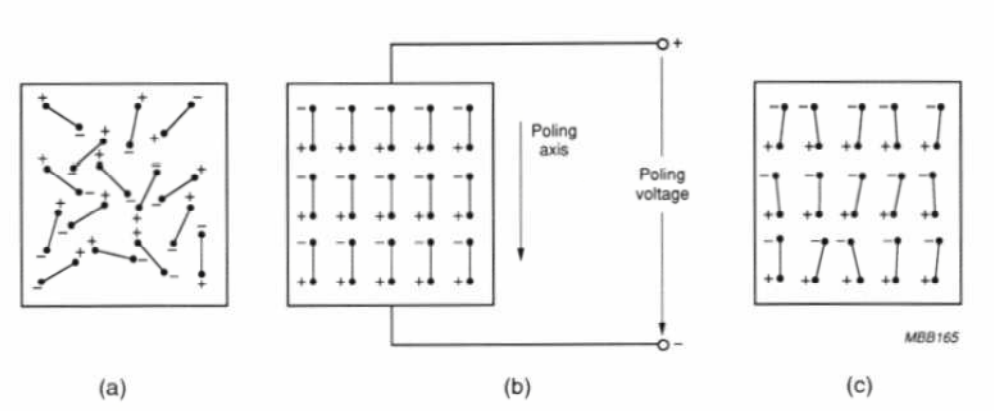

Figure 7 - Electric dipole moments. a) before polarization; b) during polarization; c) after polarization.[50]

As mentioned before, piezoelectricity is the capacity of a material, to create an electrical field when submitted to a mechanical deformation, or the inverse. The relationship between the mechanical strain produced by an applied electrical field is given by the piezoelectric constants, in this case, strain constants or "d" coefficient value, which can be calculated by equation 1 or the inverse by equation 2. The units are meter per volt (m/V) for equation 1 and Coulomb per Newton (C/N) for equation 2. [44, 50]

$$d = \frac{strain\ development}{applied\ electrical\ field}\ (\frac{m}{V}) \quad (1)$$

$$d = \frac{short\ circuit\ charge\ density\ (C)}{applied\ mechanical\ stress\ (N)} \quad (2)$$

These physical constants are tensor quantities and relate the direction of the applied stress or electric field to their perpendicular axis. The constants have two subscript indices referring to the direction of each axis of the related quantities (Figure 8). [50]

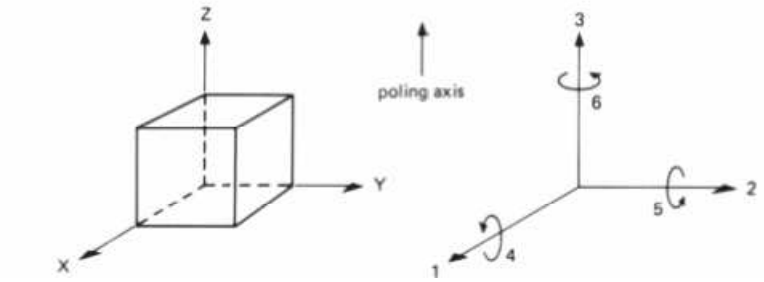

Figure 8 - Designation of the axes and the directions of deformation. [50]

Piezoelectric constants can be represented by a matrix (Figure 9) where the first subscript refers to the direction of the polarization at E=0 and the second to the direction of the applied stress. Two special constants are:

- d_{33} which refers to a force in the 3 directions (along the polarization axis) impressed on the same surface on which the charge is collected;
- d_{31} for when the charge is collected on the same surface as before, but the force is applied at right angles to the polarization axis. [50]

$$\begin{pmatrix} d_{11} & d_{12} & d_{13} & d_{14} & d_{15} & d_{16} \\ d_{21} & d_{22} & d_{23} & d_{24} & d_{25} & d_{26} \\ d_{31} & d_{32} & d_{33} & d_{34} & d_{35} & d_{36} \end{pmatrix}$$

Figure 9 - Piezoelectric constants matrix. [12]

When evaluating the converse piezoelectric effect, the constant measured is g, the voltage constant, which is related to the electrical field produced by the mechanical stress applied to the material. It is expressed in volts per meter per Newton (Vm/N) and calculated by Equation 3. [44, 50]

$$g = \frac{Open\ circuit\ field}{Applied\ mechanical\ stress}\left(\frac{Vm}{N}\right) \quad (3)$$

The piezoelectric effect is exhibited by a number of naturally-occuring crystals like quartz or tourmaline. This effect can also be noted in other groups of materials:

- Ceramics - Lead Zirconate Titanate (PZT), Barium Titanate ($BaTiO_3$), Apatite (Ap);
- Polymers - Polyvinylidene Fluoride (PVDF), Poly(L-Lactic acid) (PLLA)) and Collagen. [13, 51]

The first application of piezoelectric materials was done during the World War I as electrical transducers. Nowadays these materials are used in the quotidian as sensors, health monitoring systems, wireless devices, and more recently in Tissue Engineering as substrates for tissue growth. [13, 52]

Piezoelectricity in bone is a known phenomenon, but where does it come from? Experiments with human and ox femurs demonstrated that stress-generated potentials had their origin in the shear forces applied in collagen and on the deformation of fluid-filled channels (Haversian and Volkmann). While hydroxyapatite (HA) is vital for bone strength it is not fundamental for the generation of stress potentials because in its absence these potentials were still produced inducing that collagen is the basis for this process. [53]

Yasuda and Fukada determined the piezoelectric constants for human bone with the symmetry axis Z inclined about 10º to the side from the bone axis, knowing that the magnitude of the constant depends on the angle between the applied pressure and the axis of bone. The resulting values and the matrix can be seen in Table 1 and Figure 10, respectively. [12]

Table 1 - Piezoelectric constant of human bone measured by static and dynamic methods. (c.g.s. e.s.u – CGS system and Gaussian Sub-system). [12]

Direct Effect		**Converse Effect**
Static	Dynamic	Dynamic
2.0×10^{-9}	2.9×10^{-9}	2.9×10^{-9}
2.2×10^{-9}	3.6×10^{-9}	3.5×10^{-9}

$$\begin{pmatrix} 0 & 0 & 0 & d_{14} & 0 & 0 \\ 0 & 0 & 0 & 0 & -d_{14} & 0 \\ 0 & 0 & 0 & 0 & 0 & 0 \end{pmatrix}$$

Figure 10 – Piezoelectric constant matrix for human bone. [12]

One of the main factors affecting piezoelectricity in bone is its hydration. Water distribution through pores and extracellular space decreases over time with progressive mineralization, and its presence decreases the piezoelectric coefficients due to the absorption of free water. Another factor is the state of the biological tissue. It is known that 10-15% of bone is remodeling at any instant and over time, depending on age, gender, anatomical location, nutritional factors and hydration. If the chemical composition varies the electrical properties of bone are affected. [53]

At the cellular level, the conversion of the received mechanical or electrical stimulus into an action potential is initiated by upregulation and downregulation of important signaling molecules, which facilitates the propagation of highly specialized signals by chemical and electrical cues. Electrical fields, generated from both mechanical stimuli and external electrical devices, exert forces on ions through the cellular membrane and interstitial fluid creating a flux. The influx and efflux of ions passes faster through the membrane due to alterations in the double layer, suggesting that the membrane is the primary site of electromagnetic field interactions. The action of electrical fields alters the membrane configurations and consequently the cell homeostasis changes. Tests with osteoblasts were done to prove this with positive results. [53]

According to the model proposed by Adey *et al.* [54], electrical stimulations seem to be affected at the cellular level by a number of events where calcium has a relevant role, being them humoral stimulation, Signal Transmission and Intracellular response. [54]

On Figure 11 is described how calcium levels affect directly the concentration of parathyroid hormone (PTH) and consequently the bone resorption mechanism. When PTH is released, it acts under the influence of the enzyme cyclase which regulates the cyclic adenosine monophosphate (cAMP) second messenger and prevents bone formation. However, when the pressure increases or electrical stimulation is inducted, cAMP is inhibited and the calcium uptake increases. [53]

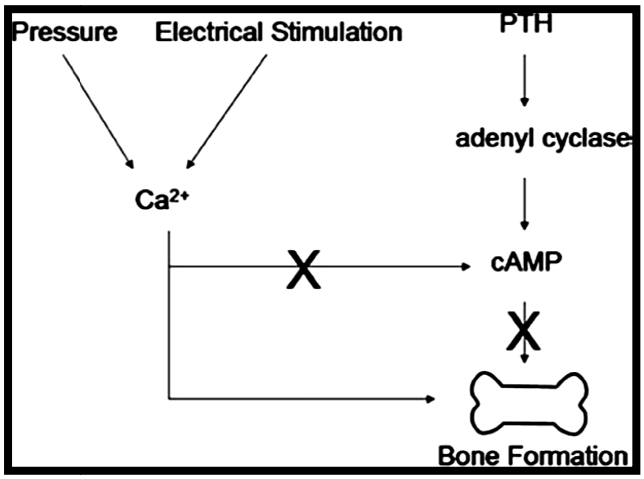

Figure 11 - Influence of calcium levels in bone formation, being PTH the parathyroid hormone and cAMP enzyme cyclic AMP. [53]

Cellular migration and orientation is also impacted by ion fluctuations through the membrane (Figure 12). This has been used in therapies based on induced osteogenesis. By implanting electrodes in the human body it was possible to observe that the passive influx of Ca^{2+} on the anodal side increased the local intracellular concentration of this ion, whereas passive efflux and/or intracellular redistribution decreased the concentration on the cathodal side. These changes in concentration give rise to push-pull effects and lead to cell migration toward cathodes. Osteoblasts, as well as other cells with a negative membrane potential, when exposed to DC, move. This movement is also termed galvanotaxis and is described by the attraction of Ca^{2+} to the hyperpolarized side of the membrane, where the anode is, while the cell contraction is driven towards the opposite side, the cathode side. [53]

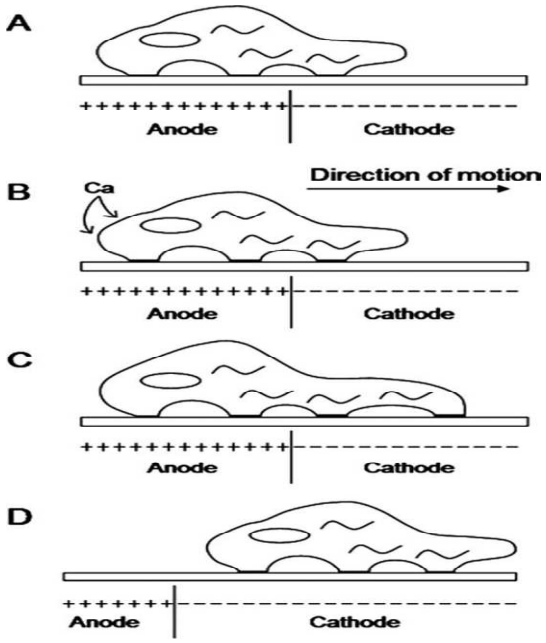

Figure 12 - Cell migration mechanism through electrical stimulation. [53]

The studies regarding bone growth started many years ago. Nowadays, following the new paradigm of Regenerative Medicine this type of investigation has been inserted in the emerging area of Tissue Engineering, where direct tissue regeneration is explored either *in situ* or *ex situ.* TE is now well developed, and has many interested experts. Despite the “novelty factor”, this field already counts with many published works, including *in vivo* studies involving humans. This new area contributes to a totally new way of approaching the healing process in all type of tissues. [55]

.

2.3 Healing Assisted Strategies

2.3.1 Bone Tissue Engineering

The activities of TE have expanded from repairing and replacement of bone, vascular organs such as the heart and kidneys, to the nervous system itself. The first objective is now to create environments and structures that allow the proliferation of a cell type, such as three-dimensional matrices, also known as scaffolds. Scaffolds consist of porous 3D platforms with the ability to support cell growth, differentiation and organization. Scaffolds are largely used for bone because they mimic its architecture, and by being porous, allow the vascularization and cell migration through it. [55]

Bone Tissue Engineering (BTE) can be undertaken through many approaches, either by tissue transplantation or by extracorporal strategies. Extracorporal strategies rely on the biological interaction of bone cells with the extracellular structure, assisted or not by growth factors. Cells

should be seeded on temporary structures or scaffolds produced from materials of controllable degradability. The ideal scaffold must allow cell attachment, promote vascularization and withstand soft tissue forces. The degradability is very important because the material must decompose without leaving any toxic residues for the organism. Different materials can be used to create the perfect platform for bone regeneration. The material is chosen according to the site and type of the defect and host health state. [55, 56]

Bioceramics are composed by calcium and phosphate, a composition similar do the bone, which gives them an outstanding osteocompatibility, and their degradation leaves no toxic products. Despite the advantages, ceramics are brittle materials and are not exempt of triggering an immune response. Composites, being a combination of different materials, gather the desired properties from each one making them suitable for almost any kind of device. However, biocompatibility is not guaranteed and a negative response by the host is also a possibility. Natural derived matrices have their origin in primary components of the bone matrix which favors the affinity with growth and osteoconductive factors. Being apparently the best hypothesis, natural materials can also trigger an inflammatory response once they are very difficult to sterilize. Finally, synthetic materials like polymers are easy to produce and sterilize, allowing different designs and consequent application on innovative devices like drug release capsules. The biggest problem is their degradation products that can be toxic. [55, 56]

The structures can have different macro and microstructures depending on the application. For bone regeneration, the most common ones are 2D structures like films (thick or thin) and 3D ones, the scaffolds. Generally these structures are made of polymers, calcium phosphate ceramics or the combination of both. Polymers have been the centre of attention regarding the medical sciences investigators due to their versatility. A lot of polymers have been considered smart materials due to their special properties that can go from flexibility to electrical conduction/isolation capacity. [3, 57]

Regarding the bioelectricity aspect, electrical properties became more and more appealing to research and development, giving rise to new therapies, initially based on electrodes alone and later helped by a smart material substrate, both having an *in situ* and *ex situ* application.

2.3.2 Electric Stimulation Therapies

Therapies using electric and electromagnetic fields have been used in orthopedics and focus in the promotion of bone healing in the presence of fractures, more specifically, nonunions. The three modalities most commonly used are Inductive Coupling, Capacitive Coupling and Direct Current. Inductive and Capacitive coupling are non invasive techniques based on the external application of an electrical field using electrodes or wires. Direct current is an invasive technique where wires are implanted in the fracture site, subcutaneously. [58, 59]

Therapies based on surface properties of materials

The application of biomaterials for bone regeneration has been largely used and the capacity of these materials to bind to a tissue relies mostly on their surface properties. The surface properties of a biomaterial important for cell adhesion are: hydrophobicity/hydrophilicity, charge, roughness, and chemical composition. [60]

Focusing on electrical influence in bone tissue regeneration, charge represents the factor in study. According to many studies, the amount of surface charges has a strong influence on cell behavior, namely charges density. When density increases cell adhesion and proliferation also increase. Many researchers reported the improvement of biocompatibility by using positive and negative ions, for example, Schneider *et al.* [61] who used HEMA (2-hydroxyethyl methacrylate) hydrogels incorporated with charges and observed a more significant cell attachment and spreading of osteoblasts and fibroblasts related to the positive charges comparing to the negative and neutral ones. The results are demonstrated on Figure 13. Makohliso *et al.* [62] performed a similar experiment on neuronal cells and the results were similar: positively charged coating materials such as polylysine improved neuronal attachment *in vitro*. Other researchers reported similar results with different materials and cells. [60]

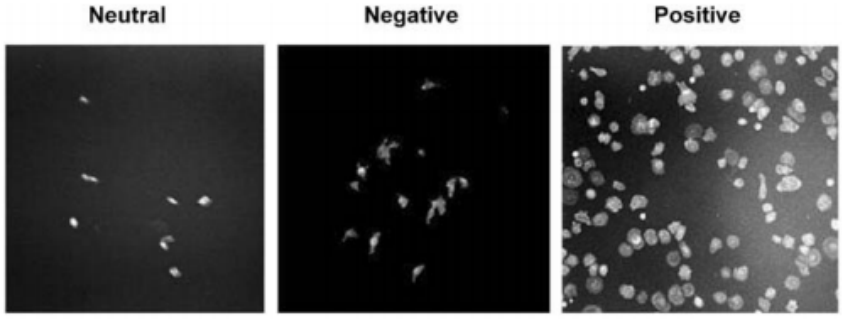

Figure 13 – Influence of charges at HEMA hydrogel surface on osteoblasts. A more significant cell attachment and spreading of osteoblasts to the positive charges comparing to the negative and neutral ones can be observed. [61]

Cells behavior can also be modified by surface charges, namely through the chemical functionalities of polymers. Lee *et al.* [63] prepared polyethylene (PE) surfaces with differently chargeable functional groups (-COOH, $-CH_2OH$, $-CONH_2$ groups) by Corona discharge treatment, graft copolymerization and substitution reaction to evaluate Chinese hamster ovary cell behavior. The best spreading rates were recorded on polar and positively charged surfaces. Another possibility is that surface charge may modulate protein adsorption to direct integrin binding and specificity, thereby controlling cell adhesion. [60]

Although the molecular mechanisms and cellular activity charge dependence still remain poorly understood, these latest findings confirm that surface charges plays an important role on the application of cell biology and TE. Based on the previous concepts and presented studies on the

electric properties of bone, it makes sense to investigate and test materials with electrically charged surfaces, able to create electric fields to accelerate bone remodeling/repairing. [60]

Materials displayed surface reactivity at the interface with the host bone tissue, playing a key role in regeneration. These materials are named bioactive because its connection with the host tissue is attributed to the formation of a CaP interfacial layer due to their structure and composition, which mimics the inorganic part of the bone. The bone-bonding mechanism of bioactive ceramics seems to be based on the electrostatic chemical bond between the negatively charged oxygen at the material surface and the amine groups of the amino acids in the surrounding proteins. The influence of surface charge has been studied in many types of materials, since bioglass and hydroxyapatite, well known bioceramics, to biocompatible polymers like collagen and PLLA. A few studies on the matter are presented below. [3]

Bioglass (BG)

Several authors emphasized the importance of the formation of an apatite layer at the material surface to promote bioactivity. Li *et al*. [64] suggested that a material to be a successfull candidate in this matter should at least have or be able to develop a negatively charged surface with abundant OH^- groups. According to the previous studies, surface charges generated by electrical polarization regulate the migration of ions, proteins and cells due to their surfaces polarity. The attractive effect of the surface charges on polarized HAp has been confirmed by the overgrowth of the CaP layer in Simulated Body Fluid (SBF), proliferation of certain cells in cultivation systems and osteoconductivity in the body. The deposition of CaP layer is higher in the negatively charged surface of HAp. [65, 66]

The process of HAp electrical polarization, results of protons migration. BG has a high ionic conductivity due to sodium ions so an electrical polarization is expected for this case too. Despite the fact that BG electrical properties haven't been deeply studied, Obata *et al.* [66] confirmed by thermally stimulated depolarization current (TSDC) that BG 45S5 was able to store large electrical charges in comparison with HAp, registering values of stored electrical charges between 80 and 190 $mCcm^{-2}$. Moreover, bioglass was assumed to have an electrical polarizability due to sodium ion transport. This was confirmed *in vivo* by the observation of calcium phosphate growth on the surface of polarized BG merged in SBF. In this study BG was polarized with different electrical fields using the system presented in Figure 14. [66]

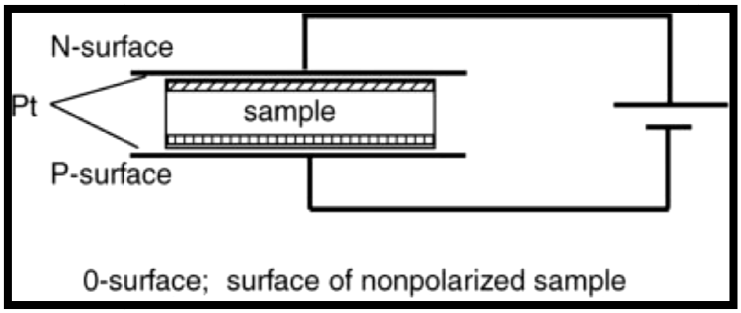

Figure 14 - Electrically polarization treatment. The negatively and positively charged surfaces are designated “N-surface” and “P-surface,” respectively. The nonpolarized surface is the “0-surface”. [66]

Hydroxyapatite (HAp)

The investigation of surface charges effects on osteogenesis has been a subject of interest during the past few years. It started with Hench *et al.* [67] who proposed that bone-bonding mechanism of bioactive ceramics was via electrostatic chemical bond between the negatively charged oxygen of the material surfaces and the amine groups of the amino acids. Others came after searching for answers, like Davies *et al.* [68] who proposed that cells modulation was determined by adsorbed proteins affected by the substrate charges. In his study, Davies used polymer beads to demonstrate, *in vitro*, that osteoblastic cells changed their morphology and process of colonization by surface charge influence. [69]

In Nakamura *et al.* study, negatively and positively charged surfaces of electrically polarized HAp ceramics were investigated. Nakamura implanted these materials in wide defects of canine femurs, and compared the results with uncharged surfaces. The HAp ceramic samples were polarized electrically in a DC field and the confirmation of the polarization charges at the samples were made by TSC (Thermal Stimulated Current) from room temperature to 500 ºC in air atmosphere at a heating rate of 5 ºC/min. The maximum value for stored electrical charge was 10.5 μCcm^{-2} for samples poled at 300 ºC. Almost complete bone regeneration was accomplished after 28 days being registered an high osteoblastic activity. This extensive osteoconduction process was attributed to the cooperative reaction of the surface bioactivity of HAp as well as to the large surface charge induced by electrical polarization. [69]

Collagen

Natural polymers are very similar, often identical, to macromolecular substances which are recognized by the organism. This characteristic eliminates problems like toxicity, stimulation of chronic inflammatory reaction and lack of recognition by cells. Other convenient aspect is that thanks to its similarity to natural molecules it is easier to design biomaterials that function biologically at the molecular level, rather than the macroscopic. [3]

Collagen is a piezoelectric polymer highly studied, being recently used for many biomedical purposes. It is one of the major components of bones, as it was seen, but many of its properties are not completely understood, namely the dielectric ones. In order to study the dielectric

properties of collagen, many measurements were made in different states: dry fibers, hide powder and in solution of suitable salt, using dielectric spectroscopy. Irastorza *et al*. [70] studied the dielectric behavior of hydrated collagen powder by Time Domain Reflectometry (TDR). The process consisted on changing the water content in samples which resulted in a polarization process with relaxation frequency in the region of 0.3-0.4 GHz. From the observed variation of the relaxation frequency when hydration is changed, Irastorza and coworkers concluded that the origin of polarization could be due to the charge distribution of the lateral chains of collagen molecules, in other words, a polarization mechanism sensitive to changes in the medium rigidity i.e. changes in the medium manifest into the mobility of the collagen lateral chains which in turn produce variations in polarization. [70]

Hence it would be interesting to have a material capable of stimulating cells electrically with the 2 main features for TE, biocompatibility and biodegradability. One of the materials being studied and that sparked curiosity for this study was Poly (L-lactic acid) (PLLA).

2.4 Poly (L-lactic acid)

2.4.1 PLLA main features and processing methods

Biomedical engineers select biomaterials according to their properties, the most closely as possible for the application. Mainly due to the biodegradability requirement, a substantial part of the materials used in TE is composed of polymeric matrices. Depending on their intrinsic chemistry and structure polymers can be processed through various techniques giving rise to different shapes, structures and morphologies [7]

PLLA is a U.S. FDA (Food and Drug Administration) approved biocompatible and biodegradable polymer used in the fabrication of different medical devices. Its biodegradation rate and mechanical properties (Table 2) can be altered by changing the quantity and characteristics of the crystalline phases through the processing conditions. [7, 8]

This polymer is preferred in applications where high mechanical strength and toughness are required (sutures and orthopedic devices), but now is largely used as a soft injectable product in facial plastic surgery (such as lipoartrophy after HIV therapy). [16, [71]

PLA is linear aliphatic polyester that has different applications in the field of medicine and TE. Lactic acid is a chiral molecule that exists in two stereoisomeric forms that yield four morphologically different polymers, stereoregular D-PLA and L-PLA (PLLA) (Figure 15), the racemic form D,L-PLA and the *meso*-PLA. [3]

The polymers obtained from the optically active D and L monomers are semicrystalline and the ones derived from the racemic form are amorphous, which has a big influence on the respective application. Racemic forms are used for controlled drug delivery where it is important to have a homogenous dispersion of the active species within the carrier matrix. The semicrystalline form frequently used is L-PLA because its hydrolysis yields L(+)-lactic acid, a natural occurring

stereoisomer of lactic acid. The L(+)-lactic acid enters the tricarboxylic acid cycle, of the cell respiration cycle, and is excreted as water and carbon dioxide, not leaving any significant amount of polymer in vital organs. PLLA can have different molecular weights, according to the number of atoms present in the structure. [7]

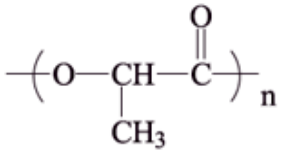

(a)

Figure 15 - PLLA chemical structure. [72]

Table 2 – Thermal and mechanical properties of PLLA, for a maximum molecular weight (M_w) ≈ 6000 g/mol. [73]

Property	Poly(L-lactic-acid)
Melting Temperature (T_m) (ºC)	170
Glass Transition Temperature (T_g) (ºC)	50-65
Enthalpy ∆H (J/g)	93-203
Density (g/cm^3)	1.25-1.30
Tensile strength (MPa)	120-2260
Young's Modulus (GPa)	6.9-9.8
Elongation at break ε_B (%)	12-26
P^d_{wo} (37ºC – period until becomes water in saline water)	3-5 years
P^e_{t50} (37ºC – period until tensile strenght becomes 50% in saline water)	6-12 months

PLLA is usually produced through the ring-opening polymerization (ROP) of its diester monomer, L-lactide (LA). Recently, a new technique was developed, direct polycondensation (DP). On ROP, the terminal end of the polymer chain reacts with cyclic monomers, by opening their rings. The ring opening (Figure 16) can be done in two ways: via bond-angle strain or steric repulsions between the atoms at the center of the ring. [74, 75]

In the process of direct polycondensation (Figure 17), the terminal groups of PLLA form coordinate bonds with the catalyst center, if the metal used is Sn (II). The number of terminals hydroxyl and carboxyl depend on the molecular weight of PLLA, if it is high, the number of

coordination sites increases and the catalyst center does not get filled with the terminal groups. The vacancy sites will origin reactions of decomposition of the LA monomer causing discolorations and racemization of PLLA. Due to the high number of open sites, proton acid is added in the beginning of the reaction in order to fill those coordination sites and enable the side reactions, accelerating the whole reaction. Water is always a product of these two reactions, however on ROP, it is difficult to eliminate without using toxic substances. In DP, the proton acid stimulates the dehydration eliminating the water excess. [76]

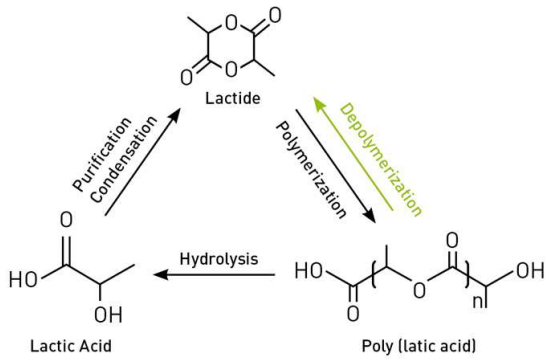

Figure 16 - PLLA synthesis via ROP. [77]

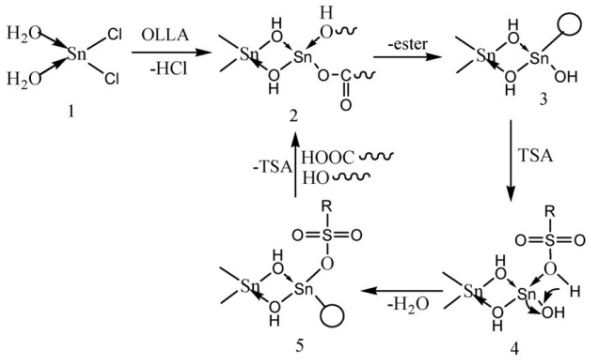

Figure 17 – PLLA synthesis via DP. [76]

In terms of solubility, PLLA can be dissolved using many solvents, being the most common dioxane, benzene and chloroform. Using these solvents the degradation happens by simple hydrolysis of the ester group even in the absence of hydrolase. [6]

In TE it is known that a good integration of the biomaterial with cells or tissues also depends on the structure of the materials. A study by Kwon *et al.* [78] on cells adhesion by using nano and microfibrous scaffolds of different compositions of PLLA, PCL and blend of poly(L-lactic acid-co-caprolactone) (PLCL) as cell culture substrate showed that different results could be obtained depending on the size of the fiber scaffolds. The smaller-diameter scaffolds (0.3-1.2 mm) exhibited better adhesion and proliferation comparing to the bigger ones (0.7 mm). The role of hydrophobicity

and of appropriate functional groups at the surface of the materials was considered relevant for the understanding of cells response. [79, 80]

Later studies showed that these finding do not necessarily mean that the material cannot be used in TE, for example, Mann demonstrated that in the case of slow adhesion, the materials may stimulate the early production of extracellular matrix components to permit cell growth and proliferation, in other words, their surface must be modified. In a recent study, nanofibrous PLLA scaffolds with surface modifications were fabricated and tested, being the results positive once the production of extracellular matrix components and cell adhesion increased. Proliferation was maintained for more than 2 weeks. [79]

PLLA was also used for electric stimulation therapies but its electrical properties, in particular, piezoelectricity, initiated a new series of studies in the most different areas. [14]

2.4.2 PLLA crystallization process

During the crystallization process of an amorphous polymer, the polymer is subjected to fusion or dissolution and then crystallized at a lower temperature. The first stage is melting, which is considered a first order phase transition. For amorphous polymers the soften process starts when the glass transition temperature (T_g) is reached but the melt only happens at the melting temperature (T_f), always higher than the glass transition temperature. [81]

Several factors can affect a polymer T_g, in aliphatic esters like PLLA, T_g decreases while the number of CH_2 units and side groups increases. At longer aliphatic side groups, T_g increases as side-chain crystallization sets in, impeding chains motion, making the material become waxy. Polymers cannot attain full crystallinity due to chain entanglement that slows down the crystallization rate. [81]

When polymers are crystallized from dilute solutions they form lamellar-shaped single crystals. These crystals usually exhibit a folded chain habit and can be of the order of 100-200 Á thick. When the polymer is crystallized from the bulk spherulites are formed. Spherulites are broadly defined as densely branched polycrystalline solidification patterns that can adopt various forms (Figure 18). [82]

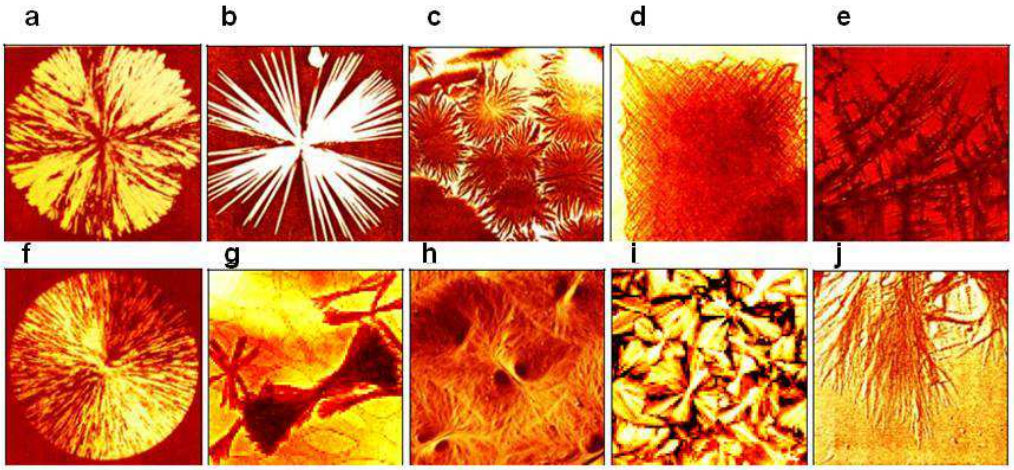

Figure 18 – Spherulitic morphologies. a) Densely branched; b) “Spiky”; c) Arboresque in polypropylene; d) and e) Quadrites; f) Formed in pure selenium; g) Crystal sheaves; h) Category 2; j) Arboresque in polyglycine. [82]

Crystallization of a polymer implies a series of factors, highlighting molecular weight and temperature as major parameters for spherulite formation. Spherulites derive from a polymer melt at moderate or high undercoolings. The appropriate material for spherulites growth must be thick enough to support an unrestricted growth in all directions, considering the spherulite as a sphere with a radius R. Firstly, monolayer crystals are formed through successive melt crystallizations when the temperature is lowered, followed by multilayer spiral growth crystals and then hedrites (Figure 19). When the temperature is lowered and maintained, hedrites are replaced by spherulites. For isothermal crystallization, spherulites are usually formed at temperatures between 120 and 130 ºC, which are the best temperatures do crystallize PLLA. [83, 84]

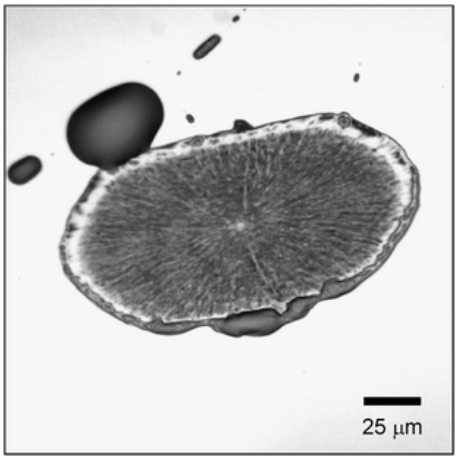

Figure 19 - PCL Hedrite oberved by optical microscopy. [85]

According to the growth process, spherulites can be divided in two categories [86, 87]. In category one, spherulites grow radially from the nucleation site, posteriorly branching intermittently

in order to maintain a space filling character. In category two they grow as thread-like fibers and subsequently form new grain at the growth front. Each spherulite exhibits an extinction cross, also called Maltese cross (Figure 20). This extinction is centered at the origin of the spherulite, and the arms of the cross are oriented parallel to the vibration directions of the microscope polarizer and analyzer. [82]

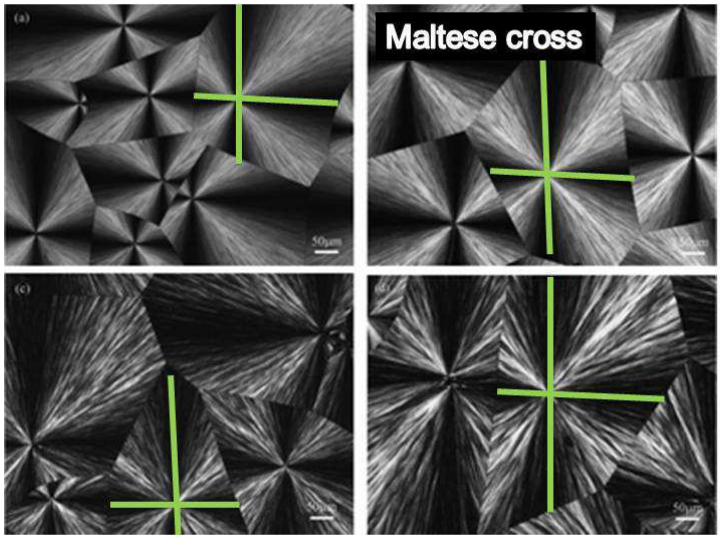

Figure 20 - Maltese cross diagram on poly(ethylene succinate-*co*-ethylene adipate) spherulites observed by optical microscopy.

During the initial stage they are spherical but in latter stages they start impinging on each other. When nucleated at different times, different sizes arise and their boundaries form hyperbolae. The spherulite formation process is resumed in Figure 21. [82]

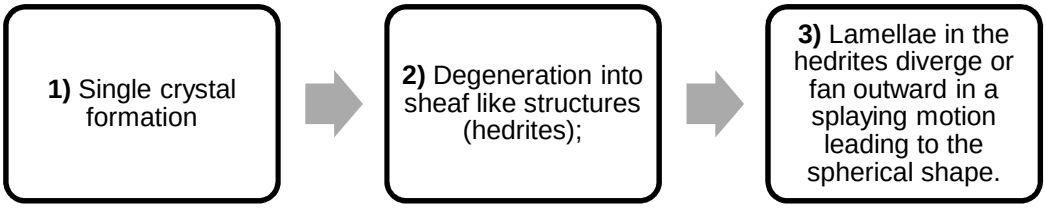

Figure 21 - Spherulite formation general process. [81]

There are several methods to crystallize a polymer but the easiest and most common one is isothermal crystallization. In this method the process starts with a sample in the amorphous state. The amorphous polymer is in a glassy (vitreous) state below its glass transition temperature and transits to the rubbery (viscoelastic) state when above it. In non-cross-linked polymers the viscoelastic behavior is attributed to chain entanglements because the macromolecules tend to form aggregates or microcrystallites. [81]

Polymers in the glassy state are seldom in thermodynamical equilibrium. By cooling an amorphous polymer down from above its glass transition temperature, a thermodynamically nonequilibrium state is formed, followed by a slow relaxation that leads to equilibrium. This kind of relaxation process is referred to as volume-enthalpy or thermodynamical relaxation because it involves a decrease of the specific volume and enthalpy. The volume change can be measured dilatometrically and the enthalpy change calorimetrically. The thermodynamical relaxation affects mechanical, dielectric and thermal properties. [81]

Crystallization affects mechanical, chemical, electrical and many other properties as it was mentioned before. Changing this parameter can lead to different results for the same material under the same conditions, especially on polymers whose structure is not well defined due to the fact that they are amorphous or semi-crystalline. Recent studies on polymers like PLLA showed that different crystalline degrees lead to distinct properties, especially regarding to the electrical character that is highly dependent on the material structure. [6, 9, 44, 73, 83, 88]

2.5 PLLA as a piezoelectric material

Piezoelectric polymers were first discovered by Kawai *et al.* in 1969 [89] in their work with Polyvinylidene Fluoride (PVDF), a polymer on which this property has been extensively studied. [89-91]. [44]

Comparing to piezoelectric ceramics, that possess a high piezoelectric coefficient, polymers show moderate values, for example, Barium Titanate has a d_{33} varying between 350-560 pC/N while PVDF d_{33} is around 20-30 pC/N. The applications emerged in many niches, since hydrophones to pressure sensors, especially after the appearance of polymer-ceramic composites and nanocomposites that allowed the spreading to many other engineering areas. In terms of piezoelectric structure, polymers belong to the orthorhombic mm^2 symmetry group, which means its tensor is described by five piezoelectric coefficients: longitudinal (d_{31} and d_{32}), transverse (d_{33}) and shear (d_{15}a and d_{24}) (Figure 22). [44, 92]

$$d = \begin{pmatrix} 0 & 0 & 0 & 0 & d_{15} & 0 \\ 0 & 0 & 0 & d_{24} & 0 & 0 \\ d_{31} & d_{32} & d_{33} & 0 & 0 & 0 \end{pmatrix}$$

Figure 22 - Polymer tensor. [44]

The different materials presented on Table 3 prove the influence of structure in the polarization. Comparing to quartz, the crystal of reference for piezoelectric analysis, PZT is softer than quartz but the piezoelectric coefficients d_{33} and d_{31} have higher values, however g voltage coefficients are still low due to the large dielectric constant of ferroelectric materials. PVDF is even

softer than both ceramics but only displays moderate values for the d and g coefficients. Cellular polypropylene is extremely soft but shows large d_{33} and g_{33} coefficients because of its softness and low dielectric constant. [44]

Table 3 - Comparison of piezoelectric polymers with piezoelectric ceramics quartz (SiO_2) and PZT. [44]

Material	E (GPa)	d_{33} (pC/N)	g_{33} (Vm/N)
Quartz	72	2 (d_{11})	0.05 (g_{11})
PZT	50	171	0.01
PVDF	2	20	0.2
Cellular polypropylene	0.002	200	30

Piezoelectric properties of PLLA have been highly studied. In 2012 Barroca *et al.* [14] studied the decay of kinetics of polarization decay on PLLA for both α and α' crystalline forms, which have different mechanical properties, like Young modulus and elongation at break. The relationship between the electrical response and crystalline form of the polymer is not studied yet but is suggested that different crystalline forms may have different polarization behaviors, namely, regarding the polarization stability. In their study Barroca *et al*. [14] demonstrated that, when poled at room temperature, both PLLA crystalline structures presented a rapid loss of the polarization but it was α-PLLA that showed better results in terms of polarization stability along time. Once α phase has a more ordered structure it consequently has more stability, and, when polarized above T_g, the PLLA films showed a durable polarization of approximately 10 days (Figures 21 and 22). The densely ordered packed crystal structure of α-PLLA allowed the dipoles to take more time to lose the induced orientation. These results proved that the material in study was appropriate for TE platforms for the study of the interaction poled substrates-proteins-cells. [14]

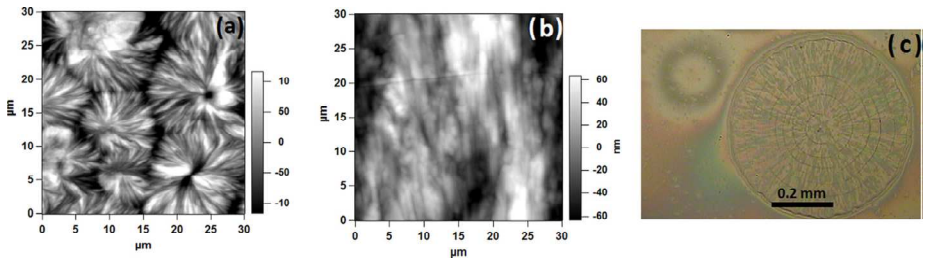

Figure 23 - Topography acquired by AFM of PLLA film crystallized at 80 ºC (a); PLLA film crystallized at 140 ºC (b); Topography of PLLA film crystallized at 140 ºC acquired by optical microscopy (c). [14]

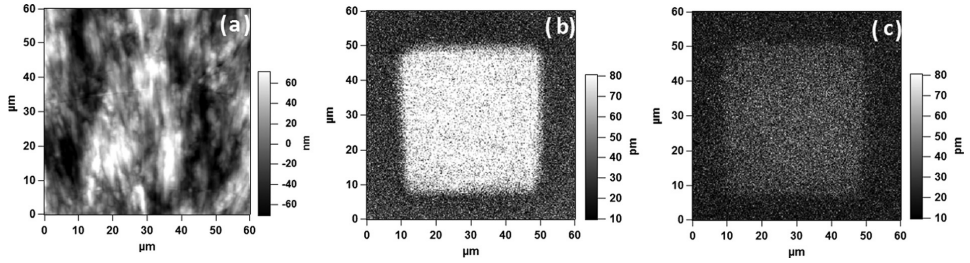

Figure 24 - Polarization decay after poling a PLLA films above glass transition temperature: topography (a); PFM amplitude after 30 min (b); and after 10 days (c). [14]

The material structure directly affects the electrical properties of a material, and for polymers, the manipulation of the material structure can have the most amazing and unexpected outcomes. Varying properties like substrate thickness and material crystallinity leads to an alteration in the electrical and piezoelectric properties worth to be studied. [93]

Chapter 3

Materials and Methods

Chapter 3 - Methodology

This chapter explains the techniques used for the process and for the characterization of the three types of PLLA membranes. The base protocol for the membranes production was already established by *Barroca et al.*, [94] and it is based on the technique solvent casting, which is the most used one, according to the literature, to prepare polymeric membranes, especially when using PLLA. Firstly, the techniques used are explained and secondly demonstrated their implementation method in this experimental work. [83, 95]

3.1 Experimental Techniques

3.1.1 Solvent casting technique

The solvent casting technique was developed almost two centuries ago, being the oldest one for processing plastic films. Initially it was applied in the photographic industry but nowadays it is used in diverse areas when high quality is a requirement. The use of solvent casting is increasing over the years for many reasons, namely for the unique final properties that are possible to obtain: uniform thickness distribution, maximum optical purity, isotropic optical orientation, which provides an excellent flatness and dimensional stability, and low haze. In terms of processing, the films can be produced in-line, with an optical coating design, and, finally, the huge growth of new crystals during the process provides a whole new range of applications like engineering plastics, optical and medical films and sheet forming or electronic applications. [96]

There are 9 key elements in solvent casting technique: (1) raw materials, (2) dope preparation, (3) casting process, (4) the caster, (5) the drying process, (5) in-line coating, (6) solvent recovery (7) handling, (8) recovery and (9) incineration. In this academic work is used the basic form of solvent casting which includes only the first 5 key elements. In order for the process to work adequately the raw materials must be soluble in a volatile solvent or water and the resultant solution must be stable with a minimum solid content the final film must be homogeneous and easy to release from the casting support. [96]

The first step consists on the dissolution of the solid polymer in pure solvents or mixtures. This process can be done in various types of mixers as soon as the mechanical shear rate and dope temperature are carefully controlled. These two parameters influence the quality of the gel particles, the solvent evaporation, the skin formation and the degradation of polymer chains. The time to attain full dissolution is usually hours and, if needed, the solution is posteriorly filtrated. The casting process can occur in a Belt Machine, cast in-line machine and in a drum machine. The equipment controls the uniformity of the film surface. The caster, embed in the complex, distributes the liquid homogeneously in order to maintain the thickness, at constant pressure and temperature. The die shape can also vary, according to the application. [96]

Finally, the drying process can include indirect heating, heating by radiation and/or air-stream drying methods. Industrially, this step is divided in two phases because of polymer-solvent systems have different diffusion regimes, so when the solvent concentration is high, the glass transition temperature falls below the process temperature causing fast evaporation of the solvent. Once dried, the film comes out of the support easily. [96]

3.1.2 Polymers crystallization process

The crystallization process, more specifically the crystallization temperature, influences the final properties of a polymer. By controlling the crystallization stage it is possible to control the spherulite morphology and, consequently, the degree of crystallinity. [83]

Thermodynamically, the crystallization kinetics can be seen as two independent phenomena: the (I) initial crystal nucleation and (II) crystal growth. It is possible to crystallize a sample from the amorphous state, isothermal crystallization, or from a crystalline state, cold crystallization. The amorphous state is attained by heating the sample until the T_f, keeping it at that temperature for 2 or 3 minutes in order to achieve full melt. The polymer is then instantly cooled. [83, 97]

According to literature, pure PLLA T_f is between 175 and 180 ºC, depending on the D-lactate content, the more it is the bigger the reduction. Usually 1% of D-unit implies a 5 ºC reduction in melting temperature. Experimentally, 200 ºC is the used fusion temperature to assure that the polymer is completely melted and that the chains have the maximum motion. The studies made by *Iannace et al.* [23] showed that the ideal crystallization temperature is 120 ºC, where both α and α' phases are present, being the last one the most disordered one, conferring a lower modulus, barrier properties and a high elongation at break when compared to the α phase. Hoffman's theory states that before 163 ºC, for a high molecular weight, a regime II spherulite is present represented by a low lateral growth and a high crystal nucleation. After 163 ºC the regime present is I which leads to an axialite formation, a multilayered aggregate of lamellar crystals. [83, 97]

It is known that the crystal morphology affects directly the structure and molecular mobility of the polymer chain, so for a process with high undercoolings, the chain mobility will decrease, the crystal growth will be slower and the nucleation rate will increase. High undercoolings bring consequences like a high number of small crystals, increasing the amount of interconnected chains between the crystals that were not adsorbed in the lamellar thickness. Once tied, the chain does not have as much mobility as the ones present in the bulk amorphous phase, meaning it does not assume a liquidlike movement above the T_g. [97]

According to the studies made on kinetics and melt crystallization of PLLA, for isothermal crystallization there is not a secondary crystallization. It is known that high temperature increases molecular mobility and consequently crystallization just before the melting of the formed crystals. Iannace experiments showed a melting point for PLLA around 206.2 ºC, similar to the literature that states a value of 170 ºC. The crystallization temperature (T_c) may range between 100 and 130 ºC, but *Iannace et al.* [23] demonstrated that the highest crystallinity degree was obtained at 135 ºC,

for pure PLLA with high molecular weight. From 90 to 105 ºC most of the molecular chains become part of several nuclei, and after 110 to 120 ºC a regime transition from athermal to thermal occurs. In the thermal regimen a higher number of nuclei are formed once the T_c is still low, leading to the formation of higher numbers of crystals with smaller sizes, increasing the crystallization degree. Before 105 ºC the spherulites growth accelerates and nucleation decreases, diminishing the crystalline percentage of polymer. [72, 97]

3.1.3 Polarization methods - Corona discharge

The polarization process consists in the application of an electric field that induces the deformation of atoms electronic cloud in the opposite direction of that same field leading to the formation of a dipole. In a dipole the negative and positive charges of the atom are separated and oriented according to the applied electric field. [93]

PLLA has a flexible molecular chain with a dipole formed by the double covalent connection between carbon and oxygen. Due to its structure it is a nonpolar molecule, however, when submitted to an electric force it possesses a dipole polarization that occurs below the 10^6 Hz. [93, 98]

There are several methods available nowadays to pole a material, for example, the application of voltage by using platinum electrodes or the Corona discharge, being the latter method one of the most popular ones being used as an ionizer in areas like research and industry. [99, 100]

The Corona discharge happens when the intensity at the conductor surface electric field surpasses an established critical value, creating an electronic discharge, or also called “electron avalanche”. The electrons possess an inherent negative charge which makes them accelerate towards the conductor positive half cycle. The discharge can be detected visually, audibly and by radio influence interference. Visually it can be represented is under the form of a plume, a brush or a simple glow (Figure 25). Audibly, the sound is generated by the air disturbances around the discharge, which are provoked by the movement of positive ions. [101]

Figure 25 - Three types of Corona discharge. From left to right, Brush, Glow and Plume. [95, 102, 103]

3.2 PLLA films characterization methods

3.2.1 XRD – X-Ray Diffraction

The XRD analysis allows the characterization related to the crystallinity and structure of the material. This technique leads to the identification of all the present phases in the material and their composition, preferred orientation and also defects. It also measures strain state, grain size, epitaxy and thickness of thin and multilayered films, as well as the atomic arrangement of amorphous materials. For polymers, it is the most reliable technique is terms of classification and crystallization measurements, like the crystallization degree as can be seen on Equation 4. [104]

$$X_c = \frac{I_c}{I_c + I_a} \times 100 \quad (4)$$

Where I_c is the area of the crystalline peak and I_a the area of the amorphous phase that is the remaining area under the fitting curve.

A major advantage of this technique is that it is non destructive. As the name suggests, when the analysis is performed the X-rays interact with the phase of the substance and diffract creating a pattern. It is an efficient tool thanks to its atomic range that allows an application to different materials. [105-107].

The patterns appear as peaks indexed according to the Miller indexes system. The attribution of indexes can be done by comparison of the measured XRD pattern with a standard data base, by analytical or by graphical methods. The plot is built with intensity versus diffraction angle. An example of XRD spectrum is represented on Figure 26. [106]

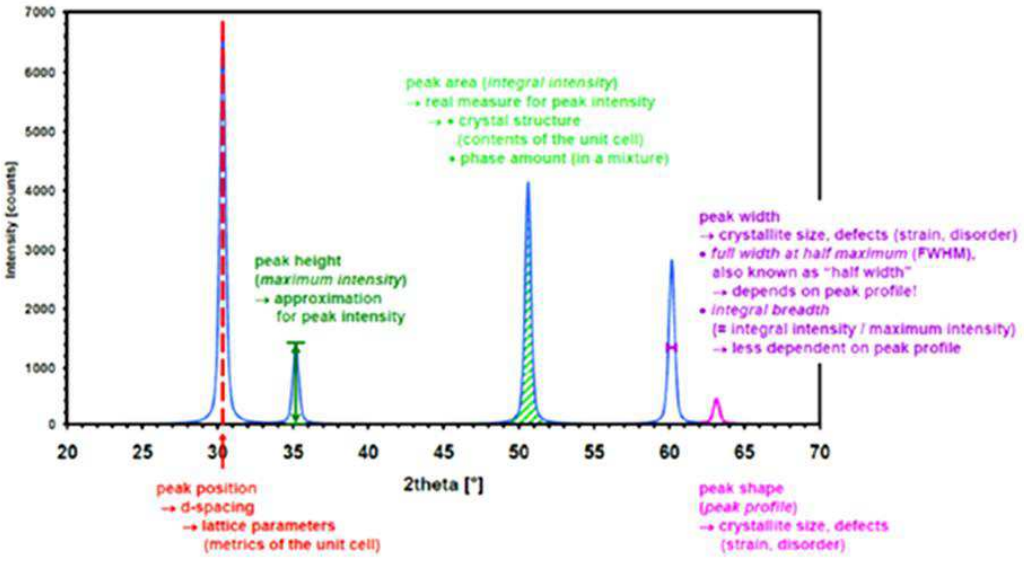

Figure 26 - XRD spectrum interpretation. [106]

3.2.2 DSC – Differential Scanning Calorimetry

The DSC analysis projects the variations in the physical properties according to thermal changes along time. It yields peaks relating to endothermic and exothermic transitions showing changes in heat capacity. Also holds quantitative information relating to the enthalpic changes in the polymer (Figure 27). [81, 108]

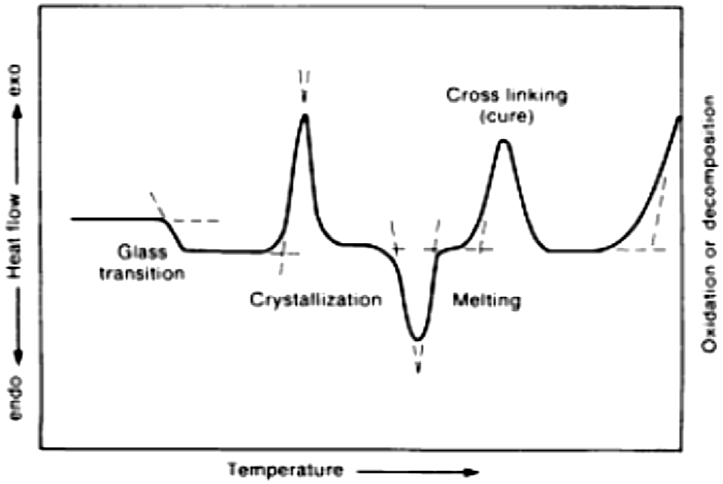

Figure 27 - DSC interpretation. [109]

DSC is used not only for thermal analysis but also to determine the degree of crystallinity. The degree of crystallinity affects both crystallization and glass transition temperature. If the polymer is crystallized by high undercoolings, the mobility of the amorphous region is reduced, increasing the T_c. The rigid fraction indicates the amount of molecules not moving when T_g is attained, and consists on the sum of the rigid amorphous fraction and the crystalline part, in percentage. If the percentage of rigid fraction is high, the T_g in the material increases because the degree of crystallinity is also higher. Once the X_c depends on the amount of amorphous fraction, the more amorphous it is the bigger is its chain mobility, allowing a higher crystallization. In order to calculate the X_c, the initial and final enthalpy (ΔH_c) must be known, as well as the heat of fusion (H_f) of the material. The parameters to calculate the X_c are gathered in the following Equation (5):

$$Xc = \frac{\Delta Hc}{Hf} \quad (5)$$

To have the percentage, the result is multiplied by 100. [97, 110]

3.2.3 SEM – Scanning Electron Microscopy

SEM is a technique that allows the researcher to see a material surface highly magnified, in the order of 10 to 300 000 times, with a resolution in the nanometer scale. SEM is a very versatile tool, having new applications emerging each year. The biggest application is for microstructural analysis like the detection of grains, their size and shape. It is also used for X-Ray and Crystallographic analysis. [107]

The SEM works in vacuum using an electron source that is focuses into a fine probe that travels along the surface of the specimen. The electrons penetrate the surface and interact with the material causing electron and photon emissions that are captured by a detector. At the output occurs the modulation of the brightness of the electron beam. The beam strikes the sample in multiple sites, and each point is recorded and mapped directly onto the screen. The magnification value is marked directly in the micrograph and can be seen in the screen in real time. The scheme of a SEM apparatus and micrographs are presented on Figure 28. [107]

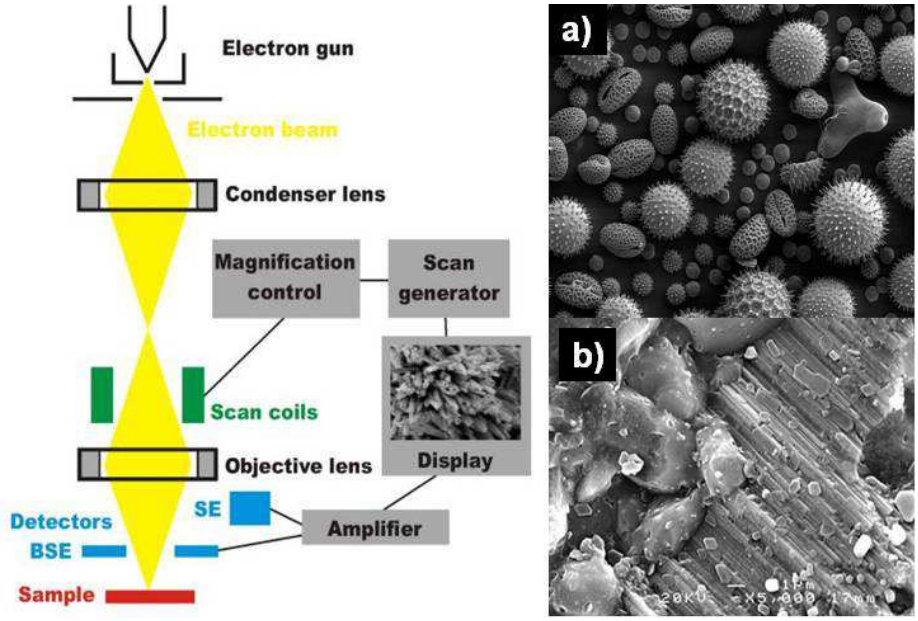

Figure 28 - Right: SEM internal system. Left: SEM micrographs, a) Pollen grains; b) Alumina surface. [111-113]

The samples must be prepared according to their nature and also should be vacuum compatible. If the sample is conductive then no previous preparation is needed, only the right size and shape is required in order to fit the chamber. When the sample is an insulating material, it is coated with a thin film of carbon, gold or other metal. The coating is usually done by sputtering. [107]

The image can be processed through various methods, from the mathematical smoothing to the image subtraction. The posterior treatment involves changes in brightness and contrast being

done with the appropriate software. These two final steps allow the maximum extraction of information from the micrograph. [107]

3.2.4 POM – Polarized Light Optical Microscopy

The POM is a light microscope that uses a polarizer between the lights path and the sample. This type of microscope is preferred among biomedical scientists once it has a polarizer that makes the light vibrate in one direction only, enabling the user to isolate specific properties, in specific orientations, unlike the normal light microscope that allows it to vibrate in every direction. The POM captures images that permit a vast analysis of the sample, like morphology, size, transparency, crystal system, the degree of crystallinity, polymorphism and others (Figure 29). [107, 114]

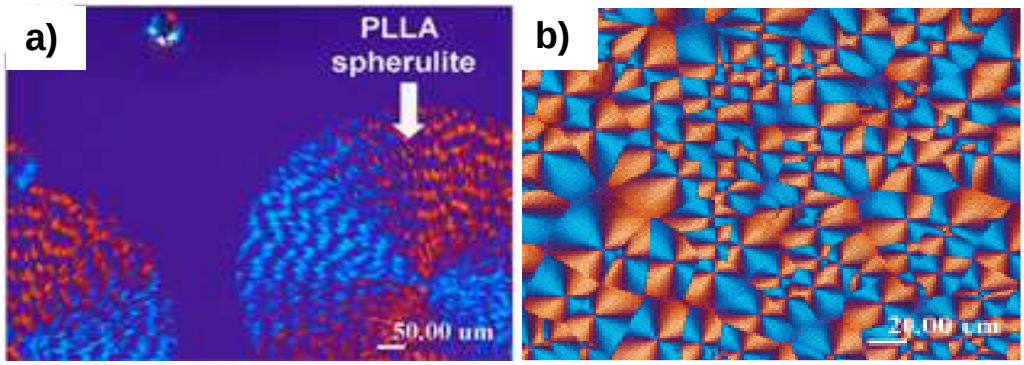

Figure 29 - POM images - photomicrographs. a) Poly (L-lactic acid) spherulites; b) poly(nonamethylene terephthalate) spherulites. [115]

The use of polarized light provides the researcher with an aesthetical visualization of the crystals, enhancing their colors and shapes. This ability comes from the right combination of four parameters related to the electromagnetic radiation: intensity, frequency, polarization and phase. [114]

These microscopes are equipped with a camera that allows the recording of the analog images into digital formats, using the adequate software. After its capture, the photomicrograph must be treated in terms of quality once its quality is never better than the one presented by the microscope in real. The conversion from analog to digital has limitations in terms of resolution, and to surpass that the resolution of the camera and computer must be similar to the micrograph. [114]

Color balance is also a problem because the detecting elements in the camera cannot respond to the light wavelength changes with same speed. Once captured, this parameter must be adjusted using the appropriate software. [114]

In resume, the photomicrograph must be a perfect replica of the real image observed by the researcher, a fact that is now possible thanks to the high camera resolution of the devices used nowadays and to the existence of efficient image treatment softwares like Adobe Photoshop®. [114]

3.2.5 Surface Roughness – Rugosimeter

Every material surface has topography. The topography consists on the distribution of curves and valleys along the surface in study and can be measured with a rugosimeter. [116] The rugosimeter measures the material surface roughness by recording altitude variations. This measurement is essential for determination of the wearing and natural degradation rate and the adhesion capability. It is done by establishing a height, width and direction of the measurement site. [117]

R_a is the arithmetical mean deviation and translates the height along the established length. The higher the number of samples the more significant is the resulting average result. As it can be seen in Figure 30, the Rugosimeter has several components, which one having a different function. [117]

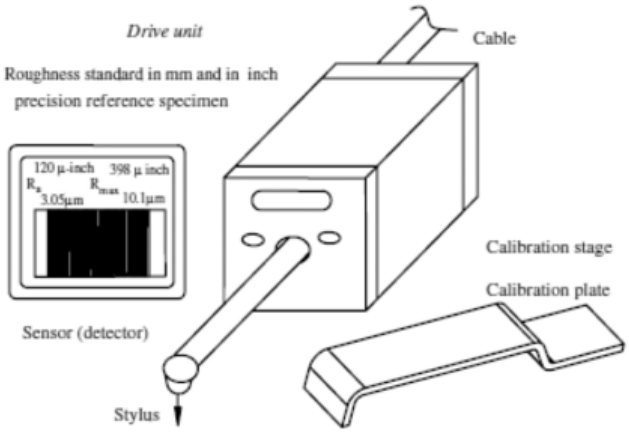

Figure 30 -- Rugosimeter scheme. [117]

The measurement is executed by a sapphire that runs along the material surface and detects the ups and downs on it. The sensor is responsible for the sapphire orientation, the monitor for showing the measurements and the AC adapter for supplying the monitor. For a portable Rugosimeter, the position can also be perfected by using a system of screws and plates that adjust it to the right height. [117]

3.2.7 Wettability - Contact Angle measurements

Wettability is described as the ability of a material to be “wet” by a liquid. Wettability forces are common and responsible, for example, by the bead up shape of water drops in oily surfaces. The measurement is based on the angle formed between the solid/liquid-liquid interface, and can be done using direct optical method or the indirect force method. This angle is denominated by Contact Angle (θ) and varies between ≈ 0 º and 90 º (Figure 31). High wettability corresponds to angles smaller than 90 º, therefore, low wettability is present for angles higher than 90 º. When the liquid is water, the denominations are hydrophobic and hydrophilic for high and small contact angles respectively. [118, 119]

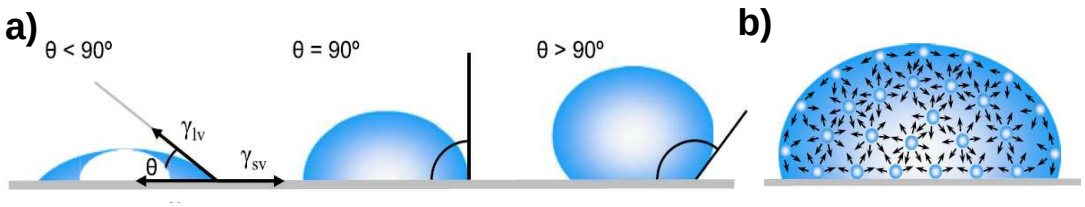

Figure 31 - Contact angle limits. a) From left to right, decreasing degree of wettability. b) Forces acting in the liquid drop by the neighbour molecules. [119]

Theoretically, in a pure liquid, the molecules are submitted to the same forces in terms of intensity and direction. In practice, the molecules of the substance surface are under the effect of heterogeneous forces once they do not have neighboring molecules in all directions. This causes an unbalance because the molecules are pulled inward, generating an internal pressure that causes the liquid to contract in search for the lowest surface free energy state, giving origin to the bead shape. [119]

Physically, Thomas Young in 1805 settled the equation that allows the calculation of the contact angle which is defined by the equilibrium of the drop under the action of three interfacial tensions (Equation 6)

$$\gamma lv \cos \theta \mathrm{Y} = \gamma sv - \gamma sl \quad (6)$$

Where γ_{lv}, γ_{sv} and γ_{sl} are the liquid-vapor, solid-vapor and solid interfacial tensions, respectively, and θY is the contact angle. [119]

In terms of techniques, the most widely used consists on the direct measurement of the tangent angle at the three-phase contact point in a sessile drop profile. For this there are several apparatus like the “telescope-goniometer”, produced and designed in 1960. The Goniometer consists of an horizontal stage where the solid or liquid sample is placed. Right up on it is a micrometer pipette responsible for a liquid drop. The illumination source and a telescope containing a protractor eyepiece are responsible for the capture. The experiment is done the by getting the tangent angle through the eyepiece. Series of improvements of the invention were done to increase precision. [119]

Nowadays, a camera can be integrated and appropriate software is used to treat the images and calculate the angles. The syringe can be motor driven so that the researcher is able to control the rate of liquid addition and removal. [119]

The advantages of this method rely on its simplicity and price, once it uses small samples (millimeters) and amounts of liquid (microliters). The disadvantage is the impurity risk due to the

small size of the drop and the substrate. For consistency, a protocol is established so that the users proceed all in the same way and then reduce the risk of error in the studies. [119]

3.2.8 Dielectric Measurements – Permittivity and Dielectric Loss

Materials with electrical features have various properties and parameters that define them and categorize them. When the material is polarized, the atoms electronic cloud deforms in the opposite direction to electric field causing the separation of positive and negative charges. In this moment a dipole is formed. There are two important measurements when evaluating the electric capacity of the material, the dielectric loss and the dielectric constant. [93]

The dielectric constant is the relative permittivity of a material, ε' or ε_r. It is the ability of a material to be polarized in response to an applied electric field (E), also named the materials polarizability. This constant is polarization dependant, so the higher the polarization degree, the higher the dielectric constant. [93] Relative permittivity can be calculated by the following equation (7):

$$\varepsilon' = \frac{C \times t}{\varepsilon_0 \times A} \quad (7)$$

Where, C is the capacity, t the thickness, ε_0 the permittivity in vacuum (8.85×10^{-12} F/m) and A the area of the polarized area, in m^2. [120]

Inorganic materials usually have higher dielectric constants than polymers because of the ions and polar groups present in their structure, which is more organized itself. For example, Titanium Oxide has a ε_r of 100 and PVDF a ε_r of 6. [93]

Polarizability is itself dependant of the free volume and frequency of the applied field. When E is applied it leads to a permanent polarization that originates a static permittivity. If the current is alternated, the field changes and polarization oscillates according to those changes. Free volume is related to the materials structure, in the case of polymers, it is the volume that is not occupied with polymeric material. The dielectric constant decreases when the free volume increases because the material has a lower density, so less polarizable groups per unit. [93]

The dielectric loss (ε'') is the loss of energy when a material is heated under the influence of an oscillating electric field. It is then the inability of the polarization to follow the rat of change of the oscillating electric field. This parameter also depends on the relaxation time (τ) which is the time took by a dipole to return to its original random orientation. If τ is equal or superior to the rate of oscillation, then ε'' is 0 or approximately 0. If not, it means that the polarization cannot follow the oscillating frequency which results in energy absorption and dissipation as heat. This can be seen on Equation 8 that gives the ratio between the dielectric loss and the dielectric constant, tgδ. [93, 121]

$$tg\delta = \frac{\varepsilon''}{\varepsilon'} \quad (8)$$

The relation between the dielectric loss and the dielectric constant relies in an inverse proportionality, in other words, if the materials maintain their permittivity values or increase them, the dielectric loss diminishes (Figure 32). [93]

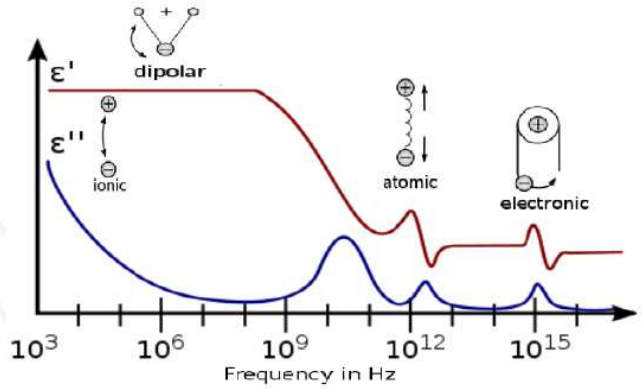

Figure 32 - Relation between permittivity and dielectric loss against frequency. [93]

To understand how the structure affects the polymer polarizability it is necessary to be aware of two concepts: segmental and normal-mode relaxations. The study of these movements provided precious information on the chain dynamics. Stockmayer classified polymers and Type-A and Type-B in terms of relaxation type. Type-A polymer have their dipoles aligned in the direction parallel to the chain contour due to the fluctuation of the end-to-end vector. This polymers experience a normal-mode relaxation, the relaxation of the global chain. Type-B polymers have a transverse dipole alignment that causes segmental-mode relaxation, the relaxation of only a few segments of the polymer chain. These relaxation modes are directly related to the temperature variations and change according to the material in question. [122]

PLA, as an aliphatic polyester, was expected to be a Type-A1 polymer, with normal mode relaxation, however, the resonance effect makes the C_2-O_3 bond act like a double bond making the rotation around this link hard. Putting this, the atoms of the backbone remain in the same plain turning every repeat unit into a virtual bond. This virtual bond possesses both Type-A and Type-B components of the dipole moment p_A and p_B (Figure 33). The same classification is given to PLLA once the only difference between it and PLA is the L monomer isomerism. [122]

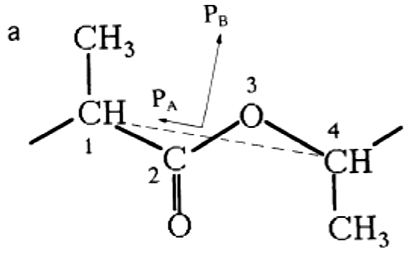

Figure 33 - Dipole moments for PLA. [122]

Ren *et al.* [122] showed that PLA has 3 types of relaxation, depending on temperature:

- 106.85 ºC – Normal-mode relaxation;
- 75.85 ºC – Segmental-mode relaxation;
- -33.15 ºC – Secondary relaxation, at 1 kHz. [122]

Hikosaka *et al.* [123] measured the ε_r on PLLA films 100 µm thick with four crystallization degrees. For the conduction, gold electrodes with a diameter of 20 mm were used. An AC voltage of 3 V_{rms} was the chosen value for the stimulation. The results showed a maximum ε_r of 6.5 in the amorphous state at 80 ºC and 10^{-2} Hz and a minimum of 3 for the same sample, at 20 ºC and $3x10^5$ Hz. His results showed that PLLA also has two types of relaxation, segmental around 65 ºC and normal between 90 and 100 ºC. [123]

3.2.9 TSDC – Thermal Stimulated Depolarization Current

Thermal Stimulated Depolarization Current is a method that measures several parameters, like the dielectric relaxation, that allow the explanation of the charging processes, decay and thermal mechanisms, the relaxation times, activation energies and others. It became an alternative for conventional bridge methods. For polymers it has been widely used to study their storage capability allowing the understanding on how the molecule behaves at different thermal states, while charged. [124-127]

The charges released during heating can be of three types:

- trapped electrons, holes or ions;
- orientational polarization (dipole);
- space charge polarization. [128]

In practical terms, the TSDC consists of a two plate capacitor and electrodes. The sample is placed between the two plates and connected to electrodes. Firstly, an electric field is applied at a determined temperature for some period of time in order to polarize the sample. After that the field is maintained while the sample cools down, in order to prevent depolarization by thermal excitation. When cooled, it is heated at a defined heating rate originating a discharge current that will be measured by the electrometer. [129]

The technique studies the charge motion based on the thermally activated release of those same charges present in localized energy levels. Basically, when the sample is heated, the trapped charges are released, which can be translated into a curve, like the glow curve of a thermoluminescent material. The curves, or current peaks, are associated with different molecular groups and respective dipoles, also known as β peaks (Figure 34). The disorientation causes a second peak to appear, α peak, associated to the space charge relaxation in the T_g zone. [88, 128]

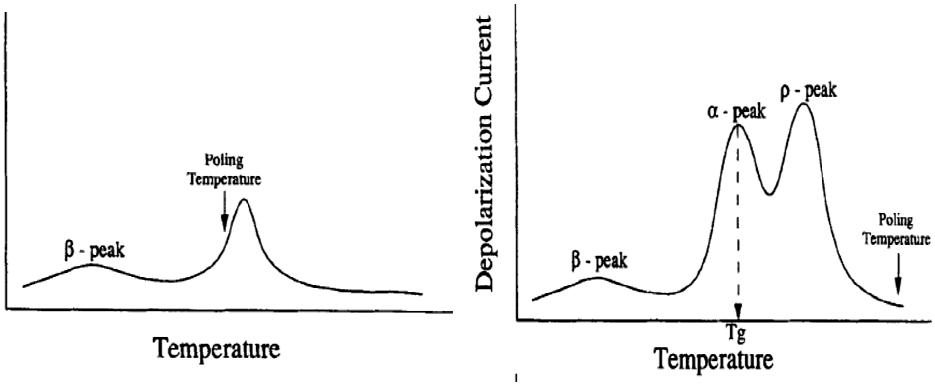

Figure 34 - TSDC peaks explanation.[130]

Non crystalline materials have different molecular conformations implying different resistances to the dipole rotation along the bulk. Since the motion of charges is not homogeneous due to the difference in activation energies, and consequently relaxation frequencies, the TSDC variation is non-linear. The number of traps of different energy levels will correspond to the number of peaks present in the spectrum. [127, 128]

3.2.10 Metabolomics Studies

Metabolomics is a science that studies the organism biochemical processes through its metabolites behavior, presence or absence. It is a recent area that came to complement Transcriptomics and Proteomics, presenting several advantages over other cell analysis techniques. Metabolomics basis is metabolites, low molecular weight organic or inorganic chemicals present in biochemical reactions, either as reactants, intermediates or product of enzyme reactions. These chemicals are not only responsible for important biochemical reactions, they are also the building blocks of structures like proteins (amino acids), genes and transcripts (nucleotides) and cell walls. [131, 132]

Technically, Metabolomics is guided by the levels of metabolites present in the organisms, once they are products of regulation processes, being highly connected to gene expression and protein production mechanisms. Despite the advantages of the technique in question, measuring metabolites can be challenging once they have rapid turnovers, varied abundance and notorious physicochemical diversity. To better measure and avoid errors derived of a rapid turnover, the metabolite must be immediately quenched by the organism so that the sample is a valid representation of the culture in study. Diversification of their chemical and physical properties is also a problem once it is very hard to find an extraction solution able to quantify all intracellular metabolites. A few extraction methods have been experiment along the years using substances like acids and bases, but it is a challenging process once each substance can only extract a group of metabolites in a determined cell type. [132]

Until now, only a few metabolomic studies were done with mammalian cells. Ritter *et al*. [133] wrote a lot of extraction protocols using Adenosine Triphosphate (ATP) as a comparison, and

Shryock *et al.* [134] worked with ANP's only. Nowadays, few techniques are available that allow and facilitate the metabolites study like the Mass Spectrometry (MS) and Nuclear Magnetic Resonance (NMR). [132]

Nuclear Magnetic Resonance Spectroscopy (NMR)

Nuclear Magnetic Resonance is a noninvasive technique that detects changes in the biochemistry of low-molecular-weight intracellular metabolites. It is a valuable tool for profiling metabolic processes once it allows the detection of different metabolites simultaneously however it is not as sensitive as Mass Spectroscopy. NMR has many advantages like, being a quantitative method highly reproducible and non-selective. The resonance allows wider spectra containing then a higher amount of information and enabling the identification of individual constituents of the sample in analysis. [132, 135]

When analyzing liquid samples, like biofluids (urine, plasma and others), the chosen technique is usually liquid NMR. But it is also possible to analyze non-homogeneous samples, as for example body tissues or even suspensions of cells. For the last, the high resolution magic angle spinning NMR technique (HR-MAS) is required, once it promotes the fast spinning of the sample and induce a higher NMR signal resolution. [132, 135]

Since it is not a destructive technique, several analyzes can be done to the same sample. The preparation process is very simple: firstly the magnetic field controller is added, usually a deuterated solvent (chloroform, for example); secondly, if needed, a chemical shift reference compound like TSP is used; finally, depending on the type of sample, a phosphate based buffer to minimize the pH-dependant chemical shift is also needed. The tubes for the experiment may have diameters ranging from 3 to 5 mm, and the volume of each sample, according to the chosen technique, can vary between 12 and 600 µl in order to completely fill the observed volume of the coil. This provides a more homogeneous magnetic field and consequently a narrow line in the spectrum. [132, 135]

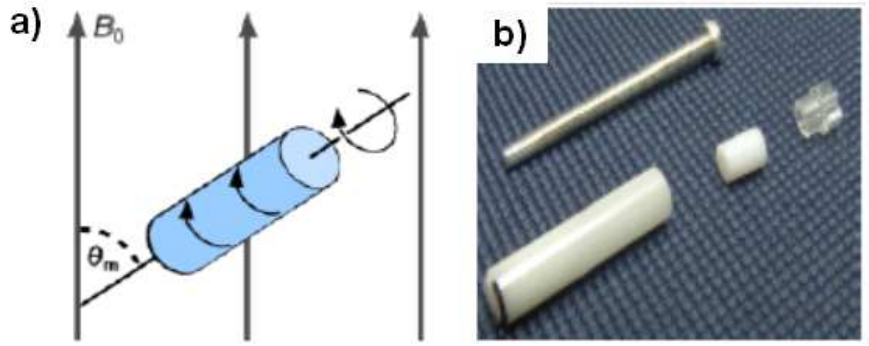

Figure 35 – a) Theoretical Magic-angle spinning. Sample rotates at high frequency inside the main magnetic field (B_0) with θ_m as the magic-angle in respect to the direction of B_0. b) Real representation of the Magic-Angle spinning. [136]

Flow injection is also an option when the researcher wants to increase the rate of sample throughout the rehearsal. In this case the sample is in a 96-well plate and is directly loaded into the magnet. When the acquisition is over, the sample is also directly transferred with a capillary tube that is posteriorly washed to avoid contamination. [132]

The low currents are controlled by shim coils in pair with wire loops, a control process called shimming (Figure 36). The shim coils produce a magnetic field which compensates for any inhomogeneity in the permanent field but the field has to be adjusted when the instrument is locked. For every sample the shimming must be repeated, if not, the peaks observed in the spectrum can appear in three different forms: asymmetric, broadened, tailed or split. [137, 138]

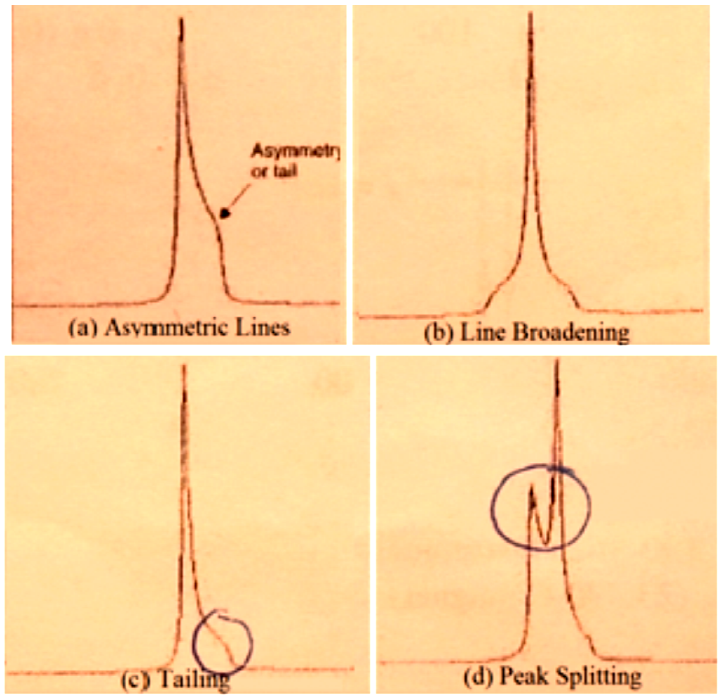

Figure 36 - Types of peak defects derived from shimming fail. [139]

3.3 Materials and Film Preparation Methods

3.3.1 PLLA films processing

PLLA films produced by the solvent casting technique were named Standard once they are the base for the production of the other two types of film that will be studied. The materials used for solution preparation were:

- Poly (L-lactic acid) (PURASORB PL 38, Purac);
- 1,4 – Dioxane (PA, Scharlau 2.5 L, LABOR SPIRIT Lda).
- Vegetal Oil.

The dope was prepared by mixing 0.55 g of PLLA with 7.8 g of Dioxane on a volumetric balloon. A thermal agitator plate (Selecta® Agimatic – N) was used as the caster. The temperature was controlled by a thermocouple (Heidolph® EKT 3001), kept at 80 ºC, and the agitation was provided by a magnet spinning at 300 rpm. The temperature of 80 ºC was chosen for being the middle term between T_g and T_f, the glass transition temperature and the melting temperature, respectively. The rotation speed was established by observation of the behavior of the magnet inside the flask, being the ideal for the agitator to cover more bottom area, to avoid gelification or de-centralization. The fume hood must be turned-off to avoid premature solvent evaporation during the whole dissolution. The dissolution time is approximately 2 hours.

After completing the dissolution, the film is immediately casted into a petri plate with 55 mm of diameter and kept in a hothouse (Heraeus® Instruments - function line) at 37.5 ºC for 3 to 4 hours. During this time the rest of the solvent evaporates and the film completes the drying process. When dried, the film starts to peel off the plate and can be removed with a tweezers. A desiccator is used to store the samples to avoid the humidity. The procedure is illustrated on Figure 37.

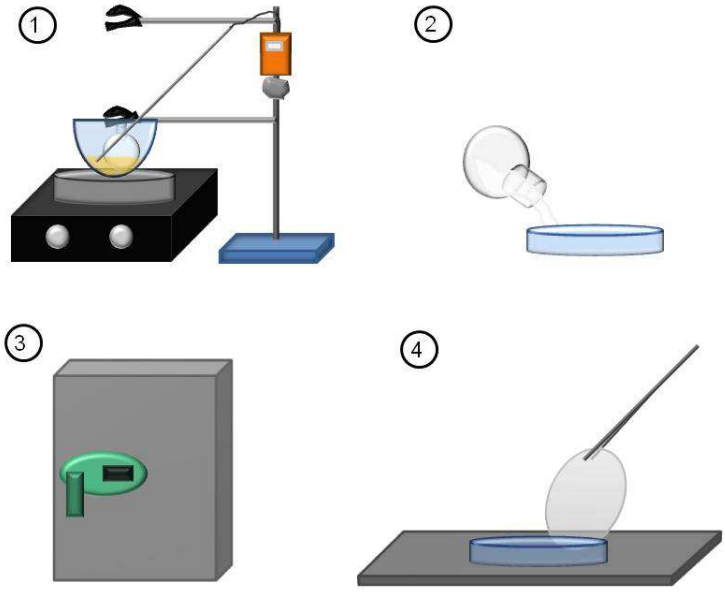

Figure 37 – Solvent casting process. 1) Polymer dissolution in a thermal agitator plate; 2) Film casting into a petri plate; 3) Drying in the hothouse at 37.5 ºC; 4) Film removal and storage.

3.3.2 Crystallization of PLLA films

Based on the literature for the crystallization process, Amorphous (no crystals) and Crystalline (higher crystalline degree) samples were produced. The temperatures chosen were 200 ºC, 120 ºC and room temperature. The samples were produced using a thermal plate (Bit Micro technology, Agitador magnetico V5). For the amorphous films the polymer was heated until 200 ºC and kept at this temperature for 3 minutes, to be sure that the melting is complete, and then cooled in a bowl filled with water to induce a thermal chock. To crystallize the samples (Figure 38), after the 3 minutes at 200 ºC, the temperature is decreased to 120 ºC, a process that takes around 8 minutes. Once reached the 120 ºC the temperature is maintained for 55 minutes allowing the spherulites to grow. Once crystallized, the sample is stabilized at room temperature for 6 hours. All the samples are then stored in the desiccator.

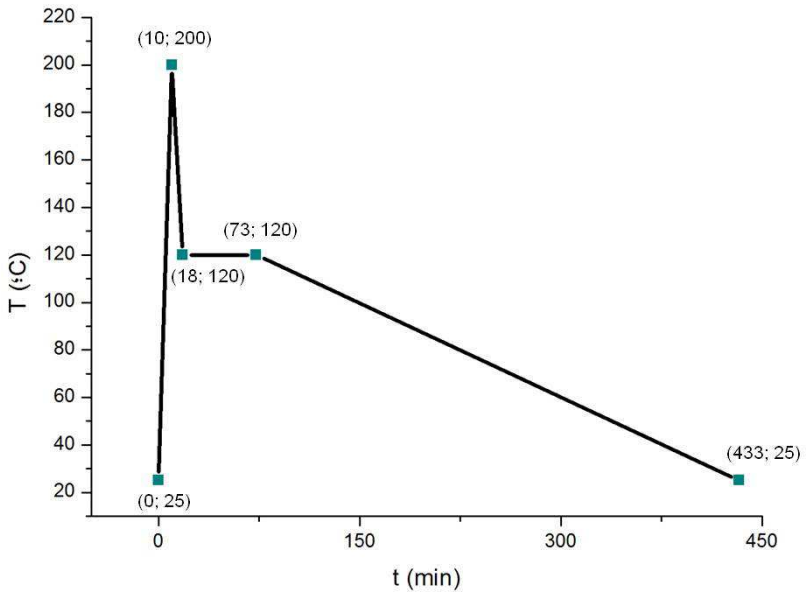

Figure 38 - PLLA films crystallization process.

3.3.3 PLLA polarization process

The films were polarized via Corona discharge using an apparatus conceived especially for the investigation group that can be seen in Figure 39. The films preparation consists on their attachment to silver paper with isolating carbon tape and posterior fixation inside the Corona, with the help of a fixation ring.

The polarization process is divided in three steps and is described on Figure 40:

- Temperature raise until 80 ºC;
- Polarization at 80 ºC;
- Polarization upon cooling (until room temperature).

The temperature maximum limit was chosen based on the material T_g. It is known that the segmental-mode relaxation of the polymer starts near the T_g, which means that at a temperature a little higher than that enables enough molecular movement, consequently dipoles rotation. The voltage ranges from 8.2 to 8.6 kV and is applied using 3 time intervals: 30 minutes, 1 hour and 2 hours. The current is maintained during cooling in order to freeze the dipoles. When room temperature is attained the voltage is turned off and 1 minute later the sample can be taken, being stored in a desiccator. Based on the previous results the only source used was negative once the positive one had no interest for this study.

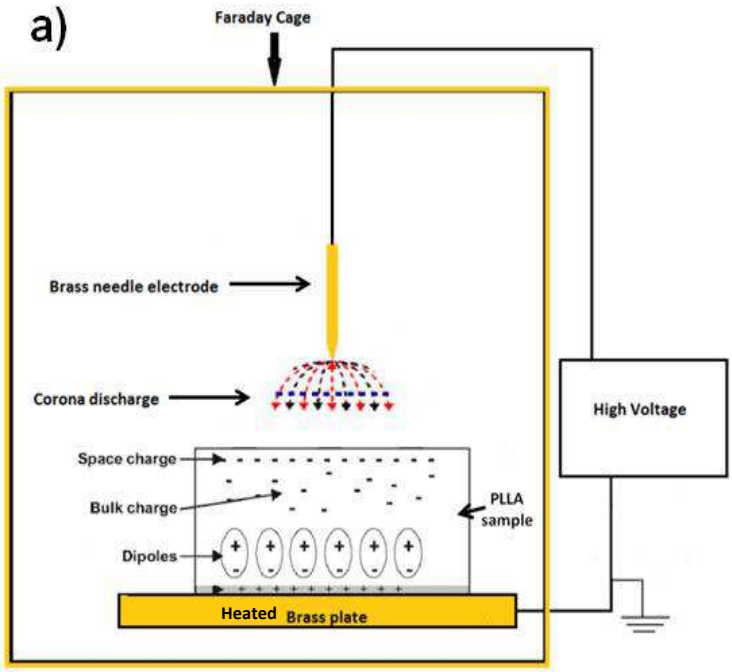

Figure 39 – The polarization device "Corona" (image kindly supplied by Nathalie Barroca from a paper under submission; [94]

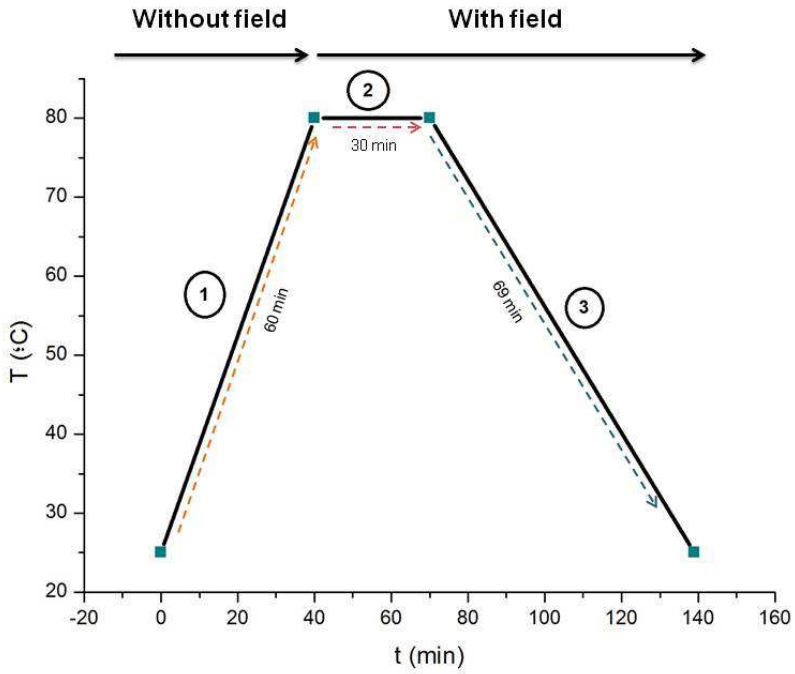

Figure 40 - Polarization process. 1- Temperature raises until 80 ºC for about 60 minutes; 2- Polarization at 80 ºC during 30 minutes. Dipole alignment; 3- Continuous polarization upon cooling, lasting around 69 minutes. Dipole Freezing.

3.4 PLLA films Characterization Methods

3.4.1 PLLA membranes X-Ray Diffraction

In order to determine the crystalline phases, a WAXS analysis was performed with Rigaku equipment, model Geigerflex. The PLLA films analyzed had different crystallization degrees: standard, crystallized and amorphous. The results were compared to previous XRDs made on PLLA and the planes were also determined according to that literature. [140]

3.4.2 Analysis of Crystallization and Thermal behaviour of PLLA films by DSC

The thermal behavior of the different films and their crystallinity degree was evaluated by DSC analysis performed in a DSC-50 Shimadzu equipment, at a heating rate of 10 ºC/min, from 0 to 250 ºC. The results were analyzed and compared with the literature. The software Origin Pro 9® was used to generate the plots and to determine the crystallinity degree (X_c) by integration of the area below the curves. [123, 141]

3.4.3 Microstructural observation by SEM

The PLLA films microsructure was evaluated by SEM with equipment from Hitachi, model S4100. As a non conducting material, the films suffered a previous sputtering treatment. The Sputter used was a Polaron Lda. SEM coating unit E5000. For the sputtering the samples were left in vacuum for about 10 minutes and then, by using a Pt/Au target, a layer of the conducting material was deposited on them for 3 minutes.

3.4.4 POM analysis of the PLLA films

For photomicrographs acquisition a Nikon Microphot Camera Infinity 1 was used. The samples suffered no previous preparation and were analyzed under 10.100x, 20x and 40x magnifications. The images were captured using the Infinity Capture® software and treated with Image J® for crystallization studies.

3.4.5 Topographic Analysis

The films topography was analyzed using a rugosimeter Mahr Perthometer M1. The sample was placed on a lamella covered with a paper sheet. The paper sheet allows the control of the tip position while it slides along the sample, working as a reference in case the tip passes the sample boarders. This assures that the values correspond to the material surface roughness. The tip is

placed in one edge and travels along the surface for a determined pre settled length. In the end the measurement is presented in a monitor.

Three samples, one of each type, were examined two times for three different directions: horizontal (→), vertical (↓) and diagonal. The parameter measured was the average between the results obtained for the three directions.

3.4.6 Contact angle measurements on PLLA films

The contact angle was measured using a goniometer (Kino model SL200HT), linked to the software UEye. Neutral and polarized samples of all the three produced types of PLLA films were analyzed. These samples were placed in a stage between the camera and the light source and a water drop of 2 µl was carefully placed on the PLLA film. All the process was recorded and saved as time frames, being the best frame chosen for posterior calculation of the contact angle. Using the Cast 3.0, the Young-Laplace angle was calculated.

3.5 Electrical Measurement Methods

3.5.1 Dielectric measurements on PLLA films

The dielectric measurements were done in all 3 types of films, crystallized, standard and amorphous, for polarized and non polarized state. The experiment included frequency and temperature variations and for that an oven (THMSE600 from LINKAM) was connected to the electrometer.

Before the measurement the samples were submitted to a sputtering treatment with an Au target and a mask in order to create electrodes that can conduct the current. Each side of the sample suffered two depositions in vacuum with 3 minutes each, using the same sputter as for SEM analysis. Once the electrodes were deposited, the samples were placed in a sapphire substrate and fixed with carbon tape. Stainless steel wires were attached with silver glue, one on each side of the electrode to allow a more precise measurement.

The electrodes were previously tested. The measure starts at 27 ºC and ends at 140 ºC with a varying cycle of frequencies ranging from 10 kHz to 2 MHz, for each change in temperature. The parameters established were a resistance of 10 GΩ and a voltage of 100 mV. Once reached the 140 ºC the data is saved and posteriorly treated using Origin 9 Pro®.

3.5.2 TSDC of PLLA films

For this analysis the samples and respective preparation were the same as for the dielectric measurements. The analysis was performed using the equipments Hewlett Packard 4192ALF Impedance Analyzer and Keithley 182 Sensitive Digital Voltmeter in circuit (Figure 40). The

parameters established were a resistance of 10 GΩ, a range of temperature from 24 to 140 ºC at a heating rate of 10 ºC/min, with no voltage. The oven used for the heating the samples was the same has for dielectric measurements.

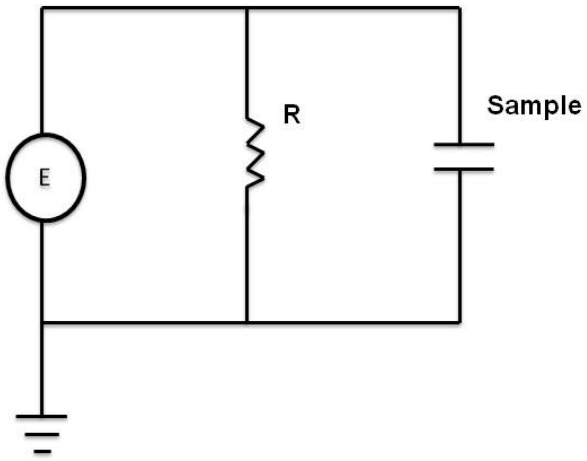

Figure 41 - TSDC circuit. E: electrometer; R: resistance of 10 GΩ.

Each sample was placed in the oven and connected to the electrodes by stainless steel wires. Once the samples were polarized, only the discharge step was performed in order to measure the depolarization. The values were then treated using OriginPro 9® and the temperature simulated on Kaleidagraph® to simulate the 10 ºC/min rate.

The current values were calculated using Ohms law (Equation 9):

$$I = \frac{V}{R} \quad (9)$$

with I representing the current, V the potential measured on each second, and R the resistance (10 x 10^{10} Ω). The polarization was calculated by integrating the peak area, using the following expression (Equation 10):

$$P = I \int \frac{1}{A}\, dt \quad (10)$$

where I is the current in ampere and A the area of the electrode, 3.14 mm^2.

3.6 Biological Assays – In vitro rehearsal for cell culture and HR-MAS

Due to cell-confluence limitations, metabolomics experiment required the preparation of 200 standard films: 100 polarized and 100 neutral. Each film had 1 cm^2 of circular area in order to fit the culture wells of a 24-well plate. The cells used were Human Osteoblasts (hOb) once the study in question was meant for bone regeneration. For the experiment to be successful 2 billion cells were needed in order to perform the NMR analysis.

The PLLA samples were sterilized with 70% ethanol for 5 minutes, washed with water for 10 minutes and finally washed with 1xPBS 10 times for ten minutes each. The PLLA samples were then placed in 24-wells plates (12 plates) and fixed with o-ring to avoid fluctuation. When the cells reached the expected confluence, 25 000 cells were trypsinated and transferred to each well containing a PLLA sample, being posteriorly incubated for 1 and 4 days. After each time point the cells were detached by trypsinization, to release the cells from the well walls and bottom, and prepared for NMR signal acquisition. The complete experiment protocol can be consulted on Annex A.

The NMR signal acquisition was performed with the Bruker Ultrashield 500 MHz/54nm equipment, and the preparation of samples, temperature settings, and other NMR-analysis related parameters were adapted for the two NMR techniques employed in the assay: NMR of liquid samples and HR-MAS NMR for the cell suspensions.

NMR signal acquisition for liquid samples (540 µL of cell culture medium) was conducted at 298 K using a reference solution of 90% H_2O + 10% D_2O. The resulting spectra were acquired and treated with the aid of software Top Spin 3.2®. Six samples were used for the analysis, each one representing the total of culture medium obtained for each of the three conditions at two different time points (Table 4).

The stock solution was prepared using a D_2O/0.25% TSP (600 µL D_2O + 300 µL TSP 0.75%). The culture medium samples were defrosted at room temperature and 540 µL of this solution was mixed with 60 µL of the stock solution (90% aqueous sample to 10% D_2O). Once mixed, 550 µL of the solution was inserted into a NMR capillary tube, gently to avoid bubble formation, and kept at 4 ºC until the analysis is performed. HR-MAS NMR signal acquisition for cell suspensions (6 samples of Hob whole cells) was conducted at 277K, with a probe rotation of 4000 Hz using the 50 µL Zirconia rotors.

Table 4 - NMR sample conditions and time points.

Conditions	Time points
S - Without PLLA film	24 and 96 hours
N – With neutral/non-polarized PLLA film	
P – With polarized PLLA film	

The spectra acquisition was made with the software TopSpin® that adjusts the phase, establishes the baseline, among other corrections. The normalization was done with MatLab®.

Chapter 4

Results and Discussion

4. Chapter 4 - Results and Discussion

In this chapter are presented all the experimental results and respective discussion. It starts with the films structural characterization, moving forward to the electrical properties and finishing with surface analysis. A resume relating all the acquired data closes the chapter.

4.1 PLLA films characterization tests

4.1.1 WAXD – Wide Angle X-Ray Diffraction

The WAXD analysis was done and the spectra can be seen on Figures 42, 43 and 44. The spectra are in accordance to the literature in terms of shape and planes. As it was expected, two crystalline peaks were observed for standard and crystallized samples and only a hum is present for the amorphous film. [140]

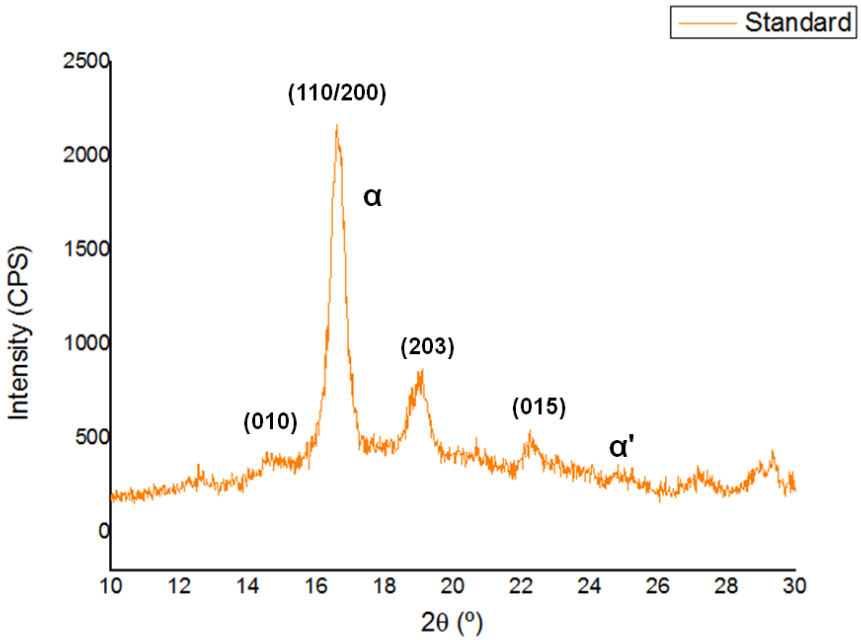

Figure 42 - WAXD for standard samples.

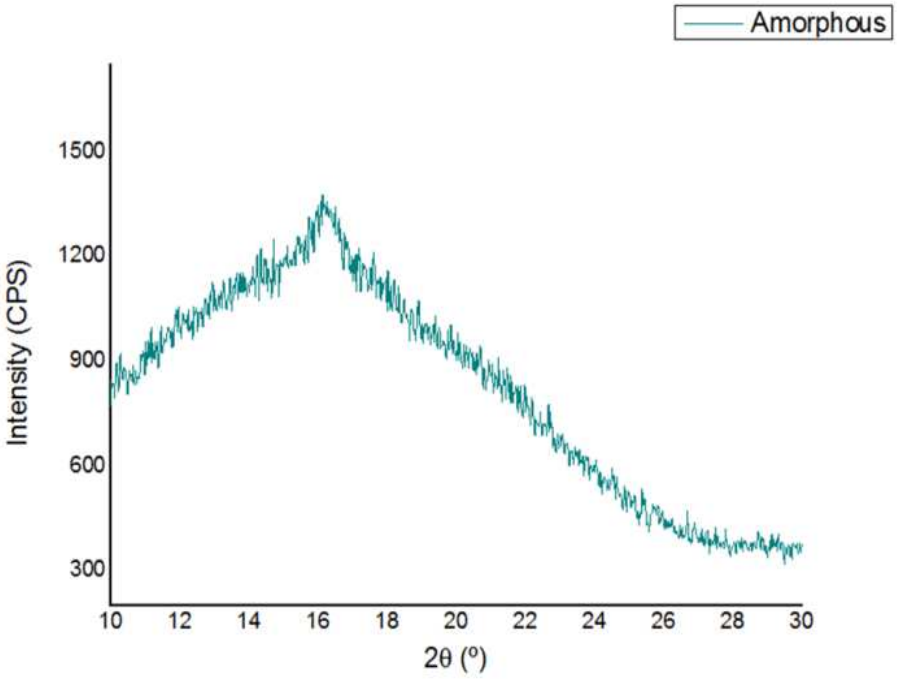

Figure 43 – WAXD for Amorphous samples.

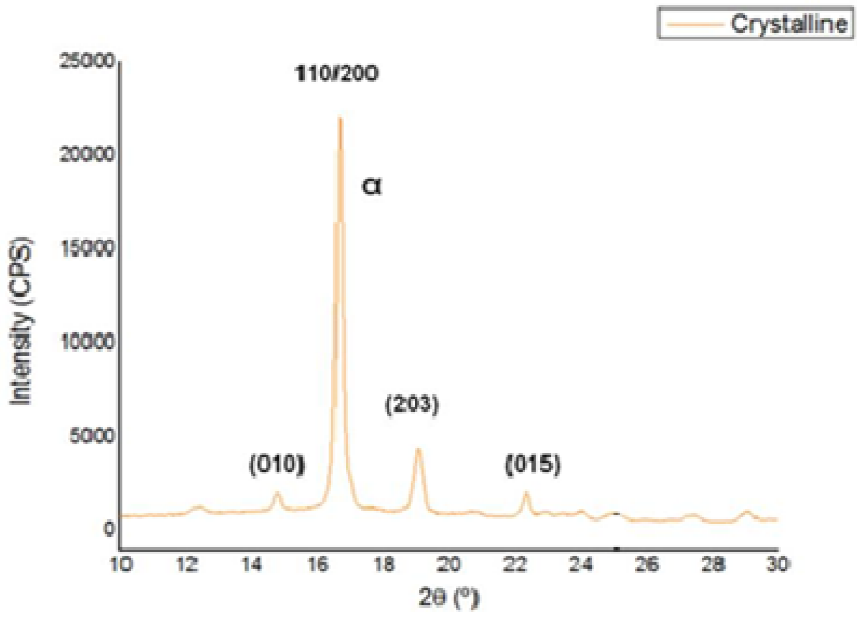

Figure 44 - PLLA films WAXD for crystalline sample.

Analyzing the spectra, an increase in intensity can be observed, directly proportional to the crystallinity degree increment. In terms of reflections, just like Cocca *et al.* [140] stated, standard

(Figure 42) and crystalline (Figure 44) samples show 110/200, 203 and 015 while amorphous samples are characterized by a hump, typical of the absence of crystals, and so no reflections. In terms of shifting, no big difference is seen. The maximum point on standard samples is located at 16.6 º and 16.65 º for crystalline. Despite the small difference, it proves that just like in Cocca studies, the peaks tend to shift to a higher 2θ when T_c increases. Finally, referring to the PLLA phases present in the films, on standard films, both α and α' can be seen and on crystalline only α phase. On standard films the appearance of α is at θ=16.6 º and α' at θ=24.8 º. The existence of α' on standard films is normal once they were crystallized below 95 ºC. On crystalline films only α phase is present, for θ=16.68 º. [140]

4.1.2 DSC analysis

The DSC analysis, of both standard (Figure 45) and amorphous films (Figure 46, up), are similar to the ones existing in the literature. Looking at the standard graphic (Figure 45) is possible to see the fusion peak located between 160 and 200 ºC. The crystallization degree measurement was done through the DSC spectra of each films, and POM images analysis using Image J®. For The crystallized film DSC (Figure 46, down) presents all 3 peaks, T_g, T_c and T_f, well defined. The T_g and T_f increase proportionally with crystallinity. In crystalline samples the T_g is ≈ 4 ºC higher comparing to amorphous and standard films. The T_c peak is in agreement with the existing literature, between 80 and 120 ºC. The fusion temperature increased slightly with the crystallinity, ≈ 2 ºC, less than the difference between glass transition temperatures. [123, 142]

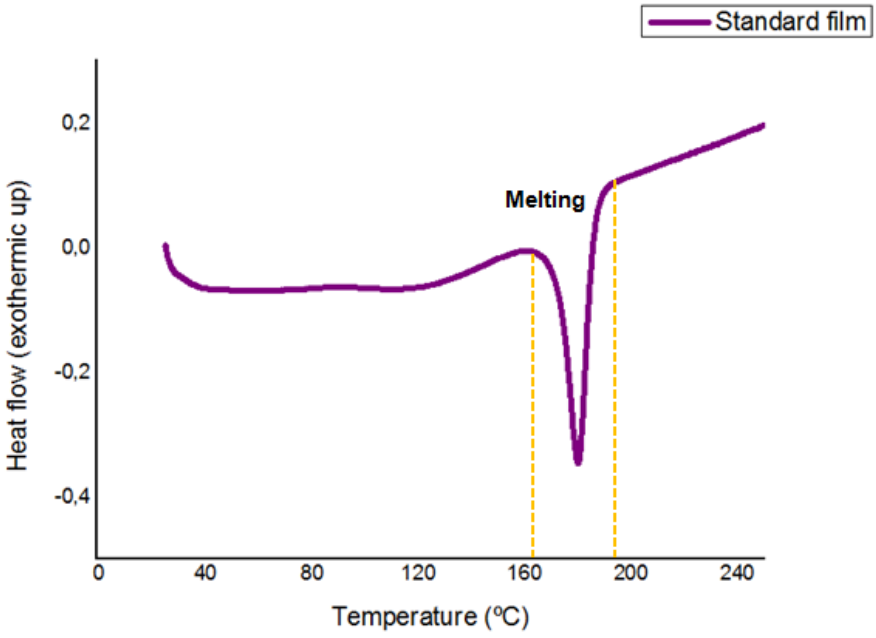

Figure 45 - DSC for Standard samples.

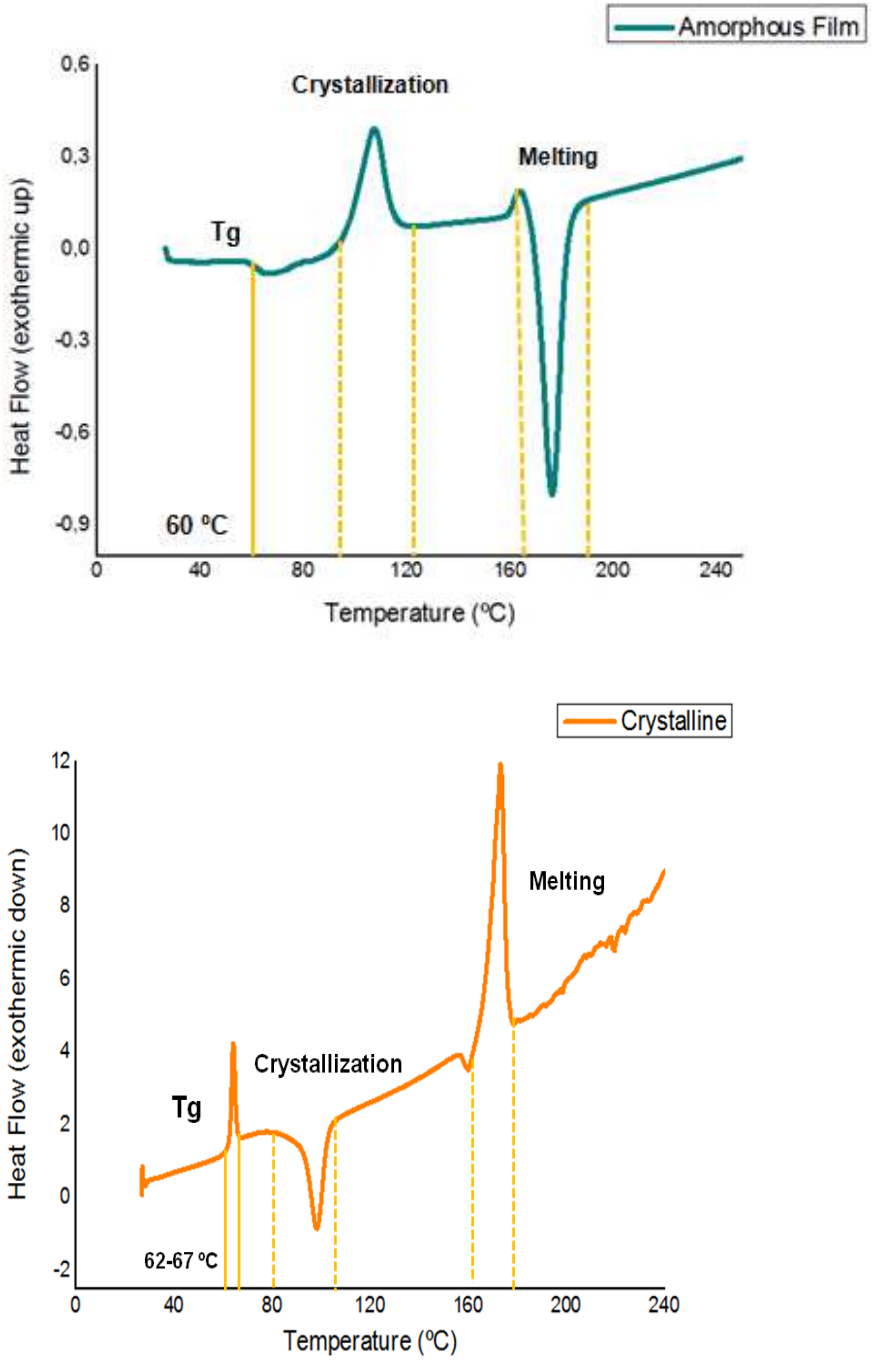

Figure 46 - DSC for Amorphous and Crystalline samples (Up and Down respectively).

The peak areas correspond to the enthalpies, so by using a mathematic function “Integrate” available in the software Origin Pro 9®, the value given was placed in the crystallization degree formula (Equation 11) in order to obtain the result.

$$Xc = \frac{Hf - Hc}{H100} \times 100 \quad (11)$$

where H_f and H_c are the fusion and crystallization enthalpies, respectively. H_{100} represents the heat of fusion for a 100% crystalline PLLA film, in the case of PLLA, 91 J/g. [142] Putting this, and making the appropriate calculations, the crystallization degrees and respective enthalpies can be verified on Table 5.

Table 5 - Enthalpies and Crystallization degree for standard and amorphous PLLA films.

Type of film	*Hf* (J/g)	*Hc* (J/g)	*Xc* (%)
Standard	2.9	0	3.18
Amorphous	5.79	4.60	1.03
Crystalline	63.35	31.63	34.86

4.1.3 POM and SEM analysis

The micrographs were taken in order to analyze the crystalline state of each sample. As it can be seen on Figure 47, not only crystalline samples have a higher degree of crystallization, as they also have bigger spherulites. SEM analysis on standard films surface was not accurate once the films bend slightly, preventing the correct capture of the image. Bending was also a problem on POM micrographs capture at big amplifications where the image would not focus as a whole.

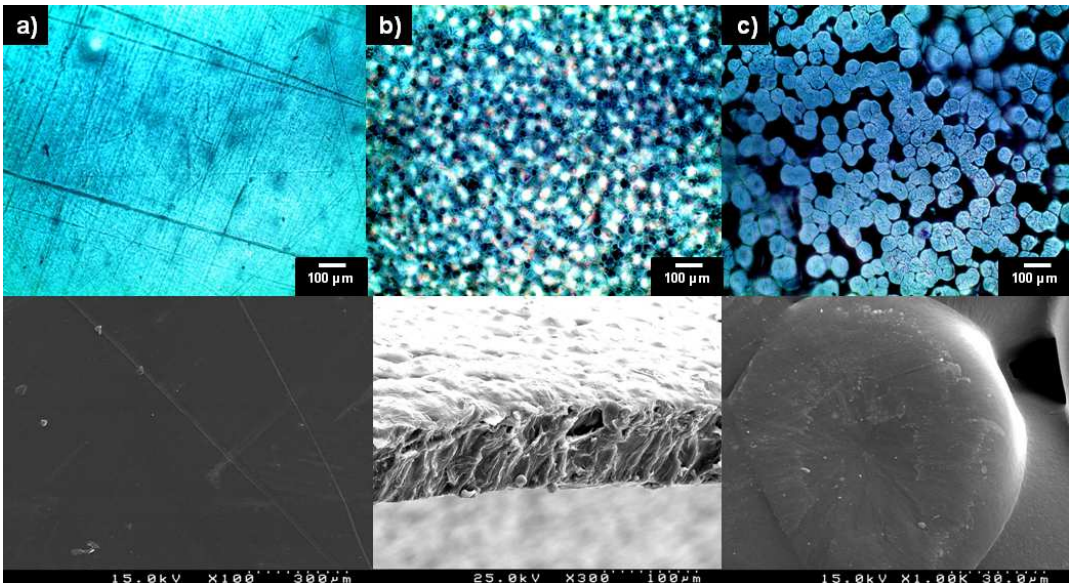

Figure 47 - From top to bottom: POM and SEM micrographs of non polarized PLLA films. a) Amorphous; b) Standard; c) Crystalline. The amplification used for POM was 10x100.

A study on the distribution of size and amount of crystals for each sample was made using Image J®. The results are presented on Table 6.

Table 6 - Spherulites size distribution for PLLA films: Standard (S), Amorphous (A) and Crystalline (C).

Radius (µm)	r ≤10	10<r≤15	15<r≤20	20<r≤25	25<r≤30	30<r≤35	35<r≤40	Total amount
C	43	35	86	73	43	5	0	285
S	305	0	0	0	0	0	0	305
A	1	0	0	0	0	0	0	1

Observing the image, for amorphous samples on Figures 47 (a) and 48 (b), the surface is plain, with only a few defects coming from their processing. In some images 1 or 2 spherulites were found, which supports the X_c obtained from the DSC, 1.03%.

Standard samples, showed a lot of small spherulites distributed along the sample. Solvent casting allows nucleation but the crystals do not grow much because the time for crystallization and temperature used is small. With a degree of crystallinity of 3.18%, a scenario like this was expected: good nucleation but a radius inferior to 10 µm (Figure 48 a)). [83]

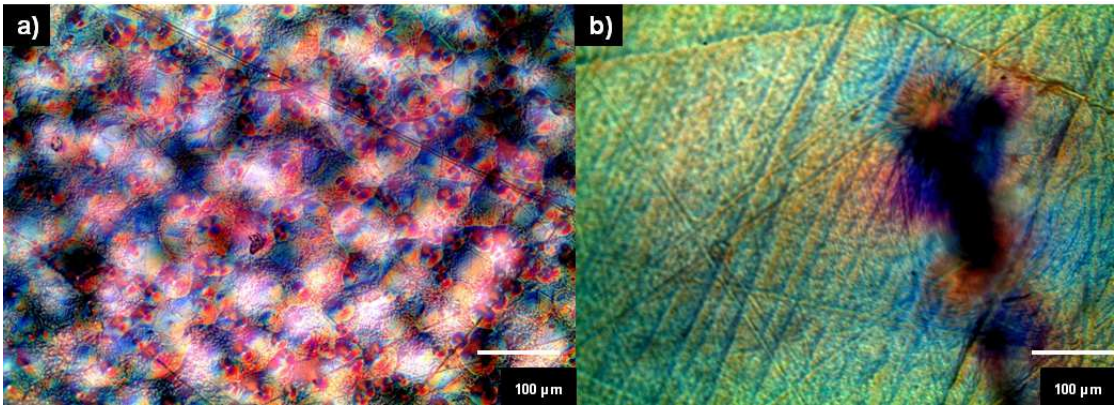

Figure 48 - Standard (left) and Amorphous (right) samples observed with a polarized light optical microscope. Amplification 20x.

Finally, on Figures 47 c), a high number of spherulites cover the surface, extending also to another layer. The sample processing favours crystallization once it starts from an amorphous state. The crystallization temperature is reported on literature as the most favourable for increasing the X_c radius varies between 10 and 35 µm, a value often found in literature for crystallization

temperatures between 120 and 140 ºC. A bigger amplification allows a more detailed observation, however the highest value possible was 40x (Figure 49). [83, 97]

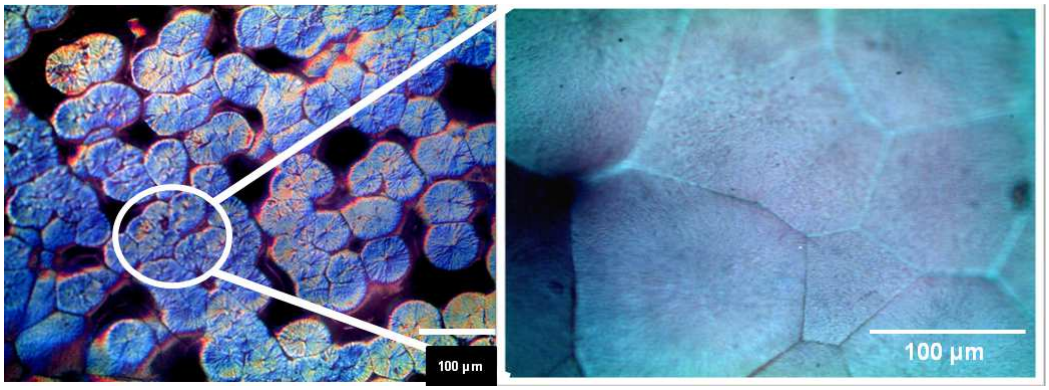

Figure 49 - Crystalline sample observed at POM microscope under two amplifications: 20x left and 40x right.

4.2 Dielectric Measurements

4.2.1 Permittivity

All the results are in accordance to Hikosaka's studies and were graphically represented on Figures 50 and 51. For all three types of samples, the tendency is for the permittivity to decrease while frequency increases. However, the contrary happens with temperature, where it increases proportionally. The difference in the values obtained, much higher for the studied cases, may be due to the strong polarization by Corona and to the different structures, higher in these samples.

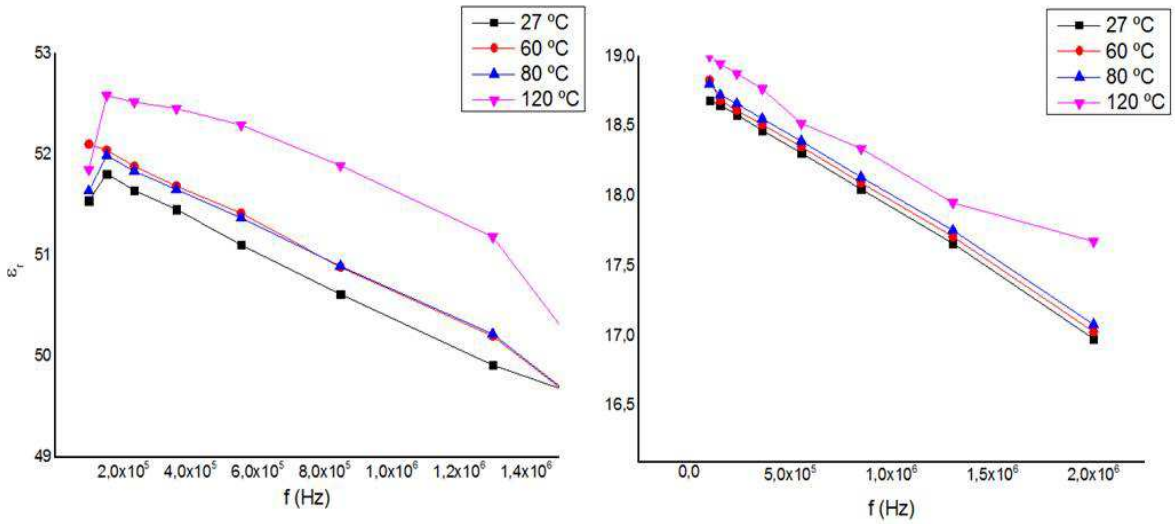

Figure 50 - Permittivity measurements for polarized samples. From left to right: Amorphous and Standard samples.

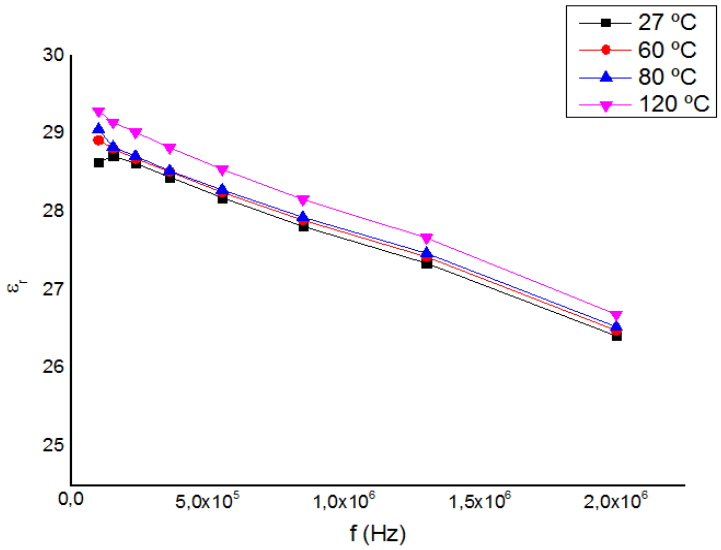

Figure 51 - Permittivity measurements for polarized crystallized samples.

By analyzing the graphics on Figures 50 and 51, it is possible to see an increase of ε_r for temperatures above 60 ºC. This increment is due to segmental mode relaxation which is the movement of some parts of the polymer chain. This movement may include rotation of some functional groups at the glass transition temperature, in the case of PLLA, around 56 ºC. The difference between values increases even more after 80 ºC, being evident for all types of samples. [123]

The increment between 60 and 80 ºC becomes less significant when crystallinity increases because, at this temperature range, the number of amorphous regions diminishes and the segmental-mode relaxation restricts the dipole orientation in the crystalline zone. To prove this, observing the first graphic on Figure 50, it is possible to observe that the amorphous samples possess higher permittivity values for all tested temperatures. [123]

Addressing now the crystalline samples (Figure 51), an increment in the permittivity is present. Comparing to the amorphous samples, the values are lower proving that high crystallinity does not lead to high capacity of polarization. As stated by Hikosaka, the key-point is the temperature increment that makes permittivity increase due to the relaxations. For the crystalline samples, the high degree of crystallinity restrains the segmental and normal-mode relaxations hampering the charge caption. [123]

In order to clarify the results, data on the samples and respective maximum permittivity results was collected and can be consulted on Table 7.

Table 7 - Samples maximum permittivity results and thicknesses.

Sample Type	Thickness (mm)	F (Hz)	≈ ε_r (27 ºC)	≈ ε_r (60 ºC)	≈ ε_r (80 ºC)	≈ ε_r (120 ºC)
Amorphous	0.31	$153x10^5$	51.81	52.04	51.99	52.58
Standard	0.11	$100x10^5$	18.68	18.82	18.80	19.00
Crystalline	0.18	$100x10^5$	28.63	28.92	29.06	29.29

The permittivity values are higher for amorphous samples just like in Hikosaka's studies. According to him, permittivity decreases when crystallinity increases. In this study, PLLA crystalline samples have higher permittivity than standard and are also more crystalline. For polymers, the thicker the material, the higher is the number of polarizable groups, and therefore the higher will be its permittivity. The values are extremely high, similar to some known ferroelectrics. Standard samples, with the initial thickness, have a ε_r similar to Barium Stannate (ε_r = 18) at 298 K for f=$25x10^5$ Hz. Crystalline samples are approximate to tellurium in a monocrystalline form (ε_r=28). Finally, amorphous samples have the highest relative permittivity, comparable to Lead Oxide at 293 K and 10^6 Hz. [93, 143]

4.2.2 Dielectric Loss

The dielectric loss happens when the polarization process cannot accompany the oscillating rate of the applied electric field, resulting in the energy dissipation as heat. It is different from polymer to polymer because each one has a relaxation time, the time necessary for the dipoles to retake their original orientation. [93]

The scenario repeats itself because, once the dielectric loss depends on the permittivity, the tendencies will be the same. As permittivity decreases, the dielectric loss increases for all samples, however the increment is not continuous because the loss stabilizes around 1 MHz. On Figure 52, it is possible to observe the results of this analysis.

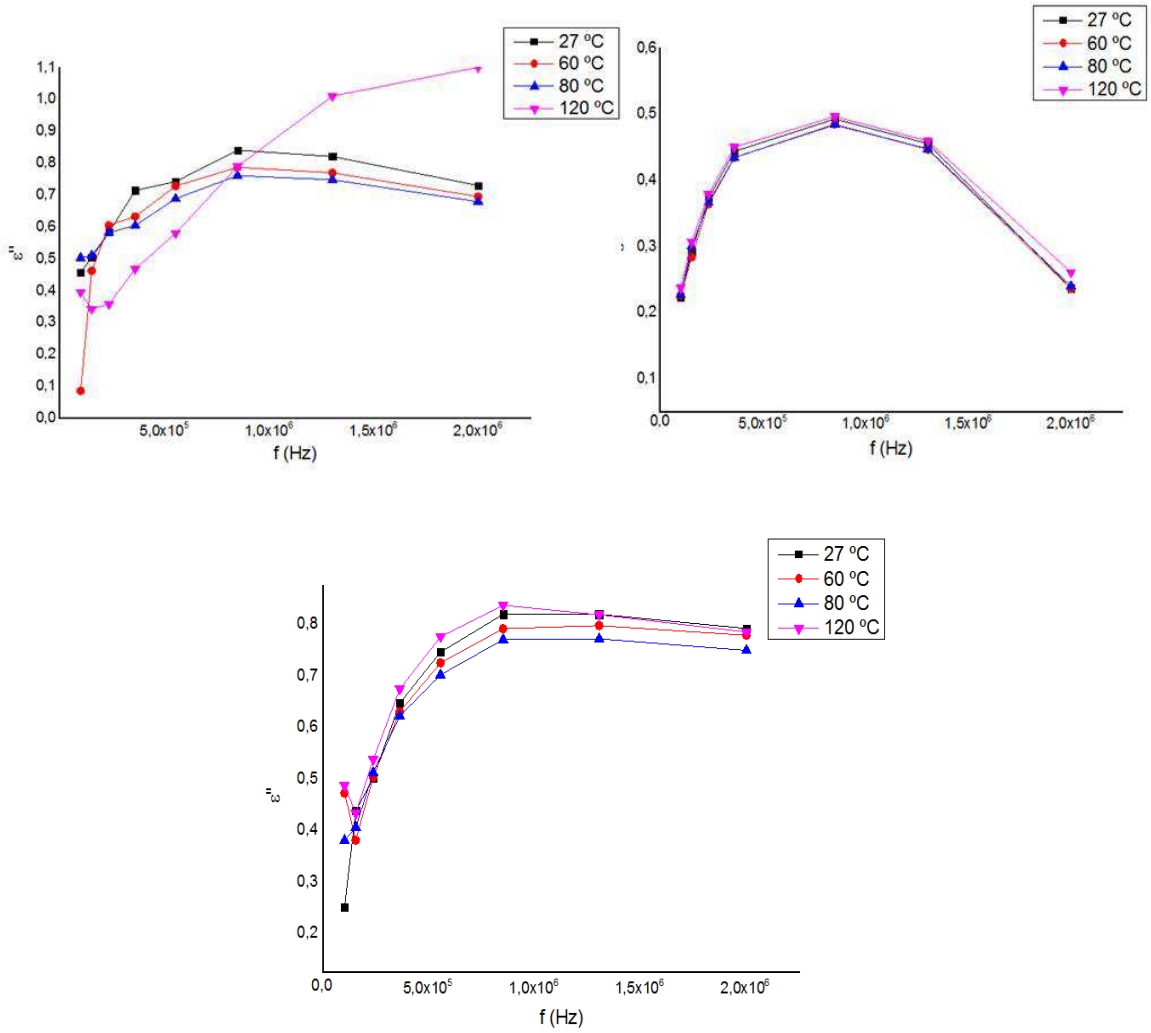

Figure 52 - Dielectric loss analysis for polarized samples. Up (from left to right) - Amorphous and Standard; Down - Crystalline.

For the amorphous and crystalline samples the same tendency is applied. For the standard samples, after 1 MHz, the dielectric loss begins to decrease and by 2 MHz it reaches approximately the initial loss value. This happens for all tested temperatures.

From 60 ºC up, ε'' decreases substantially for the amorphous samples, however, on the remaining types that does not happen and the difference is small for all frequencies. As well as in the Hikosaka's study, the dielectric loss increases when frequency and temperature increase. That is because the dipoles responsible for segmental-mode relaxation are not able to follow the frequency change of the electric field and that consequently delays their orientation. When this happens at high temperatures, where the molecular motion is higher, the loss increases significantly as showed on the amorphous sample graphic, at 120 ºC, above 1 MHz.

In terms of crystallinity degree, the higher it is the smaller is the loss. Crystalline samples have a bigger level of organization so a higher level of energy is necessary to move the molecules and disturb the chain structure. The small amount of amorphous regions directly leads to a decrease in

the segmental-mode relaxation once the chain segments are well linked, leading to a lower loss. All the data on dielectric loss is registered on Table 8.

Table 8 - Dielectric loss maximum results for all 3 types of polarized samples.

Sample Type	Thickness (mm)	F (Hz)	≈ ε'' (27 ºC)	≈ ε'' (60 ºC)	≈ ε'' (80 ºC)	≈ ε'' (120 ºC)
Amorphous	0.31	$1x10^6$	0.82	0.77	0.75	1.01
Standard	0.11	$850x10^5$	0.49	0.48	0.48	0.50
Crystalline	0.18	$1x10^6$	1.64	1.60	1.54	1.63

4.2.3 Electric Polarization

On basic terms, thermal energy affects the polarization and depolarization processes by changing their activation energies and characteristic relaxation times. [144]

Hikosaka found two well-defined peaks in the temperature dependence of the electric polarization of PLLA films. The peaks were associated to two relaxation modes. The first one related to segmental-mode and the second one to the normal-mode. The data are in accordance to the permittivity and dielectric loss results that show alterations in these same temperatures.

Our results are not totally similar to those obtained by Hikosaka. Contrarily, we have obtained for all samples only one peak. This observed behavior will be discussed below. On the study made by Hikosaka, these samples are polarized in the moment of measurement, being the amorphous samples the ones that loose more charge and faster. In this work, all the samples are polarized at least two days before the measurement, and not even a change of intensity and time of field application changed the type of obtained spectrum for amorphous ones, a straight horizontal line with no variations besides noise. It is worth noting that amorphous samples will be not farther presented in this work, since no apparent polarization was found. The samples with viable spectra were polarized during 1 and 2 hours (Figure 53) and crystalline polarized for 30 minutes (Figures 54 and 55).

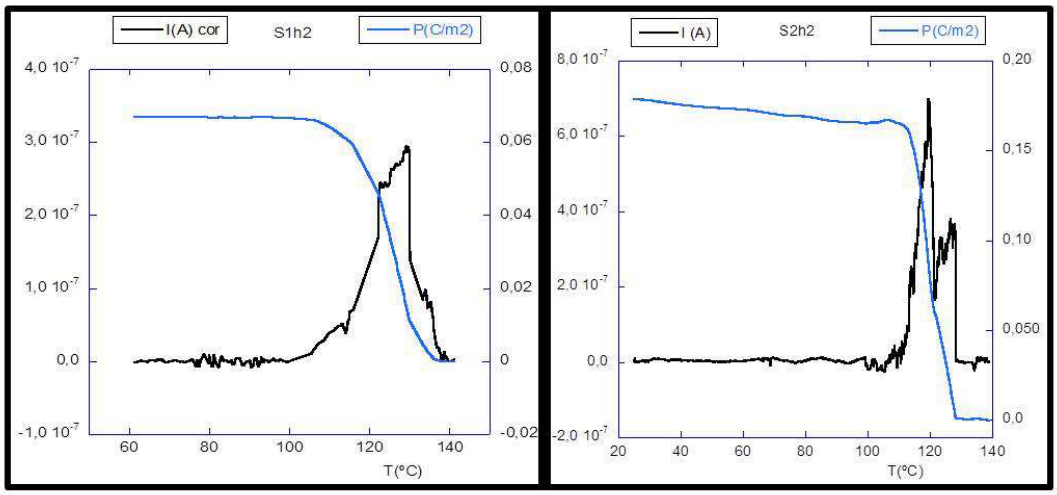

Figure 53 - TSDC for standard samples, for 1 hour (left) and 2 hours (right). Black line: Current measured; Blue line: Polarization present at that temperature.

Figure 53 shows the temperature dependence of TSDC and the corresponding electric induced polarization of two different standard samples. The anomalies observed in TSDC are irregular in shape, which can be associated with the existence of diverse polar regions, depolarizing with different activation energies. Unfortunately our data do not enable to determine them due to rather high electric noise observed at depolarization temperatures. Nevertheless, the similitude of both depolarization temperatures points out to rather similar values of the corresponding activation energies. Room temperature induced polarizations are of the same order, and even similar to the values obtained for classical ferroelectrics like BaTiO3 and TGS. It is now possible to try to establish some correlation between the anomalies observed and the polarization time, in this case 1 hour and 2 hours. Standard samples showed only one peak, associated to normal-mode relaxation, the relaxation of the global chain. By observing Figure 53, for both samples the temperature at which the depolarization occurs is similar, in the range 100 to 140 ºC. Below this range no peaks were observed, and so no segmental-mode relaxation is detected. This is not surprising because PLA is a Type-A polymer where dipoles are aligned in the direction parallel to the chain contour due to the fluctuation of the end-to-end vector. Thus after poling, micro Brownian movements make the dipoles align along the direction parallel to the chain contour in the amorphous regions. [122, 123]

Regarding the saturation polarization magnitude, samples with larger polarizing times should show larger values of the electric polarization, which is clearly the case. The sample polarized for 1 hour displays a value of 7 $\mu C/cm^2$, whereas the other one polarized during 2 hours has a higher value (18.4 $\mu C/cm^2$) (Table 9).

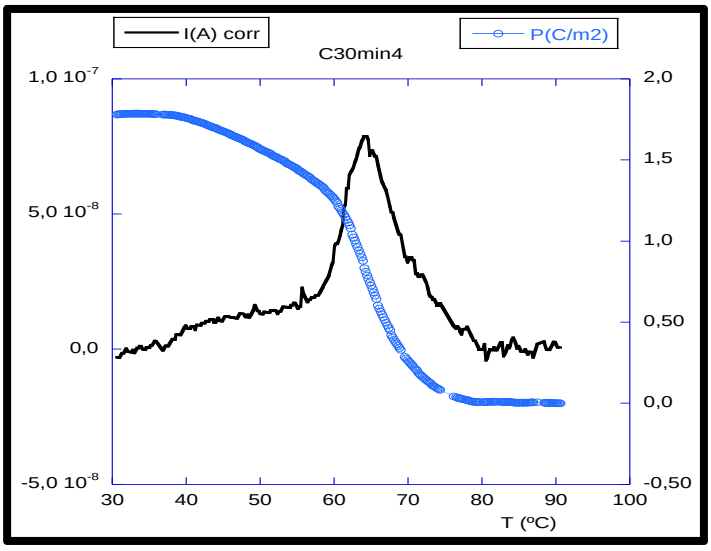

Figure 54 - TSDC of a crystalline sample poled for 30 minutes in the T_g zone. Black line: Current measured; Blue line: Calculated electric polarization.

Figure 54 shows the temperature dependence of TSDC and the calculated electric polarization of a crystalline sample poled for 30 minutes, in T_g zone. The anomaly observed in TSDC is relatively broad and it is located at ≈70 ºC. Near this temperature, Hikosaka has also found an anomaly that has assigned to α-peak, originated by a segmental-mode relaxation. This type of relaxation is likely due the transverse component of the monomeric dipoles leading to the rotation of electric dipoles. PLA can also exhibit a Type-B relaxation component that can yield a transverse alignment of the electric dipoles. In this case only a few segments of the polymer chain move, which can lead to micro Brownian movements associated with T_g. In PLLA segmental relaxation has been associated with the carbonyl groups existing in each repeating unit. [122, 123]

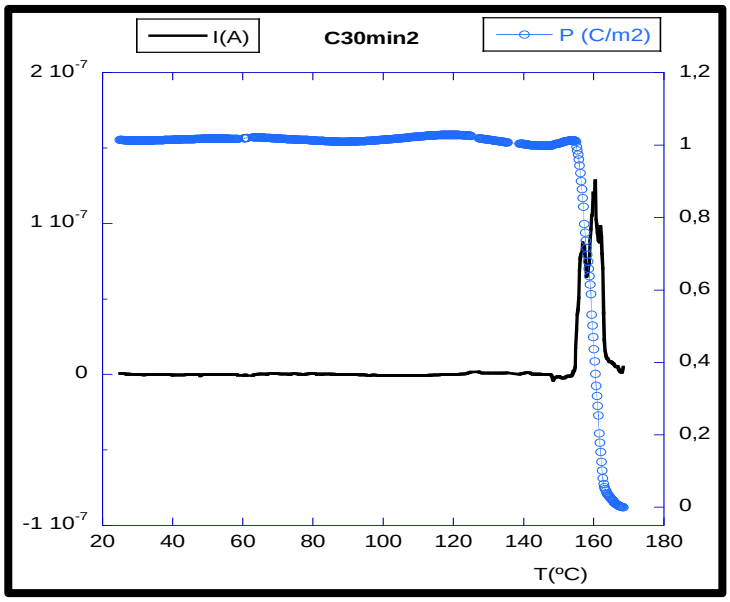

Figure 55 - TSDC for crystalline sample after Tg.

Figure 55 shows the TSDC and the corresponding calculated electric polarization of a crystalline sample but contrarily to the one of Figure 54, above T_g. TSDC exhibits a structured anomaly, which spreads from 155 to 165 ºC. This temperature is quite high, precisely close to the melting point zone, according to DSC performed. For a highly crystalline sample, the thermal energy needed to move the chain is relatively large and it is expected that the depolarization temperature can occur in the vicinity of the melting zone leading to a normal-mode relaxation associated with the whole polymeric chain. The magnitude of the electric polarization saturates below 150 ºC in a value of 100 µC/cm^2 (Table 9). Albeit, this value is ≈30% lower than the one observed for the sample in the T_g range (Figure 54), which is in good agreement with Hikosaka's results. Moreover, it is worth noting that the magnitude of both crystalline samples is about one order of magnitude larger than the one obtained in standard samples in terms of polarization measurements.

Table 9 - Polarization values obtained for Standard and Crystalline samples, and respective temperatures. T_0 is the temperature at which saturation of polarization occurs.

Sample	≈T_g(ºC)	≈T_f (ºC)	Date of polarization	Date of measurement + time difference	T_o(ºC)	Saturation Polarization (µC/cm^2)
S1h2	65	180	17/11/2014	25/11/2014 (7)	138	7
S2h2	65	180	18/11/2014	20/11/2014 (2)	130	18.4
C30min4	62-67	180	13/11/2014	25/11/2014 (11)	80	180
C30min2	62-67	180	14/11/2014	21/11/2014 (6)	160	100

In summary, crystalline samples can exhibit higher values of electric polarization, since electric dipoles can be more efficiently oriented, by using external polarizing techniques. Though the depolarizing temperature for one of the crystalline sample is lower than of the standard samples, the highest depolarizing temperature is obtained for the sample with the largest degree of crystallinity. Consequently, a high degree of organization, corresponding to larger activation energy, may prevent the structure to be easily modified by the effect of thermal energy, and thus keeping its polarizing state for a longer period of time. The influence between the dates of polarization showed its influence as it can be seen from samples S2h2 and S1h2. Despite the duration of field application, the values of polarization are almost double for S2h2 that was measured only 2 days after the corona discharge.

In quantitative terms, the polarization values obtained are larger than those presented in literature, but that can be due to the contribution of interfacial charges, spherulites behavior as grain frontiers and other unknown phenomena. The behavior observed is the same as in electrets. On electrets, charge storage and dipole orientation depend many features like chemical impurities, chemical constitution, polymer conformation, macro-molecular arrangements, degree of crystallinity, interface at amorphous-crystalline regions and mechanical stress. The polarization displayed by the electret is suggested to be related to the charges at the surface or in the bulk, also called the “real polarization”. It can also be due to the induced polarization which is the “true polarization”. The influence of both is possible.[47, 145] Eliminating such contributions will lower the obtained value, suggesting a new polarization value, ≈100 μC/cm^2 for the crystalline samples and ≈10 μC/cm^2, for standard samples.

Comparing to Hikosaka’s studies, the values of polarization are significantly higher (almost 4 orders of magnitude), however both the samples used and type of polarization differ a lot. Hikosaka’s samples were 100 μm thick, while in this work the thinnest film was ≈120 μm. The polarization method is also different. Whereas our samples were poled by Corona technique, which can yield high polarizing magnitudes, Hikosaka’s samples were poled locally during the measurement. [123]

4.3 Surface characterization

4.3.1 Surface roughness

Topography of the sample was evaluated by measuring both roughness and contact angle. The values obtained for roughness are presented on Table 10. The data shows that crystalline samples have the highest value which can be justified by its high degree of crystallinity. Observing the sample at the naked eye, and touching them, it is possible to feel the heterogeneity of the surface, and on SEM and POM that information is clear. Usually a high value of roughness is not

desirable, but for biomedical applications it becomes a high advantage. Polarization does not affect roughness. [60]

It is known that cell attachment is a process involving different variables like, cell behaviour, material surface properties and environmental factors. Surface properties comprise the hydrophobicity/hydrophilicity, charge, roughness, softness and chemical composition of the biomaterial surface itself. Roughness has a direct influence on cells morphology, proliferation and phenotype expression. Depending on the type of cell, the perfect roughness can be in the macro (100 µm to mm), micro (100 µm to 100 nm) or nano scale (100 nm or less). Many studies are available showing that cells differentiate and proliferate better on microrough surfaces, for example, one made using rat osteoblasts that showed a had higher proliferation on rough surfaces with approximately 0.81 µm. Rough surfaces are more adherent, which in cellular perspective means a high protein adsorption, consequently, high efficiency. [60]

The cells used for *in vitro* experimentation were human osteoblasts, being these cells considered big cells, and recalling the previous studies on osteoblasts, crystalline samples would be the most appropriate once they have higher roughness values, more similar to the ones showed on Lees study (0.81 vs 2.777 µm). [146]

Table 10 - PLLA films surface roughness.

Sample	Medium Roughness (µm)
Amorphous P	0.271
Standard P	0.260
Crystalline P	2.777

4.3.2 Contact Angle

Roughness studies are not enough to predict the cells behavior when in contact with the material. The films used for cellular experiments are polarized, but polarization does not affect topography. To complement that information, contact angle measurements were done (Table 11) in order to understand the effects of polarization in the surface. Hydrophilicity is one of the main requisites for protein adsorption, and to attain that the contact angle needs to be inferior to 90 º. For osteoblasts, a study made by Wei *et al.* reported a decrease of the adhesion when the contact angle increased from 0 º to 106 º. [60]

By measuring the contact angle on the processed PLLA films (Table 11), two facts became evident: Hydrophilicity increases with polarization, crystallinity and roughness. Polarized samples have smaller contact angles being the crystalline samples the ones with lower values. The difference between Standard and Crystalline samples is not significant, but combined with the values of roughness Crystalline samples become the best candidates to promote cell adhesion,

being the best choice for bioapplications. Standard samples can be used for other types, perhaps smaller, once they do not require much roughness, for example, fibroblasts that adhere properly with angles between 60 º and 80 º. [60]

Table 11 - Contact angle values for polarized and non polarized samples.

Sample	Contact Angle: Young-Laplace (º)
Amorphous NP	103.274
Amorphous P	92.504
Standard NP	89.646
Standard P	74.810
Crystalline NP	81.201
Crystalline P	72.87

The studies based on surface modification to increase wettability include not only the addition of charged substances but also electric treatment. Yaszemski's groups investigated negatively charged oligo(poly(ethylene glycol)) hydrogels and proved that the negative surface promoted hydrophilicity and consequently chondrocytes differentiation and collagen and glycosaminoglycans expression. Cairn used e-beam irradiation on PLLA samples and also saw a significant increase in surface wettability. In terms of type of irradiated samples, the contact angles didn't change much corroborating the values obtained in the present study. The difference between the contact angle of a nonpolarized and a polarized film can be seen on Figure 56. [60, 147]

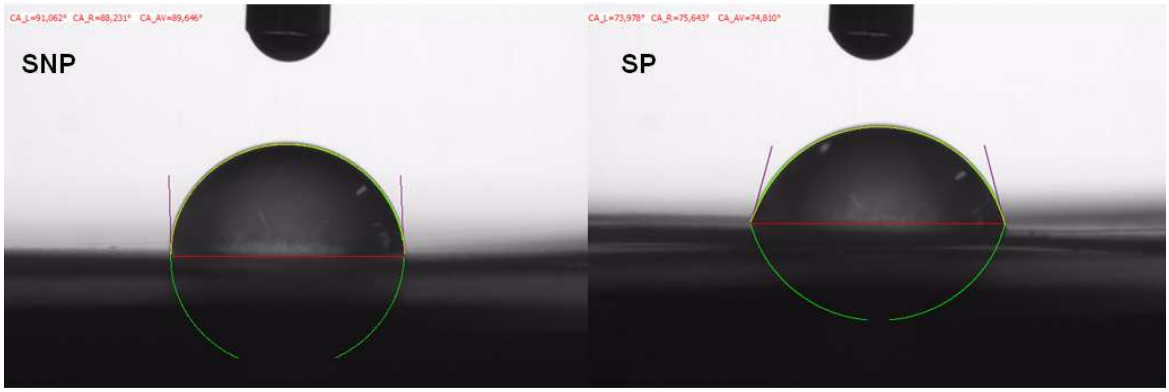

Figure 56 - Contact angle measurement for Non Polarized (NP) and Polarized (P) Standard samples.

4.4 Biological Assay - Metabolomics Study

The results obtained from the first rehearsal with HR'-MAS were not very conclusive (Figures 57, 58 and 59), being this type of analysis complicated to perform and interpret, two more experiments will be conducted in order to clarify the information. In all samples it was observed instability in the TSP peak resonance. This phenomenon could be associated to:

- The type of cells;
- The TSP interference with the cell components.

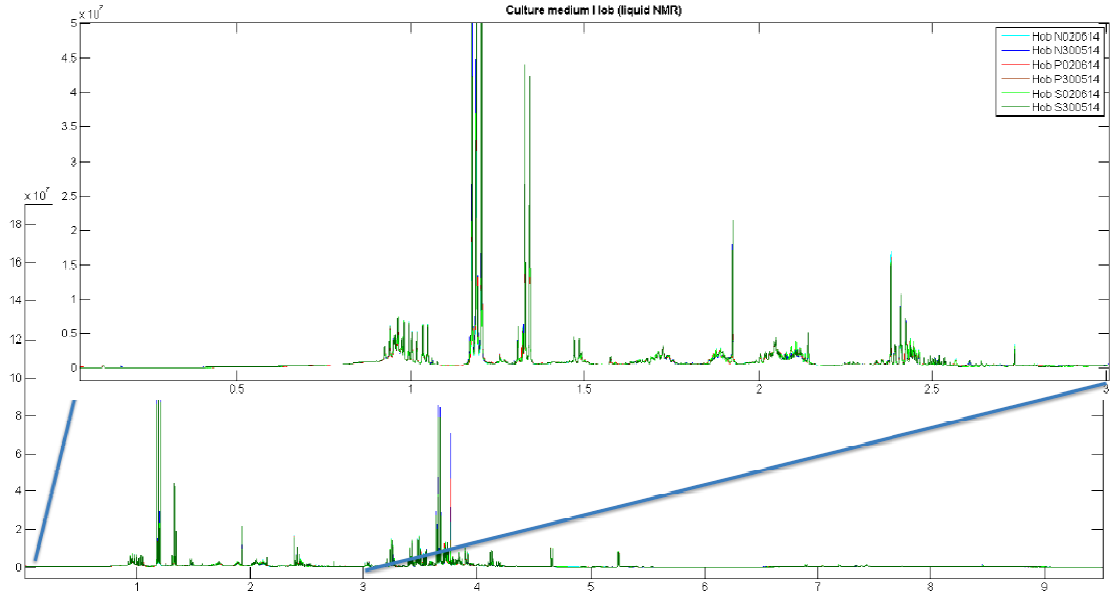

Figure 57 - HR'-MAS spectrum corresponding to 96 hours, treated by MatLab. Green: Without PLLA; Blue: Non Polarized Samples; Red: Polarized Samples (from 0 to 3 ppm).

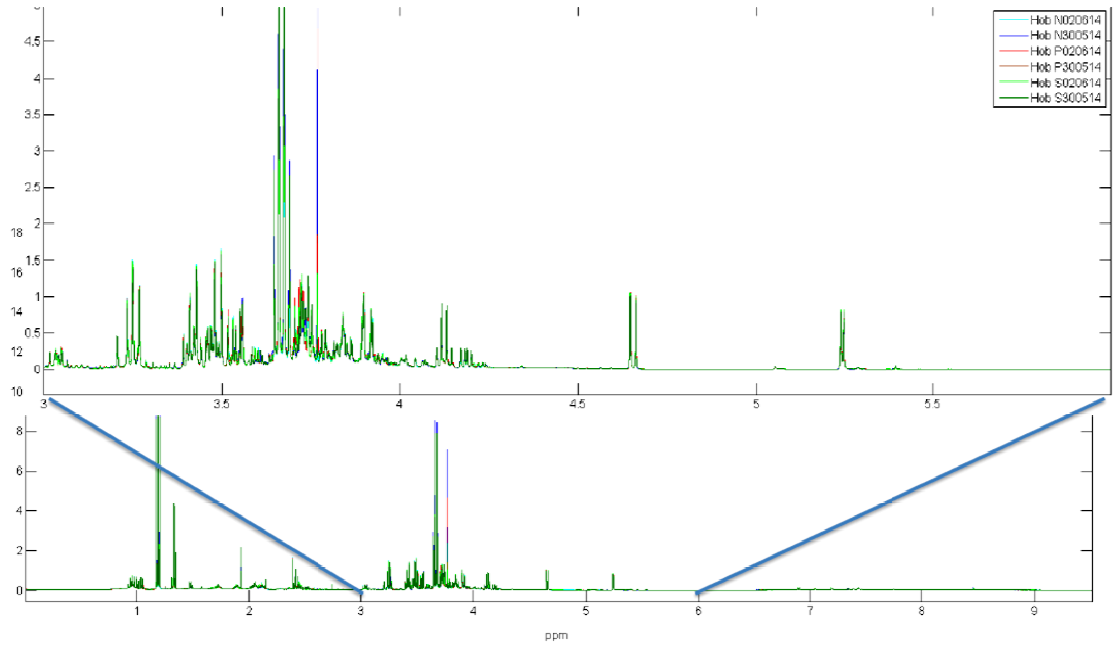

Figure 58 - HR'-MAS spectrum corresponding to 96 hours, treated by MatLab. Green: Without PLLA; Blue: Non Polarized Samples; Red: Polarized Samples (from 3 to 6 ppm).

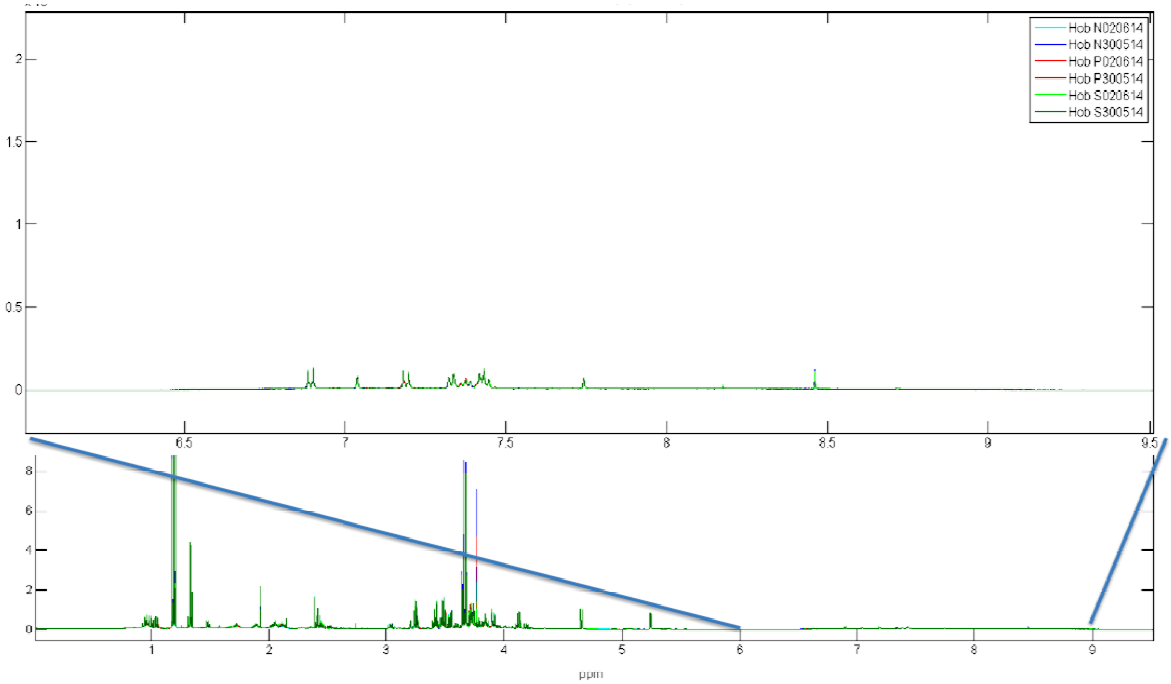

Figure 59 - HR'-MAS spectrum corresponding to 96 hours, treated by MatLab. Green: Without PLLA; Blue: Non Polarized Samples; Red: Polarized Sample (from 6 to 9.5 ppm).

On Figures 57, 58 and 59 it is possible to see a difference between the polarized and non polarized samples. As a primary analysis, the presence of peaks can be associated to many factors, from the cellular growth to the appearance of new metabolites. It can also be just an increase of the number of cells or metabolite that where already present in the solution, being this ambiguity of certainties associated to the repetition of the experiment.

At this moment it is not yet possible to display a list of the metabolites present in the samples, and their variation or correlation in metabolic pathways, since this information can only be advanced after at least three full independent assays are achieved. Nevertheless, from the primary analysis of the spectra obtained so far, we can state that none of the cytotoxic related metabolites were observed. Furthermore, we could already observe differences in the relative intensity of some resonance peaks that can be associated to many factors, from the cellular growth to the cell adhesion and differentiation.

4.5 Effect of polarization on cell adhesion

On previous studies it was proved that osteoblasts have a preference for positively charged surfaces, in this case negatively polarized by Corona. The polarization values obtained were significantly high after 11 days following the polarization process. Crystalline samples displayed the maximum polarization as it was expected. Combining the polarization values obtained and its duration with the surface measurements, both standard and crystalline films are acceptable candidates for bone tissue regeneration, once the high polarization will accelerate the process and the low contact angles will improve cell adhesion. Between standard and crystalline samples, the

latter are the most appropriate and worth investment because the range of applications is bigger due the better results in both types of measurement.

Considering possible applications, the range of options is huge once it is possible to vary films polarization and respective duration. Small bone fractures would be a good start once the healing mechanism is simpler. The target point would be the first phase, bone repair. In the first 8 hours cells divide attaining a maximum 24 hours after the injury. This activity happens in the surroundings of the injury, but it diminishes along time, being confined to target zone a few days later, maintaining itself above normal levels for weeks. Once the films are highly polarized and surely guarantee a polarization after 24 hours, their use could possibly improve the healing time by accelerating and increasing cell migration, adhesion and consequently increase proliferation. [148]

Regarding that bone callus is still weak until the 4^{th} or 6^{th} week, depending on each organism, maintain the polarization that long, could be the key to accelerate bone regeneration, consequently improving callus strength earlier. Bone remodelling starts almost along with callus ossification and continues along months until the bone regains its natural mechanical strength, shape and structure. [148]

Chapter 5

Conclusions and Future Work

5. Chapter 5 – Conclusions

In this chapter are presented the main conclusions of this project, and presented the future work and possible improvements in some experimental procedures.

5.1 Conclusions

The study of PLLA electrical properties started a long time ago with researchers like Hikosaka *et al.* [123] who explored parameters like the crystalline degree in order to see the influence on electrical polarization of PLLA films. The use of polarized PLLA for TE started with Barroca *et al*. [14, 15] who studied the relation between the material crystalline form and the duration of polarization, on thin films. A biological study on PLLA polarized films, using Fibronectin, was also done in order to see the influence of surface charges on cell adhesion and viability. [14, 15]

Giving continuity to the studies done before, in this academic work, PLLA films with different crystalline degrees were intensively characterized in terms of structure, thermal, surface and electrical properties. For structure characterization, SEM, POM and XRD analysis done showed that the temperatures and time of crystallization were successfully chosen once the maximum crystallization degree obtained was approximately 35% with well developed spherulites, with radius varying between 10 and 30 µm. The electrical measurement showed that crystallinity improves polarization durability, as it was expected, but decreases permittivity. The Corona polarization influenced both dielectric and polarization results for the values obtained were significantly higher than the ones presented on literature. Relative permittivity attained values of 50 for amorphous samples, and the dielectric loss was small proving the capability of PLLA to be polarized. The TSDC analysis confirmed the presence of polarization in standard and crystalline films, even 11 days after the corona discharge, displaying values similar to some known ferroelectric materials. In terms of surface, contact angle measurements showed that polarization and high degree of crystallization definitely increase hydrophilicity on PLLA films. The angle difference between non polarized and polarized crystalline samples, for example, was of 9 º. Hydrophilicity is one of the main requirements for a good protein adsorption and consequently cell adhesion, suggesting that, just like in previous results, cell viability may increase in these samples. The metabolomics assay, in an initial phase of study, demonstrated that negatively charged PLLA causes alteration on metabolites, however, the results are not complete enough to make more specific conclusions. Replicas of the assay must be done in the future to confirm that influence and the origin of it.

5.2 Future Work

In the future, some new experiments must be done and procedures must be improved in order to have better results. A few suggestions are given on Figure 60.

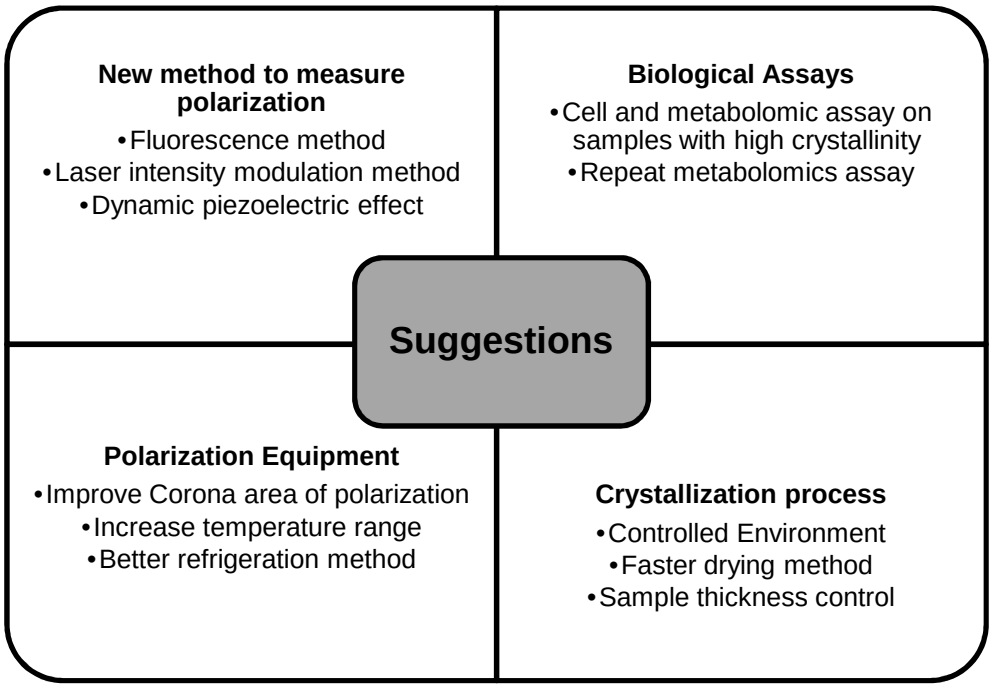

Figure 60 - Suggestions of new techniques and procedures improvement in the future. [149, 150]

Chapter 6

References

1. *U.S. Markets for Orthopedic Biomaterials for Bone Repair and Regeneration*, 2013.
2. Salgado, A.J., O.P. Coutinho, Reis, R.L., *Bone Tissue Engineering: State of the Art and Future Trends.* Macromolecular Bioscience, 2004. **4(8)**: p. 743-765.
3. Ratner, B.D., Hoffman, Allan S.,Schoen, Frederick J., Lemons, Jack E., , *Biomaterials Science, An Introduction To Materials in Medicine*. 2nd edition ed.
4. *Biomaterials - A Global Market Overview*, 2011.
5. Ikada, Y., Tsuji, Hideto, *Biodegradable polyesters for medical and ecological applications.* Macromol. Rapid Commun., 2000. **21**: p. 117–132.
6. Xiao, L., Wang, Bo, Yang, Guang, Gauthier, Mario, *Poly(Lactic-acid)-based biomaterials: Synthesis, Modification and Applications*, in *Biomedical Science, Engineering and Technology*, P.D.N. Ghista, Editor. 2012. p. 902.
7. Mistry, A.S.a.A.G.M., *Tissue Engineering Strategies for Bone Regeneration.* Adv Biochem Engin/Biotechnol, 2005. **94**: p. 1-22.
8. Barroca, N.B., Wu, A., Daniel-da-Silva, A. L., Fernandes, M. H., Vilarinho, P. M., *Poly(L-lactic)acid as stimulator of bone growth: Piezo-force microscopy study of the local piezoelectric properties.*, in *NanoSpain2008*2008: Braga, Porto.
9. Fukada, E., *Piezoelectricity of biopolymers.* Biorheology, 1995. **32**(6): p. 593-609.
10. Watkins, B.A., Lippman, H. E., Bouteiller, L., Li, Y., Seifert, M. F., *Bioactive fatty acids: role in bone biology and bone cell function. Progress in Lipid Research.* Progress in Lipid Research, 2001. **40(1-2)**: p. 125-148.
11. Barrère, F., Blitterswijk, C. A., Groot, K., *Bone regeneration: molecular and cellular interactions with calcium phosphate ceramics.* Int J Nanomedicine, 2006. **1(3)**: p. 317-332.
12. Fukada E., Y., I., , *On the Piezoelectric Effect of Bone.* Journal of the Physical Society of Japan, 1957. **12**: p. 1158-1162.
13. Barroca, N., *Scaffolds à base de polímeros piezoeléctricos para regeneração óssea*, in *Departamento de Engenharia de Materiais e Cerâmica*2008, Universidade de Aveiro. p. 142.
14. Barroca, N., Vilarinho, Paula M., Fernandes, Maria Helena., Sharma, Pankaj., Gruverman, Alexei.,, *Stability of electrically induced-polarization in poly (L-lactic) acid for bone regeneration.* Applied physiscs letters, 2012. **101**: p. 023701-1.
15. Barroca, N., Vilarinho, Paula M., Daniel-da-Silva, Ana Luisa., Wu, Aiying., Fernandes, Maria Helena., Gruverman, Alexei.,, *Protein adsorption on piezoelectric poly(L-lactic) acid thin filmsby scanning probe microscopy.* Applied physics letters, 2011. **98**: p. 133705.
16. Turner, J.F., Riga, A., O'Connor, A., Zhang, J., Collis, J., *Characterization of drawn and undrawn poly-L-lactide films by differential scanning calorimetry.* Journal of Thermal Analysis and Calorimetry, 2004. **75(1)**: p. 257-268.
17. Nordell, B., *The dowsing reaction originates from piezoelectric effect in bone.* Pres. At the 6th Int. Svedala Symposium on Ecological Design, 1988.
18. *Downsing Rods - L shaped*. Available from: https://encrypted-tbn3.gstatic.com/images?q=tbn:ANd9GcT4RBL2YL9UYMbQiyWxk2eZctkUi3N01JYz08Lnm_emnnoKEyBA.
19. *Dowsing Rods - Y-Shaped*. Available from: http://www.perceptions.couk.com/uef/imgs/Y%20Dowsing%20Rod.jpg.
20. Marino, A.A., *Direct current and bone growth.* Foundations of Modern Bioelectricity, 1988: p. 657-709.
21. Becker, R.O., *The bioelectric field pattern in the salamander and its simulation by an electronic analog.* IRE Trans. Med. Elect., 1960. **ME-7**: p. 202-208.
22. Becker, R.O., *The bioelectric factors in amphibian limb regeneration.* J. Bone Joint Surg., 1961. **43-A**: p. 643-656.
23. Becker, R.O., Bachman, C. H., Slaughter, W., *The longitudinal direct current gradients of spinal nerves.* Nature 1962. **196**: p. 675-676.
24. Becker, R.O., *Search for evidence of axial current flow in peripheral nerves of the salamander.* Science, 134. **134**: p. 101-102.
25. Bassett, C.A.L., *Electrical effects in bone.* Sci. AM., 1965. **213**: p. 1826.
26. Bassett, C.A.L., L., Pawluk, R. J. and Becker, R. O., *Effects of electric currents on bone in vivo.* Nature, 1964. **204**: p. 652-654.

27. Friedenberg, Z.B., Andrews, E. T., Smolenski, B. I., Pearl, B. W., Brighton, C. T., *Bone reaction to varying amounts of direct current.* Surg. Gynecol, Obstet., 1970. **131**: p. 894-899.
28. Friedenberg, Z.B., Roberts, P. G., Didizian, N. H., Brighton, C. T., *Stimulation of fracture healing by direct current in the rabbit fibula.* J. Bone Joint Surg., 1971. **53A**: p. 1400-1408.
29. Friedenberg, Z.B., Zemsky, L. M., Pollis, R.P., Brighton, C.T., *The response of non—traumatized bone to direct current.* J. Bone Joint Surg., 1974. **56A**: p. 1023-1030.
30. Richez, J., Chamay, A., Bieler, L., *Bone changes due to pulses of direct electric microcurrent.* Virchows Arch. Abt. A Path. Anat., 1972. **357**: p. 11—l8.
31. Brighton, C.T., Friedenberg, Z. B., Black, J., et al., *Electrically induced osteogenesis: Relationship between charge, current density, and the amount of bone formed.* Clin. Orthop., 1981. **161**: p. 122-123.
32. Spieler, H., *Data Acquisition Handbook: A reference for DAQ and analog & digital signal conditioning*, 2004, Measurements Computing Corporation.
33. Guzelsu, N., Walsh, W. R., *Streaming potential of intact wet bone.* J. Biomech., 1990. **23 (7)**: p. 673-685.
34. Poltawski, L., Watson,, *Bioelectricity and microcurrent therapy for tissue healing – a narrative review.* Physical Therapy Reviews, 2009. **14(2)**: p. 11.
35. Marieb, E.N., *Human Anatomy and Physiology*. 5th ed, ed. K. Ueno. 2001, USA: Daryl Fox.
36. Seeley, R.D., T.D. Stephens, P. Tate, *Anatomia e Fisiologia*. 1993: Sorbona.
37. *Bone cell formation*. 22/01/2014]; Available from: http://image.tutorvista.com/content/feed/tvcs/bone20cells2020osteoblast.jpg.
38. *Bone cells*. 22/01/2014]; Available from: http://www.siumed.edu/~dking2/ssb/images/remodel.jpg.
39. *Compact Bone structure*. 21/01/2014]; Available from: http://aikidopurbalingga.blogdetik.com/files/2011/06/bone-structure.jpg.
40. *Bone growth process*. 22/01/2014]; Available from: http://classes.midlandstech.edu/carterp/Courses/bio210/chap06/Slide15.JPG
41. Pearson, O.M., Leberman, Daniel E., *The Aging of Wolff's "Law": Ontogeny and Responses to Mechanical Loading in Cortical Bone.* Yearbook of Physical Anthropology, 2004. **47**: p. 63-99.
42. *Bone remodelling process*. 22/01/2014]; Available from: http://www.umich.edu/news/Releases/2005/Feb05/img/bone.jpg
43. Liu, S.Q., *Bioregenerative engineering: Principles and Applications*, 2007, Wiley-Interscience - A John Wiley % Sons, Inc.
44. Heywang, W., Lubitz, Karl, Wersing, Wolfram, *Piezoelectricity: Evolution and Future of a Technology*. Vol. 114. 2008: Springer Series in Materials Science.
45. Nalwa, H.S., *Ferroelectric Polymers - Chemistry, Physics and Applications.* 1995, New York, USA: Marcel Dekker, Inc.
46. *Direct and Converse Piezoelectric effect*. Available from: http://resources.edb.gov.hk/physics/articlePic/AtomicPhysics/SamrtMaterials_pic01.gif.
47. Sessler, G., *Physical principles of electrets.* Electrets, 1999. **1**: p. 13-80.
48. Yang, X.L., Gu, J. W., Zhu, H. S., *Preparation of bioelectret collagen and its influence on cell culture in vitro.* J. Mater. Sci: Mater Med, 2006. **17**: p. 767-771.
49. Ramsey, N.F., *Electric-Dipole Moments of Particles.* Annual Review of Nuclear and Particle Science, 1982. **32**: p. 211-233.
50. Kholkin, A.L., Pertsev, N. A., Goltsev, A. V., *Piezoelectricity and Crystal Symmetry*.
51. Ledoux, A., *Theory of Piezoelectric Materials and Their Applications in Civil Engineering*, in *Department of Civil and Environmental Engineering*2011, Massachusets Institute of Technology.
52. Qiu, J., Ji, Hongli, *The Application of Piezoelectric Materials in Smart Structures in China.* Int'l J. of Aeronautical & Space Sci., 2010. **11(4)**: p. 266-284.
53. Isaacson, B.M., Bloebaum, Roy D., *Bone bioelectricity: What have we learned in the past 160 years? - a review.* Wiley Online Library, 2010.
54. Adey, W.R., *The sequence and energetics of cell membrane transductive coupling to intracellular enzyme systems.* Bioelectrochem. Bioenerg, 1986. **15**: p. 447-456.
55. Meyer, U., Meyer Thomas, Handschel, Jorg, Wiesmann, Hans Peter, *Fundamentals of Tissue Enginerring and Regenerative Medicine*, 2009, Springer-Verlag Berlin Heidelberg.

56. Fisher, J.P., Mikos, Antonios G., Bronzino, Joseph D., *Tissue Engineering*, 2006, Taylor Francis Group.
57. Chu, P.K., Liu, Xuanyong, *Biomaterials fabrication and processing handbook*. 2008, USA: Taylor & Francis Group, LLC.
58. Poitout, D.G., *Biomechanics and Orthopedics*, ed. Springer-Verlag. 2004, London.
59. Cain, E.L., *Stimulating Treatment.* Orthopedic Technology Review, 2002. **4 (4)**.
60. Chang, H., Wang, Yiwei, *Cell Responses to Surface and Architecture of Tissue Engineering Scaffolds, Regenerative Medicine and Tissue Engineering - Cells and Biomaterials*, E. Daniel, Editor 2011: Australia.
61. Schneider, G.B., English, A., Abraham, M., Zaharias, R., Stanford, C., Keller, J., *The effect of hydrogel charge density on cell attachment.* Biomaterials, 2004. **25**: p. 3023-3028.
62. Makohliso, S.A., Valentini, R. F., Aebischer, P., *Magnitude and polarity of a fluoroethylene propylene electret substrate charge influences neurite outgrowth in vitro.* Journal of Biomedical Materials Research, 1993. **27**: p. 1075-1085.
63. Lee, J.H., Jung, H. W., Kang, I. K., Lee, H. B., *Cell behaviour on polymer surfaces with different functional groups.* Biomaterials, 1994. **15**: p. 705-711.
64. Li, P. and F. Zhang, *The electrochemistry of a glass surface and its application to bioactive glass in solution.* Journal of Non-Crystalline Solids, 1990. **119**(1): p. 112-118.
65. Lu, H.H., Pollack, Solomon R., Ducheyne, Paul, *Temporal zeta potential variations of 45S5 bioactive glass immersed in an electrolyte solution.* John Wiley & Sons, Inc., 2000.
66. Obata, A., Nakamura, Satoshi, Moriyoshi, Yusuke, Yamashita, Kimihiro, *Electrical polarization of bioactive glass and assessment of their in vitro apatite deposition.* Willey Periodics, Inc., 2003.
67. Hench, L.L., *Bioceramics.* J. Am. Soc. , 1998. **81 (7)**: p. 1705-28.
68. Davies, J.E., Causton, B., Bovell, Y., Davy, K., Sturt, C. S., Biomaterials, 1986. **7**: p. 231.
69. Nakamura, S., Kobayashi, Takayuki, Yamashita, Kimihiro, *Extended bioactivity in the proximity of hydroxyapatite ceramic surfaces induced by polarization charges.* Willey Periodics, Inc., 2002.
70. Irastorza, R.M., Mayosky, Miguel A., Grigera, J. Raúl, Vericat, Fernando, *Dielectric Properties of Natural and Demineralized Collagen Bone Matrix*, 2010.
71. Guaraldia, G., Fontdevila, Joan, Christensenc, Lise H., Orlandoa, Gabriella, Stentarellia, Chiara, Carlia, Federica, Zona, Stefano, and G. De Santis, Pedoned, Antonio, De Fazio, Domenico, Bonuccie, Pierluigi, Martınez, Esteban, *Surgical correction of HIV-associated facial lipoatrophy.* AIDS, 2011. **25**: p. 1-12.
72. Pezzin, A.P.T., Zavaglia, Cecília A. C., Duek, Eliana A. R., *Estudo da degradação in vitro de blendas de Poli(p-dioxanona)/Poli(l-ácido-láctico) (PPD/PLLA) preparadas por evaporação de solvente.* Polímeros, 2002. **12 (4)**.
73. Auras, R., Lim, Loong-Tak, Selke, Susan E. M., Tsuji, Hideto, *Poly(Lactic Acid) - Synthesis, Structures, Properties, Processing and Applications*, 2010, Wiley.
74. Bailey, W.J., *22 - Ring-opening Polymerization*, in *Comprehensive Polymer Science and Supplements*, G.A.C. Bevington, Editor. 1989, Pergamon: Amsterdam. p. 283-320.
75. Achmad, F., et al., *Synthesis of polylactic acid by direct polycondensation under vacuum without catalysts, solvents and initiators.* Chemical Engineering Journal, 2009. **151**(1–3): p. 342-350.
76. Maharana, T., B. Mohanty, and Y.S. Negi, *Melt–solid polycondensation of lactic acid and its biodegradability.* Progress in Polymer Science, 2009. **34**(1): p. 99-124.
77. *PLLA synthesis by ROP*. 12-12-2014]; Available from: http://www.bioplasticsmagazine.com/bioplasticsmagazine-wAssets/img/online-archiv/201303/pla_depolymerization_fig_4.jpg.
78. Kwon, I.K., Kidoaki, S., Matsuda, T., *Electrospun nano-to microfiber fabrics made of biodegradable copolyesters: structural characteristics, mechanical properties and cell adhesion potential.* Biomaterials, 2005. **26**: p. 3929-3939.
79. Santos Jr., A.R., *Bioresorbable Polymers for Tissue Engineering, Tissue Engineering*, D.E. (Ed.), Editor. 2010.
80. Lin, Y., Wang, Luling, Zhang, Peibiao, Wang, Xin, Chen, Xuesi, Jing, Xiabin, Su, Zhaohui, *Surface modification of poly(L-lactic acid) to improve its cytocompatibility via assembly of polyelectrolytes and gelatin.* Acta Biomaterialia, 2006. **2**: p. 155–164.

81. Sperling, L.H., *Introduction to Physical Polymer Science*. 2nd ed. 1992, USA: John Wiley & Sons, Inc.
82. Gránásy, L., Pusztai, Tamás, Tegze, György, Warren, James A., Douglas, Jack F., *On the growth and form of spherulites.* Phys. Rev. E, 2005. **72, 011605**.
83. Saeidlou, S., et al., *Poly(lactic acid) crystallization.* Progress in Polymer Science, 2012. **37**(12): p. 1657-1677.
84. Crist, B., *Structure of Polycrystalline Aggregates*, in *Handbook of Polymer Crystallization*. 2013, John Wiley & Sons, Inc. p. 73-124.
85. *PCL hedrite*. Available from: http://pubs.rsc.org/services/images/RSCpubs.ePlatform.Service.FreeContent.ImageService.svc/ImageService/Articleimage/2009/SM/b806074f/b806074f-f4.gif.
86. Padden, F.J., Keith, H. D. , J. Appl. Phys., 1965. **36**: p. 2987.
87. Norton, D.R., Keller, A., Polymer Engineering and Science, 1985. **26**: p. 704.
88. Riande, E., Díaz-Calleja, Ricardo, *Electrical Properties of Polymers*. 2004: Marcel Dekker Inc.
89. Kawai, H., Jpn. J. Appl. Phys., 1969. **8**: p. 975.
90. Bergman, J.G., McFee, J.H., Crane, G.R. , Appl. Phys. Lett. , 1971. **18**: p. 203.
91. Nakamura, K., Wada, Y., J. Polym. Sci., 1971. **A-29**: p. 161.
92. Almusallam, A., Yang, K., Cao, Z., Zhu, D., Tudor, J., Beeby, S. P., *Improving the dielectric and piezoelectric properties of screen-printed Low temperature PZT/polymer composite using cold isostatic pressing.* Journal of Physics: Conference Series, 2014. **557**: p. 012083.
93. Ahmad, Z., *Polymeric Dielectric Materials*, 2012, InTech.
94. Barroca, N., *Article under submission.* 2014.
95. *Corona plume discharge*. Available from: http://ej.iop.org/images/0022-3727/46/29/295402/Full/jphysd469123f02_online.jpg.
96. Siemann, U., *Solvent cast technology – a versatile tool for thin film production.* Progr Colloid Polym Sci, 2005. **130**: p. 1-14.
97. Iannace, S., Nicolas, L., *Isothermal crystallization and chain mobility of poly(L-lactide).* P.le Tecchio, 1996. **80**.
98. Pan, Q.Y., Tasaka, Shigeru, Inagaki, Norihiro, *Ferroelectric behavior in Poly-L-lactic acid.* Jpn. J. Appl. Phys., 1996. **35**: p. L1442-L1445.
99. Sekimoto, K., Takayama, Mitsuo, *Fundamental Processes of Corona Discharge - Surface Analysis of Traces Stained with Discharge on Brass Plate in Negative Corona.* J. Inst. Electrostat. Jpn, 2009. **33**: p. 38-42.
100. Frias, C., Reis, J., Silva, F. Capela e, Potes, J., Simões, J., Marques, A. T., *Polymeric piezoelectric actuator substrate for osteoblast mechanical stimulation.* Journal of Biomechanics, 2010. **43**: p. 1061-1066.
101. Inc., H.P.S., *What is Corona? A Clearly Explained and Illustrated Story About Three Types of Corona Discharge and Their Relationship to Radio Interference*, 2004, Bulletin EU1234-H.
102. *Corona glow discharge*. Available from: http://www.weatherscapes.com/Photos/w-085-25.jpg.
103. *Corona brush discharge*. Available from: http://www.electrotherapymuseum.com/2009/Protocakes/Brush2.jpg.
104. Mulla, S.M., Phale, P. S., Saraf, M. R., *Use of X-Ray Diffraction Technique for Polymer Characterization and Studying the Effect of Optical Accessories.* AdMet, 2012. **OM 006**.
105. La Carrubba, V., Pavia, F. Carfì, Brucato,V., Piccarolo, S., *PLLA/PLA scaffolds prepared via Thermally Induced Phase Separation (TIPS): tuning of properties and biodegradability*.
106. Sharma, R., Bisen, D.P., Shukla, Usha, Sharma, B.G., *X-ray diffraction: a powerful method of characterizing nanomaterials.* Recent Research in Science and Technology 2012. **4(8)**: p. 77-79.
107. Brundle, C.R., Jr., Charles A. Evans, Wilson, Shaun, *Encyclopedia of Materials Characterization - Surfaces, Interfaces, Thin Films*, L.E. Fitzpatrick, Editor 1992, Reed Publishing (USA) Inc.: USA.
108. Gill, P., Moghadam, Tahereh Tohidi, Ranjbar, Bijan, *Differential Scanning Calorimetry Techniques: Applications in Biology and Nanoscience.* 2010. **21**: p. 167-193.
109. Instruments, T. *TA Q100 Differential Scanning Calorimetry - Operating Instructions*.

110. Braun, D., Cherdron, Harald, Rehahn, Matthias, Ritter, Helmut, Voit, Brigitte, *Polymer Synthesis: Theory and Practice - Fundamentals, Methods, Experiments.* 5th edition ed.: Springer.
111. *SEM micrograph polen grains*. Available from: http://upload.wikimedia.org/wikipedia/commons/thumb/a/a4/Misc_pollen.jpg/800px-Misc_pollen.jpg.
112. *SEM micrograph*. Available from: http://www.azom.com/work/UGPSC2I902ISy2o98267_files/image009.jpg.
113. *SEM apparatus*. Available from: http://www.microscopy.ethz.ch/images/sem.jpg.
114. Carlton, R.A., *Chapter 2 - Polarized Light Microscopy*, in *Pharmaceutical Microscopy*. Springer Science and Business Media, LLC 2011.
115. *PLLA spherulite*. Available from: http://www.nature.com/pj/journal/v43/n9/images/pj201163f3.jpg.
116. Vorburger, T.V., Raja, J., *Surface Finish Metrology Tutorial*, 1990, U.S Department of Commerce: U. S. A.
117. Grous, A., *Applied Metrology for Manufacturing Engineering*. Instrumentation and Measurement Series. Wiley.
118. Abdallah, W., Buckley, Jill S., Carnegie, Andrew, Edwards, John, Herold, Bernd, Fordham, Edmund, Graue, Arne, Habashy, Tarek, Seleznev, Nikita, Signer, Claude, Hussain, Hassan, Montaron, Bernard, Ziauddin, Murtaza, *Fundamentals of Wettability - Oilfield Review*, 2007.
119. Yuan, Y., Lee, Randall T., *Chapter 1 - Contact Angle and Wetting Properties*, in *Surface Science Techniques*, G. Bracco, Holst, B., Editor. 2013, Springer: Verlag Berlin Heidelberg.
120. Dann, J.H., Dann, James J., *The People's Physics Book - Electric Circuits: Capacitors*, 2006.
121. Brittanica, E. *Dieletric Loss*. 10/09/2014]; Available from: http://www.britannica.com/EBchecked/topic/162651/dielectric-loss.
122. Ren, J., Urakawa, Osamu, Adachi, Keiichiro, *Dielectric and Viscoelastic Studies of Segmental and Normal Mode Relaxations in Undiluted Ply(d,l-lactic acid).* Macromolecules, 2003. **36**: p. 210-219.
123. Hikosaka, S., Ishikawa, H., Ohki, Y. , *Effects of Crystallinity on Thermally Stimulated Current and Complex Permittivity of Poly(L-lactide)*, in *Annual Report Conference on Electrical Insulation Dielectric Phenomena*2008. p. 497-500.
124. Kalia, R., Sharma, Vandana, Sharma, J. K., *Dielectric behavior of polyetheretherketone (PEEK) using TSDC technique.* J Polym Res, 2012. **19**: p. 9826.
125. Gaur, M.S., Shukla, Prashant, Tiwari, R. K., Tanwar, Anju, Singh, S. P. and *New approach for the measurement of glass transition temperature of polymer* INDIAN J PURE & APPL PHYS, 2008. **46**.
126. Burghate, D.K., Deogaonkar, V. S., Sawarkar, S. B., Yawale, S. P., Pakade, S. V., *Thermally stimulated discharge current (TSDC) and dielectric constant of semiconducting glasses.* Bull. Mater. Sci., 2003. **26**: p. 267-271.
127. *TSDC*.
128. Hong, C.-M., Day, Delbert E., *Thermally stimulated polarization and depolarization current (TSPC/TSDC) techniques for studying ion motion in glass.* Journal of Materials, 1979. **14**: p. 2493-2499.
129. Boudenne, A., Ibos, Laurent, Candau, Yves, Thomas, Sabu, *Handbook of Multiphase Polymer Systems*. 2011: John Wiley and Sons, Ltd.
130. Sedita, J.S., O'Reilly, James M., *A Thermally Stimulated Depolarization Current Study of Polymers in the Glass Transition Region.* Polymer Engineering and Science, 2001. **41 (1)**: p. 15-22.
131. Dietmair, S., Timmins, Nicholas E., Gray, Peter P., Nielsen, Lars K., Krömer, Jens O., *Towards quantitative metabolomics of mammalian cells: Development of a metabolite extraction protocol.* Analytical Biochemistry, 2010. **404**: p. 155-164.
132. Dunn, W.B., Broadhurst, David I., Atherton, Helen J., Goodacre, Royston, Griffin, Julian L., *Systems level studies of mammalian metabolomes: the roles of mass spectrometry and nuclear magnetic resonance spectroscopy.* Chem. Soc. Rev., 2011. **40**: p. 387-426.

133. Ritter, J.B., Genzel, Y., Reichl, U., *Simultaneous extraction of several metabolites of energy metabolism and related substances in mammalian cells: Optimization using experimental design.* Analytical Biochemistry, 2008. **373**: p. 349-369.
134. Shryock, J.C., Rubio, R., Berne, R. M. , *Release of adenosine from pig aortic endothelial cells during hypoxia and metabolic inhibition.* American Journal of Physiology, 1988. **254**: p. H223-2299.
135. Hakumäki, J.M., Kauppinen, Risto A. , *1H NMR visible lipids in the life nd death of cells.* Elsevier Science Ltd, 2002: p. 357-362.
136. *Magic Angle spinning*. Available from: http://upload.wikimedia.org/wikipedia/commons/thumb/a/ab/MagicAngleSpinning.svg/220px-MagicAngleSpinning.svg.png.
137. Laws, D.D., Bitter, H. M. , Jerschow, A. , *Solid-State Spectroscopic Methods in Chemistry.* Angew. Chem., 2002. **41**: p. 3096-3129.
138. Williamson, P.T.F., Ernst M., Meier, B.H., *MAS Solid-State NMR of Isotropically Enriched Biological Samples in BioNMR in Drug Research*, O. Zerbe, Editor 2003, Wiley.
139. Bruice, P.Y., *Organic Chemistry*, 2007, Pearson Prentice Hall: New Jersey.
140. Cocca, M.C.C., Di Lorenzo, Maria Laura, Malinconico, Mario, Frezza, Vincenzo, *Influence of crystal polymorphism on mechanical and barrier properties of poly(L-lactic acid).* European Polymer Journal, 2011. **47**: p. 1073–1080.
141. Mano, J., Wang, Yaming, Viana, Júlio C., Denchev, Zlatan, Oliveira, Maria J., *Cold Crystallization of PLLA Studied by Simultaneous SAXS and WAXS.* Macromolecular Materials and Engineering, 2004. **289**: p. 910-915.
142. Di Lorenzo, M.L., *The Crystallization and Melting Processes of Poly(L-lactic acid).* Macromol. Symp., 2006. **234**: p. 176–183.
143. Young, K.F., Frederikse, H. P. R., *Compilation of the Static Dieletric Constant of Inorganic Solids.* J. Phys, Chem., 1973. **2**: p. 313-409.
144. Hashim, A.A., *Polymer dipoles relaxation and potential energy (New Simulation Model)*, in *Polymer Thin Films*2010.
145. Sessler, G.M., *Polymeric electrets.* Electrical properties of polymers, 1982(241-284).
146. Lee, S.J., Choi, J. S., Park, K. S., Khang, G., Lee, Y. M., Lee, H. B., *Response of MG63 osteoblast-like cells onto polycarbonate membrane surfaces with different micropore sizes.* Biomaterials, 2004. **25**: p. 4699-4707.
147. Wei, J., Igarashi, T., Okumori, N., Maetani, T., Liu, B. S., Yoshinari, M., *Influence of surface wettability on competitive protein adsorption and initial attachment of osteoblasts.* Biomedical Materials, 2009. **4**: p. 045002.
148. McKibbin, B., *The biology of fracture healing in long bones.* Journal of Bone and Joint Surgery, 1978. **60-B(2)**.
149. Nishijima, Y., Y. Onogi, and T. Asai, *Fluorescence method for studying molecular orientation in polymer solids.* Journal of Polymer Science Part C: Polymer Symposia, 1967. **15**(1): p. 237-250.
150. Lang, S.B. and D.K. Das-Gupta, *A new technique for determination of the spatial distribution of polarization in polymer electrets.* Ferroelectrics, 1984. **60**(1): p. 23-36.

Appendix A

Biological Assay protocol

Metabolómica – Protocolo com placas de 24 poços

1 único ensaio (HR-MAS NMR)

1º Passo: Cultura de HOb

A. Preparação dos frascos de cultura para HOb

1. Tirar o meio de crescimento de HOb do frigorífico e descontaminar com etanol 70%;
2. Pipetar 15mL de meio de crescimento de HOb à Temperatura ambiente para um frasco T-75 (idealmente manter proporção de 1mL por cada 5cm^2).

B. Descongelar e plaquear HOb

1. Remover o vial criopreservado do tanque de armazenamento de azoto líquido;
2. Descongelar as células rapidamente colocando a metade inferior do vial num banho de 37˚C por 1 min;
3. Tirar o vial do banho, secar bem e descontaminar exteriormente com etanol 70%;
4. Na câmara de fluxo, remover a tampa do vial cuidadosamente;
5. Ressuspender as células no vial, pipetando gentilmente as células 5 vezes com uma pipeta de 2mL;
6. Pipetar a suspensão celular (1mL) do vial para o frasco T-75, contendo 15mL do meio de crescimento de HOb;
7. Tapar o frasco e agitar gentilmente para distribuir bem as células;
8. Colocar o frasco na incubadora (37˚C, 5% CO_2, atmosfera humedecida);
9. Fazer substituição de meio 24h depois, para remover todos os vestígios de DMSO;
10. Mudar o meio diariamente até as células atingirem uma confluência de 60%;
11. Dobrar o volume de meio quando a cultura tiver uma confluência > 60%, ou para crescimentos durante o fim de semana;
12. Dividir células quando a cultura atingir os 80% de confluência.

C. Preparar solução neutralizadora de Tripsina

Para 200mL de solução de 5% FBS em tampão sem cálcio e sem magnésio.

1. Preparar HBSS;
2. Inactivar FBS: 30min a 56˚C (deixar arrefecer no frigorífico overnight);
3. Adicionar 10mL de soro inactivado a 190mL de HBSS – armazenar a 4˚C.

D. Dividir HOb

Tripsinizar as células à temperatura ambiente. Não aquecer nenhum dos reagentes a 37˚C.

1. Pipetar 15mL de meio de cultura para novos frascos T-75;
2. Remover o meio dos frascos com HOb confluentes por aspiração;
3. Lavar as células com HBSS e remover a solução por aspiração;

4. Pipetar 6mL de Tripsina/EDTA (solução) para o Frasco T-75. Agitar gentilmente o frasco para assegurar que a solução cobre todas as células;

5. Fechar o frasco e monitorizar o processo de tripsinização à temperatura ambiente ao microscópio invertido. Geralmente as células levam 2-4min para ficarem redondas.

6. Soltar as células redondas da superfície do frasco, batendo com o frasco lateralmente na palma da mão;

7. Pipetar 5mL da solução neutralizadora de Tripsina para inibir actividade tríptica;

8. Transferir a suspensão celular do frasco para um frasco estéril de 50mL;

9. Lavar o frasco com 5mL adicionais de solução de neutralização de tripsina e transferir para o mesmo frasco de 50mL;

10. Centrifugar o tubo a 220g por 5min para sedimentar as células;

11. Aspirar e rejeitar o sobrenadante;

12. Ressuspender o pellet celular em 5mL de meio de crescimento de HOb, pipetando gentilmente;

13. Contar as células num hemocitómetro. Inocular 10 000 células por cm^2 para crescimento rápido ou 5 000 por cm^2 para crescimento normal.

Nota: Número de células por frasco T-75 ≅ $1x10^6$ células (90% confluência). Precisamos de 1 milhão de células/amostra/tempo. Temos 3 amostras (PLLA neutro, PLLA polarizado (carga negativa), Plástico) e **2 tempos: 24h e 96h**.

2º Passo: Esterilização do PLLA

1. Círculos de PLLA polarizados e não polarizados com $1cm^2$ são colocados em placas de 24 poços (Num total de **12 placas de 24 poços**: 6 placas para o T1-24h, 6 placas para o T2-96h; T0 é definido como o tempo inicial de contacto entre as células e o polímero).

2. Introduzir os discos de PLLA nos poços, depondo um o-ring de PTFE sobre cada um.

3. Manter os discos em 70% Etanol durante 5 min, **10** lavagens com água destilada durante 10 min/cada, seguido de **10** lavagens com 1x PBS durante 10 min/cada e **3** lavagens com meio de cultura de células.

3º Passo: Adição dos HOb aos discos de PLLA

1. Adicionar as células no topo de cada disco de PLLA presente em cada poço a uma densidade de 10 000 células/cm^2 (10 000 células são depositadas por poço em 2mL de meio de cultura).

2. Colocar as placas na incubadora a 37ºC, 5% CO_2. Após **24 h** as primeiras 6 placas são retiradas da incubadora (Proceder ao 4º Passo); após **96h** outras 6 placas são retiradas (Proceder ao 4º Passo).

4º Passo: Remover as células do PLLA e lise mecânica (preparação para a metabolómica)

Protocolo para retirar as células do PLLA (tripsina)

1. Remover com cuidado o meio dos poços que contêm o PLLA com os HOb; **guardar o meio para análise por RMN.**

2. Adicionar 2mL de PBS para lavar restos do meio de cultura, remover a solução por aspiração;

3. Pipetar 1mL de Tripsina/EDTA (solução) para cada poço. Agitar gentilmente a placa para assegurar que a solução cobre todas as células;

4. Monitorizar o processo de tripsinização à T ambiente ao microscópio invertido. Geralmente as células levam 2-4min para ficarem redondas.

5. Pipetar 1mL da solução neutralizadora de Tripsina para inibir actividade tríptica;

6. Transferir a suspensão celular de cada poço para um tubo falcon estéril de 50mL;

7. Centrifugar a 1000rpm, 6min, 20˚C;

8. Aspirar o sobrenadante e ressuspender em 2mL de PBS;

9. Centrifugar a 1000rpm, 6min, 20˚C;

10. Aspirar o sobrenadante e ressuspender em 2mL de PBS;

11. Centrifugar novamente a 1000rpm, 6min, 20˚C;

12. Aspirar o sobrenadante e ressuspender o pellet de células em 1mL de PBS/D_2O, transferindo esta suspensão para um eppendorf de 1.5mL;

13. Centrifugar a 1000rpm, 6min, 20˚C;

14. Aspirar o sobrenadante e finalizar a preparação da amostra já para RMN ressuspendendo o pellet em 40µL de PBS/D_2O + 5µL de PBS/D_2O/TSP(0.25%);

15. Congelar a amostra na arca a -20˚C;

16. Levar as amostras para o **Departamento de Química** para efetuar a lise celular (protocolo em baixo).

Protocolo de lise mecânica (Metabolómica)

1. 15 seg em azoto líquido;
2. 30 seg ultrasons;
3. 15 seg em azoto líquido;
4. 30 seg ultrasons;
5. 15 seg em azoto líquido;
6. Guardar a -80ºC até análise por RMN.